ASPECTS OF QUANTUM CRITICALITY IN ITINERANT ELECTRON FERROMAGNETIC SYSTEMS

by

MARTYN LAURENCE LAWLEY

A thesis submitted to
The University of Birmingham
for the degree of
DOCTOR OF PHILOSOPHY

School of Physics and Astronomy
The University of Birmingham

September 2009

Abstract

Fermi-liquid theory is one of the standard models of condensed matter physics, supplying a valid explanation of the low temperature properties of many metals. However, non-Fermi-liquid behaviours arise in many itinerant systems that exhibit a zero temperature magnetic phase transition. This thesis is mainly concerned with such quantum critical points and is an investigation into the various phenomena seen in the phase diagram of itinerant ferromagnetic systems.

We apply a standard theory of itinerant quantum criticality to a quantum-critical end-point in a three-dimensional ferromagnet, before speculating on $ZrZn_2$ being a test-bed of our results. Then we consider two explanations for the appearance of a first-order phase transition at low temperatures and attempt to reconcile them with $ZrZn_2$.

Finally we concentrate on the wide range of novel states that appear instead of a pure quantum critical point. Such exotic phases are superconducting or magnetic in nature and we investigate whether the onset of ferromagnetic quantum critical fluctuations can give rise to a certain class of such states.

Acknowledgements

I acknowledge my supervisor Professor Andrew Schofield for all he has done to help over these past four years. The research appearing in this thesis was funded via a PhD studentship from the Engineering and Physical Sciences Research Council (EPSRC).

For my parents.

Contents

List of Figures

List of Tables

Chapter 1

Overview of the thesis

This thesis is concerned with quantum criticality, the study of phase transitions at zero temperature. In particular we concentrate on the appearance of quantum critical points in itinerant ferromagnetic systems. The generic phase diagram of such systems displays many interesting phenomena and in this thesis we will explore the physics of a number of them.

The standard low temperature treatment of metals has, for some time, been given by Fermi-liquid theory (an introduction to which is given in §2.2) and, indeed, many metallic systems are well described. However, it seems that in the vicinity of quantum critical points, regions of the phase diagrams of itinerant systems fail to comply with the predictions of Fermi-liquid theory and a wide range of anomalous behaviours - in many systems - have now been catalogued by experimental workers (see §2.5 for a review of experiments). Chapter Two of this thesis introduces Fermi-liquid theory and its subsequent breakdown near quantum criticality. The study of critical phenomena (§2.3) and itinerant magnetism (§2.4) is also introduced.

There do, however, exist theories of quantum criticality in itinerant systems. Chapter Three serves as a review of one of the most eminent, Hertz-Millis theory. To involve ourselves fully with the theory, it will be required that we develop a little mathematical machinery and so we will also be introduced to fermionic functional integrals (see §3.2), required to write down the action associated with Hertz-Millis theory, and the renormalization group (RG) procedure (§3.4). Solving a set of RG equations allows one to compute a phase diagram near a quantum critical point as well as a set of thermodynamic quantities, this is performed in §3.6.

Having developed Hertz-Millis theory, in Chapter Four we apply it to a clean, three-dimensional, ferromagnetic quantum-critical end-point. In doing so we calculate a number of quantities with which an experiment could be compared (see §4.3). Although no such quantum-critical end-point has been experimentally found in three-dimensions, we do speculate on a potential "test-bed", namely $ZrZn_2$ (see sections 4.4 and 4.5).

Hertz-Millis theory is applied to continuous quantum phase transitions. But many itinerant ferromagnetic systems, including $ZrZn_2$, are found to exhibit first-order transitions at low temperatures. Chapter Five reviews two different theories that purport to explain this phenomena. The first theory (covered in §5.2) predicts that a first-order transition is a generic feature of

itinerant ferromagnets. We consider the shape of the phase diagram it predicts and attempt to apply it to $ZrZn_2$. The second theory (covered in §5.3), on the other hand, predict first-order behaviour only for some systems and we consider some examples of where first-order behaviour might arise. Once again, we attempt to apply this theory to $ZrZn_2$.

The final chapter of content is an investigation into a set of novel phases that, more recently, have been seen to appear at quantum criticality. It turns out that as a quantum critical point is approached, systems prefer to enter some new state (often an exotic superconducting or magnetic phase) rather than continue to a naked quantum critical point. We review a number of experimental realisations of such states in §6.2 and investigate the possibility of Pomeranchuk instabilities as a ferromagnetic quantum critical point is approached (see §6.2).

The final chapter will summarise the work done in, and conclusions drawn from the thesis.

Chapter 2

Prolegomena

2.1 Introduction

This chapter is intended to be an outline of the physics relevant to the rest of the thesis. Landau's Fermi-liquid theory, the theory of metallic systems at low temperature, appeared to be a robust treatment. However, as new systems are searched for and experimentation becomes cleaner and more refined, the theory occasionally (and sometimes unexpectedly) breaks down. As such, it is necessary to introduce a variety of situations where it is either invalid or fails to apply as a concept. Fermi-liquid theory will be discussed in §2.2.

In order to discuss quantum criticality in itinerant ferromagnets, the example of Fermi-liquid breakdown we are mostly interested in in this thesis, we will need to discuss the history of not only the theoretical treatments of classical and quantum criticality, but also of itinerant magnetism. This is done in detail in sections 2.3 and 2.4.

Finally, §2.5 provides many examples of Fermi-liquid breakdown in itinerant magnetic systems. We review a host of various anomalous behaviours in a wide range of systems from the past two decades.

2.2 Fermi-liquid theory

Here we discuss one of the more successful many-body theories: *Fermi-liquid theory* [1, 2, 3]. However, it is useful to begin by considering a model which is the simplest possible for a system of fermionic electrons, namely the *free-electron model*. We investigate some properties of this model and acknowledge its unexpected successes as an explanation of the metallic state before moving on to realise the explanation for this success, leading to Fermi-liquid theory itself.

2.2.1 The free-electron model

The electrons are free in the sense that they refuse to acknowledge each other, that is, the interaction between any two electrons is ignored. We do, however, invoke the *Pauli principle* [4].

Now we switch into momentum space in which the electrons occupy single particle eigenstates labelled by the good quantum number **k**. Due to the Pauli principle, no two electrons can occupy the same state and so any electron is well defined in its own state. Therefore we can label any arbitrary state via $(\mathbf{k}, \sigma)$, where **k** is the momentum vector and σ is the spin of an electron sitting in the state. Electrons carry a spin-$1/2$ and hence any state having a momentum **k** can house two electrons, one having spin-up and one spin-down.

With the Pauli principle in mind, and still working in momentum space, we can imagine beginning to fill up our system with electrons. We place electrons, one at a time, in the unoccupied state having the lowest momentum. When we eventually run out of electrons to put into the system, we find that due to symmetry considerations the system has taken the form of a sphere in momentum space. We have therefore defined a surface which has below it occupied electron states, and above it unoccupied electron states – we call this surface the *Fermi surface*. We say that electrons at the Fermi surface have an energy called the *Fermi energy*, which we denote by ϵ_F and whose numerical value is given by

$$\epsilon_F = \frac{p_F^2}{2m}, \tag{2.1}$$

with p_F being the value of momentum of an electron occupying a state at the Fermi surface, namely the *Fermi momentum*, and m its mass. We can go further to define the *Fermi velocity* v_F via

$$v_F = p_F/m \tag{2.2}$$

and express the *Fermi temperature* T_F in terms of the Fermi energy as

$$\epsilon_F = k_B T_F, \tag{2.3}$$

where k_B is the Boltzmann constant. The physical significance of the Fermi temperature is that it is only for temperatures $T > T_F$ that a gas of free electrons behaves classically. At temperatures $T \ll T_F$, the system is dominated by the Pauli exclusion principle.

2.2.2 The effectiveness of the free-electron model

The free-electron model has been successful in predicting some properties of metallic systems. It predicts a number of experimental observations such as the heat capacity behaving linearly with temperature T [5] and the fact that the Pauli susceptibility is independent of temperature [2]. The fact that the free-electron model predicts such behaviour is somewhat surprising when we consider the fact that the theory is – by construction – one of non-interacting electrons. In reality we know that electrons, being charged and packed closely in solids, **really do** interact with each other very strongly via the Coulomb force and for any typical system of interest, the potential energy between any two electrons might well be comparable to (or larger than) an electron's kinetic energy. In fact, it turns out that a measure of the ratio of average potential energy $\bar{E}_p$ to average kinetic energy $\bar{E}_k$ is given by the mean electron-electron separation r_s:

$$\frac{\bar{E}_p}{\bar{E}_k} \sim \frac{r_s}{a_0}, \tag{2.4}$$

where a_0 is the Bohr radius. In general, r_s/a_0 is higher than one, meaning average potential energy is larger than average kinetic energy. An explanation to this almost paradoxical success of the free electron model is supplied by considerations of the work on ^{3}He by Landau in his papers on Fermi-liquid theory [6, 7, 8]. On top of this explanation, investigations motivated by Landau's work pushed metallic theory further – his Fermi-liquid theory would provide excellent theoretical results for many systems, including some where electrons are extremely strongly correlated.

2.2.3 The notion of the quasiparticle

The success of the free-electron model can be explained via an argument based on the idea of *adiabatic continuity* [9]. Let us first start with the now familiar non-interacting electron gas in its ground state, constructed as explained above. We imagine we have a knob which we can use to tune the interactions between the electrons from off (which is obviously the point we begin at) to an interaction strength which represents the realistic situation for electrons. Let us

start to adiabatically turn the interactions on and allow the system to slowly evolve. The ground state of an interacting electron gas may be constructed by the adiabatic 'turning-on' of interactions between the free electrons of the non-interacting system's ground state. Furthermore, any arbitrary excited state of the interacting system could be constructed by exciting a number of electrons of the non-interacting gas into a state above the Fermi surface, leaving an equal number of holes behind, and then allowing the system to evolve adiabatically by turning our knob to a directly corresponding excited state of the interacting system. The crux of all this is that the free electron model's success is explained by the fact that, although wavefunctions of the interacting system are markedly different from those of the free-electron system from which they are adiabatically derived, the wavefunctions' labels (that is, momentum and spin) remain robust during the adiabatic transition. The one-to-one correspondence of the non-interacting system's electron configuration (whether excited or not) to that of the interacting system provides the realistic theoretical predictions which previously were puzzling.

The new interacting system is made up of fermionic particles (therefore there exists a Fermi surface) which we shall call *quasiparticles*. These particles are not exact eigenstates of the system, hence they have a finite lifetime. Where in the non-interacting case we talked of free electrons being labeled via their momenta $\mathbf{k}$ and spin σ, we now talk of fermionic quasiparticles which share these labels.

2.2.4 The validity of Fermi-liquid theory

It is crucial to remember that the quasiparticle eigenstates we have talked about are not exact. They, given enough time, will eventually evolve into very complex, yet exact eigenstates. As discussed above, we have to make sure that interactions are turned on before this evolution starts to occur. We are keen to search for somewhere that the theory can be considered to be robust. A straightforward investigation employing Fermi's golden rule [10] can be employed to compute the lifetime τ of one of the non-exact quasiparticle eigenstates. Let us take a quasiparticle at an energy ϵ above the quasiparticle Fermi surface at zero temperature. We allow this to decay into a state with a lower energy $\epsilon-\omega$. We have to have the creation of a particle-hole pair to conserve

energy. At low temperatures, Fermi's golden rule gives the inverse of the quasiparticle's lifetime to be proportional to the square of the energy:

$$\frac{1}{\tau} \sim \epsilon^2. \tag{2.5}$$

Thus the quasiparticle states are well defined for excitation energies which are small compared to the Fermi energy. If ϵ is small, then the lifetime will be suitably large enough for the time taken for the interactions to be turned up to a realistic strength. Conversely, the theory will break down for quasiparticle energies far from the Fermi energy; a small lifetime means they decay into exact eigenstates before interactions are fully turned on. It is also true that at finite temperature the scattering rate is proportional to T^2 [11], therefore we must make sure we consider temperatures which are small in comparison to the Fermi temperature. This is not too unreasonable as most metals have a large Fermi temperature (of the order of 10^4K) compared to the temperatures at which experiments might be carried out. Hence, at low temperatures quasiparticles are well defined and Landau's Fermi-liquid theory is applicable.

Considerations of the appearance of quasiparticles has led us away from the actual individual electrons which make up any system of interest. Recall, these quasiparticles have been derived adiabatically from the original electrons and thus their wavefunctions must contain something of the wavefunctions of the electrons themselves:

$$|\psi_{\text{quasiparticle}}\rangle \sim \sqrt{z}\,|\psi_{\text{electron}}\rangle + \cdots, \tag{2.6}$$

where the ellipsis denotes higher order particle-hole excitations.

The entity z is called the *electron residue* and this acts as an order parameter for the Fermi-liquid: it is important this is non-zero as if it was zero it would imply that the desired adiabatic connection between the original electrons and derived quasiparticles no longer exists.

2.2.5 The meaning of "adiabatic"

When using the word 'adiabatic', we should be careful not to casually assume that it is fine if transitions from the non-interacting to interacting system are simply over any arbitrarily large timescale.

There is not only a need for a lower limit on the rate of interaction changes, but also a requirement that there exists an upper limit giving a range of rates within which we are safe to assume the theory holds [9]. This is brought about by the fact that the quasiparticles have a finite lifetime.

It is important to have the interactions turned on slowly enough so that our energy resolution is much smaller than the energy of the system, which is around the Fermi energy. This is the obvious condition and brings about the use of the word 'adiabatic'. On top of this we must make sure that the rate at which the interactions are turned on is not so slow that a quasiparticle has time to evolve itself into an exact, more sophisticated eigenstate. It can be shown that a rate to satisfy both upper and lower limits is quite accessible and is given by the condition

$$\epsilon^{-1} \ll t \ll \epsilon^{-2}. \tag{2.7}$$

2.2.6 Experimental observables

After explaining why the free-electron model works, Fermi-liquid theory can be used to modify the free electron model's results. Retaining labels whilst moving from free electrons to interacting quasiparticles means that the entropy also remains unchanged. However, it is true that the energy **does** change. A quasiparticle's energy will firstly change because in the new interacting system the energy spectrum differs from the non-interacting case. This, though, can be absorbed by assigning the quasiparticle with an effective mass m^* which can be found by, say, measuring the heat capacity at extremely low temperatures. The second contribution to the energy is that of the actual interaction between a system's quasiparticles, obviously this arises naturally as we turn interactions on and is recorded in Landau's *interaction function*, which describes any system within the theory by a set of various spin symmetric and spin anti-symmetric

F-coefficients. The mathematical details can be found, for example, in references [1, 2].

These two contributions to the energy can be captured in Landau's quasiparticle energy functional

$$\epsilon_{\mathbf{k}\sigma} = \frac{\hbar^2 k_f}{m^*}\left(k - k_f\right) + \frac{1}{V}\sum_{\mathbf{k}'\sigma'} f\left(\mathbf{k}\sigma;\mathbf{k}'\sigma'\right)\delta n_{\mathbf{k}'\sigma'}, \tag{2.8}$$

where $\delta n_{\mathbf{k'},\sigma'}$ is the distribution of the quasiparticle distribution function from equilibrium.

From this point onwards, one can proceed to calculate experimental properties. One can establish, for example, that the **functional** form of the heat capacity remains unchanged with the introduction of an effective mass $m \to m^*$ being the only difference from the ideal case:

$$C_v = \frac{\pi^2}{3} g\left(\epsilon_F\right) k_B^2 T, \tag{2.9}$$

where $g\left(\epsilon_F\right)$ is the density of states

$$g\left(\epsilon_F\right) = \frac{m^* k_F}{\pi^2 \hbar^2}. \tag{2.10}$$

Compare this with the free-electron model [2, 5].

The magnetic susceptibility is – too – modified. However, this time by not only making the change $m \to m^*$ in the result for the non-interacting case χ_0, but adding in an effective "screening" which means that a further factor of $1/\left(1 + F_0^a\right)$ is included:

$$\chi = \frac{m^*}{m_0}\frac{\chi_0}{1 + F_0^a}, \tag{2.11}$$

where F_0^a is a Landau parameter taken from the interaction function.

We saw above that the quasiparticle relaxation rate has the temperature dependence $\tau^{-1} \sim T^2$. This means, therefore, that the resistivity must be given by

$$\rho\left(T\right) = AT^2. \tag{2.12}$$

Here A is a constant and depends on the underlying band structure.

From a practical point of view, we now have a method of identifying a Fermi-liquid: we experiment on our system and check the results against the low temperature dependences – for example, $\rho \sim T^2$, $C \sim T$ and a temperature independent magnetic susceptibility – discussed above. However, later in this chapter we will see situations where either the concept of a Fermi-liquid fails to apply from the outset or the expected behaviour does not become apparent.

2.2.7 Examples of Fermi-liquids in nature

When formulating this theory, Landau had in mind ^{3}He: certainly a quite elemental example of a liquid of fermions. Much effort has been invested into the study of such a system and the experimental findings appear to agree extremely well with theory [12, 3]. At low temperatures, ^{3}He is the best example of a Fermi-liquid nature can offer.

As for metallic systems, many materials (including some very strongly correlated ones) are well described by Fermi-liquid theory as $T \to 0$. A striking example of its success is in the metal UPt_3, a material in which it is known that interactions are extremely strong and specific heat measurements have shown the effective mass of the system's quasiparticles to be two orders of magnitude greater than those of a the free electron model [13]. de Haas van Alphen measurements [14] have been employed to map out the Fermi surface of UPt_3's quasiparticles and accounts for the enlarged specific heat: indicating that Fermi-liquid theory can, too, apply in extreme situations.

2.2.8 Non-Fermi-liquid situations

We have discussed Fermi-liquid theory at some length, but now we wish to consider some important situations where Fermi-liquid theory is not appropriate [10]. This might be because the experimental observations differ from what is expected, or could be because the assumptions made in the conception of a Fermi-liquid simply fail to apply. But, whatever the case, there do exist metallic systems where the fermionic quasiparticle of Fermi-liquid theory apparently fails to be a valid description of their low energy excitations. Often in such cases some new quasiparticle must be considered.

In practice it is observed that many metals undergo a continuous (characterised by specific heat measurements displaying a discontinuity) transition into a superconducting state, in which the properties of the system are markedly different from the normal (metallic) state. The most dramatic property is the disappearance of electrical resistance below some transition temperature T_c.

Other properties of note are the superconducting state's expulsion of magnetic fields (the Meissner-Oschenfeld effect) and the isotope effect: the observation that the transition temperature of a given metal depends on the various masses of its isotopes M via the relation $T_c \propto 1/\sqrt{M}$. It was the isotope effect that pointed to the potential importance of the electron-phonon interaction to the superconducting state.[1]

A microscopic treatment of superconductivity was offered by BCS theory [15], in which it was displayed that the electron-phonon interaction leads to an effective **attractive** interaction between a pair of electrons living on the Fermi surface. Together these two electrons form a bound state, referred to as a *Cooper pair*, and, furthermore, it is true that their formation is independent of how weak the attractive interaction is. Therefore, the Fermi-liquid state becomes unstable in metallic systems which superconduct.

A more puzzling problem arose, beginning in the late 1980's, when a set of high temperature (high-T_c) superconductors were found to enter a zero resistance state at temperatures much larger then those seen in materials known to conventionally superconduct. The initial breakthrough [16] came with the material LaBaCuO boasting a transition temperature of 30K, adding 7K onto the previous conventional record (and pushing the upper limit predicted in BCS theory). Frantic activity yielded many new examples of similar materials and the record superconducting temperature continued to rise.

Until the recent finding of superconductivity in iron-based superconductors, the high-T_c compounds, despite often being somewhat complicated materials, were linked by the fact that they all contained a structure consisting of layers of CuO_2 (copper-oxide) planes separated by other inter-plane elements. It is due to these planes that such compounds are often referred to

[1] The stronger this interaction (which scatters electrons strongly at higher temperatures, thus constituting a "bad" metal) the earlier the system will superconduct as temperature is lowered.

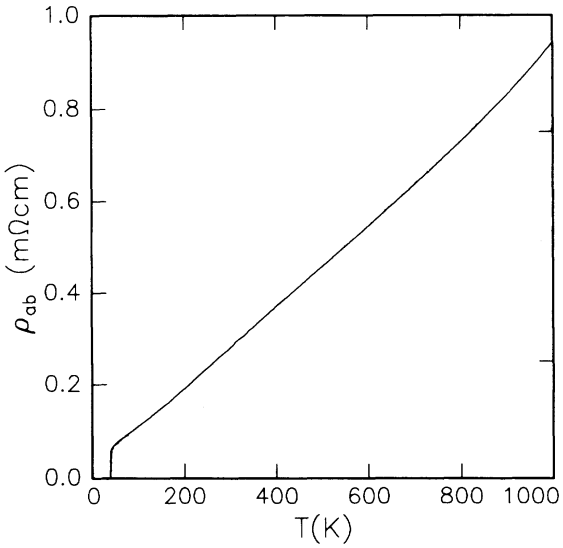

Figure 2.1: From [17]. Measurement of the temperature dependence of the resistivity for (the optimally doped) $La_{0.85}Sr_{0.15}CuO_4$. Notice the anomalous linear dependence which is not to be expected from a Fermi-liquid argument.

as *cuprates*. Under normal conditions the parent compound of these materials are insulators and show antiferromagnetic order, with the moment situated on the copper sites, and it is only when they are doped that they display their most interesting properties. Doping takes place by removing an inter-plane element and replacing with another, this extracts some electrons from the copper-oxide layers allowing metallic conduction to take place within the two-dimensional plane (the materials are so anisotropic that resistance when measured perpendicular to the plane is often two to three orders of magnitude greater than that found within the plane). Lowering the temperature causes superconductivity to arise.

Despite the interest generated by the superconductivity in these materials, and the intensity of the search for an explanation of these properties, it is in the metallic state and its non-Fermi-liquid behaviour that we have an interest here. An intriguing anomaly is the measured temperature dependences of the resistivity. Measurements of the usual electron-electron scattering rate show a linear dependence on temperature $\rho \sim T$, a relation usually associated with electron-phonon scattering. However, measurements of the Hall effect in the same systems (measurements which are expected to display the same dependences) give the usual quadratic temperature dependence $\rho \sim T^2$. Figures 2.1 and 2.2 show exactly these dependences in data

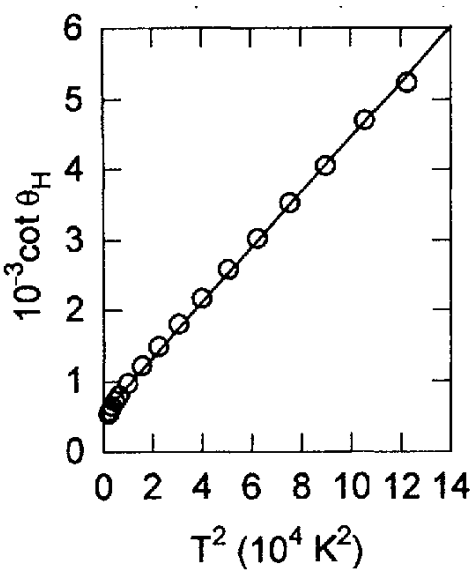

Figure 2.2: From [18]. Measurements of the inverse Hall angle in $La_{0.85}Sr_{0.15}CuO_4$. Here the electron-electron scattering rate depends on the square of the temperature. This, despite being the behaviour expected from a Fermi-liquid, differs from the linear resistivity dependence seen in the measurements of the usual scattering rate seen in figure 2.1.

from the compound $La_{1-x}Sr_xCuO_4$ at the optimal strontium doping of $x = 0.15$. As described above, Fermi-liquid theory predicts a T^2 dependence for metals, whereas measurements on the cuprates cannot even agree on a single electron relaxation time. Therefore, it is clear that the concept of a Fermi-liquid fails to apply here.

In one dimensional systems, it is impossible for there to exist well-defined (albeit not necessarily exact) electron eigenstates [10]. Performing the straightforward Fermi's golden rule analysis (discussed above for Fermi-liquids) in one dimension gives the inverse lifetime to be proportional to the excitation energy,

$$\tau^{-1} \sim \epsilon, \tag{2.13}$$

rather than ϵ^2 seen for higher dimensions. From a physical point-of-view, the complicated quasiparticle states fail to exist for long enough for interactions to be switched on. This means that we cannot create a one-dimensional Fermi-liquid from freely moving electrons via adiabatic continuity, as we have seen above.

However, all this does not mean that a metallic state is forbidden in one-dimension: a different type of adiabatic continuity has been introduced to account for one-dimensional systems

[19]. This gives rise to the *Luttinger liquid*, Fermi-liquid's one-dimensional analogue.

In a one-dimensional system, an excitation of a particle-hole pair, via some momentum transfer, will always involve the same change in energy regardless of which pair we choose to excite. It follows from this that the quasiparticle eigenstates of the Luttinger liquid arise due to *spin-charge separation*: the electrons of one-dimensional systems effectively split up into their magnetic and charge parts, separating into two experimentally observable particles: the *spinon*, which is associated with the magnetism of the electron and carries its spin, and the *holon*, which is associated with and carries the charge of the electron. It is the spinon and holon that act as the quasiparticles in a Luttinger liquid. Due to not being derivable from free electrons, therefore not sharing the same good quantum numbers seen in the case of a Fermi-liquid, metals in one-dimension constitute non-Fermi-liquids.

The final example of a non-Fermi-liquid situation is the case of metallic systems in the vicinity of quantum-critical points. As this thesis primarily concentrates on such situations, later on in this chapter we will investigate this scenario in much more depth than those discussed hitherto.

2.3 Critical phenomena

Despite, as we have seen, being one of the more successful treatments of many-body electron systems, Fermi-liquid theory fails to apply in certain situations. Such situations thus far have included the appearance of low temperature ground-states that fail to be described by the Fermi-liquid quasiparticle and one-dimensions systems in which the arguments of Fermi-liquid theory fail to apply from the outset. In the next few sections it is our aim to introduce the physics of systems that are subject to conditions such that they are near to some quantum-critical point in their phase diagram. No treatment of this would, however, be complete without a preliminary discussion of classical critical phenomena. This is our starting point.

2.3.1 Phase transitions

It is a common observation that systems change their phase when subjected to certain changes in their environment. Usually this is due to a change in temperature. Such things are often seen in everyday life, most notably the various changes that occur in water and, indeed, its phase diagram (shown in figure 2.3) is the archetypal system in this field. Let us briefly discuss some of the physics on show.

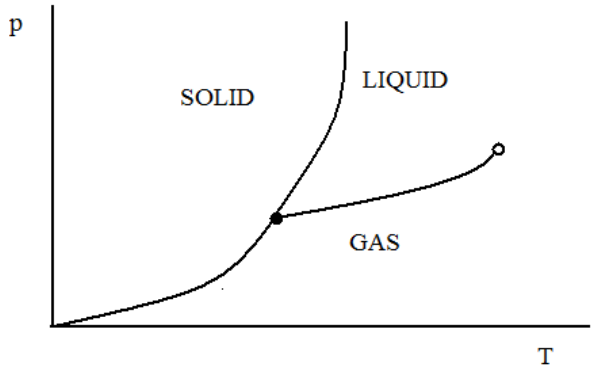

Figure 2.3: The temperature-pressure phase diagram of water. Regions of solid, liquid and gaseous behaviour are separated by lines of first-order transitions (solid lines). Special points of note are the triple point (the solid dot): the point at which all three phases can coexist, and the critical point (the open dot): the endpoint of first-order transitions beyond which one can pass between the liquid and gas phases continuously.

The thermally driven transitions of water are, when subjected to ambient conditions, seen to be first-order. First-order phase transitions, by their very nature, involve the release of some amount of latent heat at the transition temperature. There exist boundaries between the two coexisting phases near to any transition point. In fact, in the case of water it is even possible to have three coexisting phases at a unique value of temperature and and a unique value of pressure, the so-called *triple point*. The triple point is indicated in figure 2.3 by the filled dot.

Further properties are *metastability*, the preference of the "wrong" phase due to the fact that $k_B T$ is too small to overcome the various energy gaps which are associated with making the transition, and *hysteresis*: estimates of the transition temperature appear to vary depending on the direction from which one approaches the transition – a direct consequence of metastability.

Table 2.1: Various examples of symmetries broken in phase transitions and of associated order parameters.

Symmetry	System	Order parameter	Example
Ising or Z_2	liquid-gas	$\langle \rho_l - \rho_g \rangle$	H_2O
	uniaxial ferromagnet	$\langle m_z \rangle$	
	order-disorder	$\langle n_a - n_b \rangle$	β-brass
O_2	superfluid	$\langle \psi \rangle$	^{4}He
O_3	Heisenberg ferromagnet	$\langle \mathbf{m} \rangle$	Fe

Moving along the coexistence line of water and gas, one reaches a very important point of the phase diagram. Andrews [20] was the first to identify (albeit in carbon dioxide) the *critical point* (indicated, for water, by the open circle in figure 2.3): an apparent end to first-order behaviour and the point after which the properties of liquid and gas are indistinguishable; one can move from liquid to gas (and vice versa) continuously. A theoretical treatment of this was to be supplied by van der Waals [21], whose work introduced the first theory involving a mean-field.

A second important critical point is that found by Curie [22]: the continuous transition in iron at a temperature around 1000K, below which iron is a ferromagnet. This point is called the *Curie point*. Later, another mean-field theory of Weiss described this transition [23]. Continuous phase transitions such as those just discussed are very important and give rise to the study of critical phenomena. Let us review some of the more interesting concepts.

2.3.2 Continuous transitions and criticality

We have considered two examples of continuous (or second-order) phase transitions. In order to begin a more complete discussion, let us imagine an entity ϕ which we call the *order parameter*. First introduced by Landau [24], the order parameter, by definition, has the property that it is equal to zero in some disordered phase of the system and not equal to zero in some ordered phase. For the time being we assume that the order parameter is a scalar (that is, its variation in time and space is suppressed) for any given system. Examples of order parameters are given in table 2.1.

At this stage much progress can be made in extracting information about critical phenomena. Landau realised that one can straightforwardly write down the thermodynamic potential $f(\phi)$, some function of the order parameter which obeys all the various symmetries of the disordered phase. Technically this function should be quite a complicated one, but in the vicinity of criticality it is safe to assume that $f(\phi)$ can be written down as some power series in ϕ. Let us take, as an example, the Ising case with Z_2 symmetry. Here $f(\phi)$ must remain invariant with the change $\phi \to -\phi$. Therefore $f(\phi)$ may only contain terms of even powers in ϕ:

$$f(\phi) = \frac{1}{2}t\phi^2 + \frac{1}{4}u\phi^4 + \frac{1}{6}v\phi^6 + \cdots \tag{2.14}$$

So long as ϕ is small (is near criticality), one can quite quickly terminate the power series. In equilibrium the thermodynamic potential is a global minimum

$$f'(\phi) = 0, \tag{2.15}$$

which implies that the term of highest power must have a positive coefficient to make certain of this stability, in this case $v > 0$. The value of the order parameter at this minimum is that taken by the system. In order for the system to become ordered, the minimum must occur for some non-zero value of the order parameter, that is the free energy curve must become negative. One way that this can happen is for the case where $u > 0$ and t changes sign to become negative: this describes a continuous transition. If $t > 0$ and $u < 0$, then there is a first-order transition. Figure 2.4 displays this phase diagram.

We have established that the order parameter's average is zero in the disordered phase, however its fluctuations are not. As any critical point is approached, spatial fluctuations of the associated order parameter grow larger until, at the critical point itself, they actually diverge. In the vicinity of criticality, the typical length scale of fluctuations, a quantity known as the *correlation length* ξ diverges with an exponent ν:

$$\xi \sim t^{-\nu}, \tag{2.16}$$

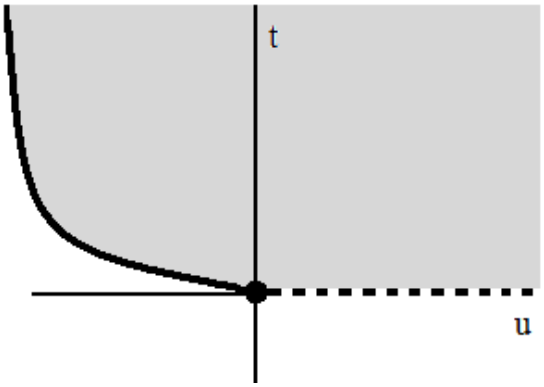

Figure 2.4: The $t - u$ phase diagram of the Landau theory given by equation 2.14. The shaded region is the disordered phase and the unshaded region the ordered phase. Variation of the parameters t and u might give rise to either a continuous phase transition (dotted line) or a first-order transition (bold line). A tricrital point (dot) separates the two behaviours.

where t is the "distance" from the critical point itself. For example, $t = (T - T_c)/T_c$ if criticality is at some temperature $T = T_c$. The time scale over which fluctuations decay also diverges as the critical point is approached, this time with an exponent z given by

$$\tau \sim \xi^z = t^{-\nu z}. \tag{2.17}$$

This is known as *critical slowing down*.

A more stringent treatment of the criticality of classical system than that of Landau above might proceed as follows: firstly, one writes down the Hamiltonian of the system in terms of a kinetic term $H_{\text{kinetic}}(p)$, dependent only on momenta, and a potential term $H_{\text{potential}}(q)$, dependent only on position:

$$H(p,q) = H_{\text{kinetic}}(p) + H_{\text{potential}}(q), \tag{2.18}$$

and continues to write down the partition function Z, which decouples the statics and dynamics as follows

$$Z = \int dp e^{-H_{\text{kinetic}}/k_B T} \int dq e^{-H_{\text{potential}}/k_B T} = Z_{\text{kinetic}} Z_{\text{potential}}. \tag{2.19}$$

Integrating out all degrees of freedom other than those associated with the order parameter gives

Table 2.2: A list of critical exponents of note for the magnetic case.

Quantity	Exponent	Relation
specific heat	α	$\mathrm{c} \sim t^{-\alpha}$
order parameter	β	$\phi \sim (-t)^{\beta}$
susceptibility	γ	$\chi \sim t^{-\gamma}$
correlation length	ν	$\xi \sim t^{-\nu}$
dynamic exponent	z	$\tau \sim \xi^{z}$

rise to some Landau-Ginzburg-Wilson functional $\Phi(M)$ whose form obeys the various order parameter symmetry considerations and looks like

$$\Phi(M) = \int d^d r M(\mathbf{r}) \left(t - \nabla^2\right) M(\mathbf{r}) + u \int d^d r M^4(\mathbf{r}) - B \int d^d r M(\mathbf{r}). \tag{2.20}$$

Through the partition function

$$Z = \int D[M] e^{-\Phi(M)}, \tag{2.21}$$

and then the free energy

$$F = -k_B T \ln Z, \tag{2.22}$$

one can compute many statistical quantities of interest. In doing so, their dependences on the parameter t give rise to more critical exponents. A list of some of the more usual exponents is given by table 2.2. Furthermore, a scaling analysis actually links these exponents by a set of *scaling relations*.

We are now in a position to discuss one of the main results of this analysis. The critical behaviour of any system can be defined by its set of critical exponents. However, many widely different critical systems are sometimes described by the same set, often due to sharing a dimension and the basic symmetries of the systems being the same. We say that when two differing systems share the same critical exponents, they fall into the same *universality class*. This phenomena, known as *universality*, arises because at criticality the correlation length's divergence averages over microscopic details of the Hamiltonian. A more rigorous approach is that of the renormalization group [24, 25] which gives a firm grounding to the study of critical phenom-

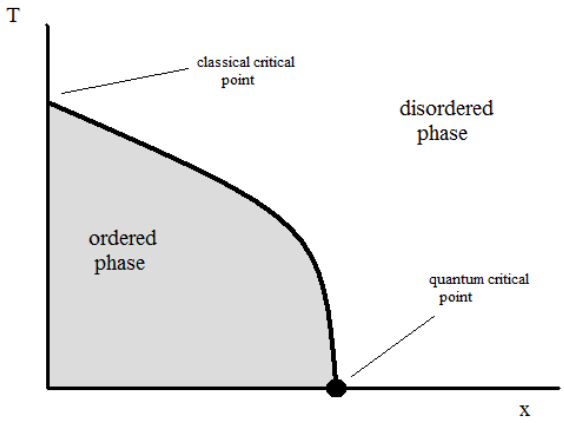

Figure 2.5: The most basic continuous quantum critical point. The transition temperature from some disordered state to an ordered state can be lessened with the application of some other parameter x. At some critical value of x, the transition temperature has been forced to zero and the transition is between two quantum mechanical ground states.

ena and derives the exponents and relations discussed from a more fundamental and physical starting point.

To complete this overview of classical criticality, let us note the importance of fluctuations. It is true that fluctuations become more and more important in lower dimensions and, below a certain dimension, eventually they are so strong that a mean-field treatment is inappropriate. It turns out that in cases discussed here the *upper critical dimension* is four. For $d < 4$ fluctuations must be taken into account. There also exists a *lower critical dimension*, below which no order is actually possible.

2.3.3 Quantum phase transitions

Let us now reconsider the above treatment, but for a different kind of transition. Instead of causing a phase transition in the classical way, *i.e.*, via thermal fluctuations, imagine varying some other parameter of a system's Hamiltonian x to cause a phase transition at zero temperature – a *quantum phase transition* [26]. Such parameters might be pressure, magnetic field or chemical doping. We refer to the point at which this transition occurs as a *quantum critical point*. See figure 2.5 for the simplest type of phase diagram to have both a classical and quantum critical point.

Table 2.3: The value of the dynamic exponent z for various systems

z	System
1	free magnons
2	itinerant antiferromagnetism
3	itinerant ferromagnetism (clean case)
4	itinerant ferromagnetism (dirty case)

As the transition occurs at zero temperature, it is between two quantum mechanical ground states of the system and in such cases "melting" occurs because of fluctuations due to the Heisenberg uncertainty principle rather than thermal fluctuations. It must be true that quantum mechanics is important at zero temperature as any characteristic energy scale of the system $\hbar\omega$ is most definitely bigger than $k_B T$. At finite temperatures, sufficiently close to the transition, thermal effects always play a more important rôle than quantum ones – all finite temperature transitions are classical.

Quantum effects become important when $\hbar\omega$ is larger than temperature. It is known that time scales diverge at criticality and, in turn, this means that energy scales go to zero as

$$\hbar\omega \sim t^{\nu z}, \tag{2.23}$$

where now is varied by variation of x, for example, $t = (x - x_c)_c$ where criticality is found at $x = x_c$.

The *dynamic exponent* z is a system dependent quantity [27]. For a list of various values of z in itinerant systems see table 2.3.

This gives a condition for quantum mechanics to be important, namely when

$$t^{\nu z} > k_B T. \tag{2.24}$$

In quantum mechanical systems, equation 2.18 has to be modified – position and momentum

now become non-commuting operators $\hat{q}$ and $\hat{p}$:

$$\hat{H}\left(\hat{p},\hat{q}\right)=\hat{H}_{\text{kinetic}}\left(\hat{p}\right)+\hat{H}_{\text{potential}}\left(\hat{q}\right), \tag{2.25}$$

and therefore it is no longer possible to write down equation 2.19. The statics and dynamics of a quantum phase transition of some system are linked and this can be attributed to the non-commutability of the terms in its Hamiltonian. We can no longer, therefore, solve them independently and we have to treat them equally in what is to follow.

The formulation of a Landau-Ginzburg-Landau theory must now include imaginary time τ. Generalising equation 2.20 would give rise to a thermodynamic potential which, *e.g.*, in the case of an insulating magnet where $z=1$, look something like

$$\begin{aligned}\Phi\left(M\right) &= \int_{0}^{1/k_{B}T}d\tau\int d^{d}rM\left(\mathbf{r},\tau\right)\left(t-\nabla^{2}-\frac{\partial^{2}}{\partial\tau^{2}}\right)M\left(\mathbf{r},\tau\right)\\ &+ u\int_{0}^{1/k_{B}T}d\tau\int d^{d}rM^{4}\left(\mathbf{r},\tau\right)-B\int_{0}^{1/k_{B}T}d\tau\int d^{d}rM\left(\mathbf{r},\tau\right),\end{aligned} \tag{2.26}$$

and the re-calculation of critical exponents would, in general, give different results from the classical case. This would, it follows, give rise to a new universality class.

A result pertinent to our previous discussions is the fact that the mixing of statics and dynamics gives rise to an apparent increased dimension $d\rightarrow d+z$. This would imply that the majority of quantum critical systems would lie above the upper critical dimension – mean-field theory would suffice to explain the critical behaviour.

Sometimes quantum critical points are first-order in nature, we will see examples later in the thesis in various itinerant ferromagnetic systems where the usual second-order phase transition becomes first-order with the application of some other parameter x. The line of continuous transitions meets the line of first-order transitions at some critical end-point. The application of a further tuning parameter, x' say, can, in some cases, suppress the first-order nature and drive the critical end-point to zero temperature. This creates a quantum-critical end-point and such points are of high importance in this thesis. Figure 2.6 shows the phase diagram that is

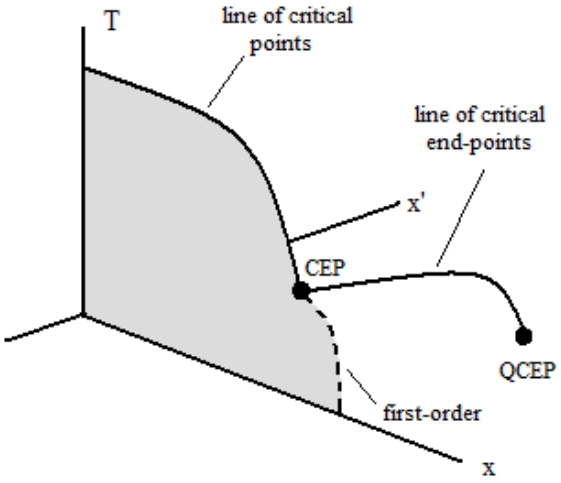

Figure 2.6: Diagram showing the realisation of a quantum-critical end-point. Imagine a system with a classical continuous transition as temperature is lowered. The application of some further parameter x lowers the transition temperature towards a quantum critical point in the manner discussed above. However, this line of critical points ends at a critical end-point (CEP) and the transition is afterwards first-order. Application of a further parameter x' could push this critical end-point to zero temperature, in the process suppressing the first-order transition, thus reaching a quantum-critical end-point (QCEP).

described in this paragraph.

This thesis is primarily concerned with quantum criticality in itinerant systems. We will analyse such physics in great depth in the next chapter when we consider the leading theory, namely Hertz-Millis theory.

2.4 Introduction to itinerant ferromagnetism

Here we wish to briefly discuss the historical theoretical treatment of itinerant ferromagnetic materials. Such treatments are from a microscopic viewpoint and therefore differ from the phenomenological Fermi-liquid theory of Landau on which we have concentrated previously.

2.4.1 Classical magnetism

Magnetic materials have been used for a variety of scientific or engineering pursuits since antiquity and magnetism has been a fascinating subject for many millenia, research into the subject and its application has been intense throughout the centuries. Despite this, a theoretical expla-

nation of the properties of magnets has often been difficult to provide and has regularly been the subject of much controversy. Arguably the viewpoint adopted today can trace its roots back to the work of Langevin [28, 29], whose interpretation of magnets as consisting of a set of free individual moments of equal size successfully explained the well-known Curie law observed in experiments. The inclusion of a moment's interaction with other moments was via a mean-field approach and was due to work by Weiss [23]. The Langevin-Weiss theory gives the temperature dependence of the magnetic moment below the transition temperature T_c to be

$$M \sim \sqrt{T_c - T} \tag{2.27}$$

and the magnetic susceptibility above the magnetic transition temperature to be

$$\chi \sim \frac{1}{T - T_c}. \tag{2.28}$$

Despite the fact that the functional form of equations 2.27 and 2.28 agree with most investigations into ferromagnetic materials, the results fail to quantitatively agree with experiment: extremely modest temperatures would be enough to destroy any ordered state. It was only with the advent of quantum mechanical theories that this issue was addressed.

2.4.2 Localised quantum magnetism

If we assume that the Russell-Sanders scheme is valid[2], then quantum mechanics gives the total angular momentum (a good quantum number) of an atom to be written as $\mathbf{J} = \mathbf{L} + \mathbf{S}$, where $\mathbf{L}$ and $\mathbf{S}$ are, respectively, the total orbital angular momentum and the total spin of electrons residing in the atom. These, too, are both good quantum numbers meaning the eigenstates of the atom are given by $\mathbf{J}$, $\mathbf{L}$ and $\mathbf{S}$. The energies of these eigenstates are described by Hund's rules and any degeneracies existing between the lowest of these energy states is lifted by spin-orbit coupling $\mathbf{L} \cdot \mathbf{S}$. If the lowest energy state is separated from the rest of the states by an amount of energy greater than $k_B T$, then the atom has fixed angular momentum and a fixed

[2]Which is usually the case for atoms that are not too heavy.

magnetic moment. This is the origin of localised magnetism.

Statistical treatments are corrected by this quantum mechanical viewpoint [5, 30] and the classical results are re-obtained in the limit that the magnitude of the total angular momentum diverges, $J \to \infty$. The archetypal model for studying localised magnetism, for cases where the moment is seen to be fixed, is the Heisenberg model [31], whose Hamiltonian depends on the spin operators of a system's individual electrons (which are located on sites labelled here by i or j) and some coupling strength J_{ij} between them:

$$H = -\sum_{ij} J_{ij} S_i \cdot S_j. \tag{2.29}$$

Equation 2.29 is notoriously difficult to solve for many situations. However it can be used to derive many important types of magnetism and is a highly studied model in the field of critical phenomena.

2.4.3 The tight-binding model

If the magnetism discussed above consisted of localised moments in real space, itinerant magnetism, a subject of much interest to us in the remainder of this thesis, consists of moments localised in reciprocal space. Such moments are those associated with those electrons that are free to delocalise from their parent atoms.

In a realistic metal, where neighbouring atoms are separated by a few Ångströms, the electronic orbitals in which the atom's electrons reside often remain very localised in their extent. However, occasionally one of these tightly bound orbitals, which houses a valence electron, might overlap sufficiently with suchlike orbitals of a neighbour. The electrons are able to delocalise. The *tight-binding model* (for a discussion of the model, whose origins derive from work by Slater on nickel [32], see [5, 30]) provides a method of describing these delocalised electrons whilst retaining the atomic sites which are not present in the free-electron model[3].

[3]The *nearly-free electron model* treats electrons moving in some regular potential which is assumed to arise from the atomic sites. This model is the simplest to predict band-gaps, explaining why some metals become insulators.

The tight-binding model (in a similar vein to the Hubbard model which we will discuss next) somewhat reconciles the Bloch picture of electrons existing as plane-waves extending throughout a metal and that of localisation of electrons on atomic sites. It is one possible starting point to the derivation of magnetism in metals.

The tight-binding Hamiltonian contains two terms, the first is the energy of an electron which sits on some atomic orbital (such orbitals, it can be shown, can be suitably described by Wannier states) and the second is some "hopping" term which allows the electrons to move from site to site.

$$H_{\text{tight-binding}} = \sum_{\sigma} \sum_{i} \sum_{\mu} \epsilon_{\mu} \hat{a}^{+}_{i\sigma} \hat{a}_{i\sigma} + \sum_{\sigma} \sum_{ij} \sum_{mn} t^{mn}_{ij} \hat{a}^{+}_{im\sigma} \hat{a}_{jn\sigma}. \tag{2.30}$$

Here ϵ_{μ} is the energy of an electron sitting in a band, labelled by μ, of an atom and t^{mn}_{ij} is the "hopping integral" between the m$^{\text{th}}$ Wannier state on an atom labelled by i and the n$^{\text{th}}$ on site j. This term represents the gain in kinetic energy of a delocalised electron. $\hat{a}^{+}$ and $\hat{a}$ are, respectively, the usual creation and annihilation operators.

The tight-binding Hamiltonian can be applied to systems of varying complexity and used to (for example, via diagonalisation on a Bravais lattice) extract information on the band-structure of metals. A striking realisation of this model is that **any** metal consisting of a band only partially filled by electrons should be a metal. This is sometimes seen to not always be the case in reality: some materials, which are expected to be metallic, are seen in practise to be insulators. The reason for this is that, thus far, we have overlooked the Coulomb interaction between electrons.

We now move on to add an extra term to the Hamiltonian of equation 2.30 which incorporates the Coulomb interaction's repulsion between electrons. We also simplify the other terms in the tight-binding Hamiltonian somewhat, as we consider a very important model of many-body physics, the Hubbard model.

2.4.4 The Hubbard model

As we have seen, the tight-binding model fails to explain certain systems which happen to be insulators rather than the expected metals. Let us consider a model which includes two terms. Firstly, a tight-binding-like hopping term which transports electrons from one atomic site (which we assume to have a single band only) to a neighbour:

$$\hat{T}_{\text{Hubbard}} = -\sum_{\langle ij \rangle} \sum_{\sigma} t_{ij} \hat{a}^{+}_{i\sigma} \hat{a}_{i\sigma}, \tag{2.31}$$

here the angled brackets indicate a summation only over nearest neighbours.

The second term, that introduced by Hubbard, incorporates (rather crudely), the Coulomb repulsion via the term

$$\hat{V}_{\text{Hubbard}} = U \sum_{i} \hat{a}^{+}_{i\uparrow} \hat{a}_{i\uparrow} \hat{a}^{+}_{i\downarrow} \hat{a}_{i\downarrow}, \tag{2.32}$$

which pays an energy cost U if and when two electrons (necessarily of opposing spin due to the Pauli principle) attempt to occupy the same atomic site which is labelled by i.

Together equations 2.31 and 2.32 constitute the Hubbard model, described by the Hamiltonian

$$\begin{aligned} \hat{H}_{\text{Hubbard}} &= \hat{T}_{\text{Hubbard}} + \hat{V}_{\text{Hubbard}} \\ &= -\sum_{\langle ij \rangle} \sum_{\sigma} t_{ij} \hat{a}^{+}_{i\sigma} \hat{a}_{i\sigma} + U \sum_{i} \hat{a}^{+}_{i\uparrow} \hat{a}_{i\uparrow} \hat{a}^{+}_{i\downarrow} \hat{a}_{i\downarrow}. \end{aligned} \tag{2.33}$$

Much research has been conducted into attempting to solve equation 2.33 (recently highly motivated by the high temperature superconductors showing behaviour similar to certain analysis of the Hubbard model), with only modest success and, indeed, a complete understanding of the physics of the Hubbard model remains one of the field's important goals. It was argued by Mott [33] that at half filling (*i.e.*, there is on average one electron per site) there exists a transition from a metal to an insulator (coined the *Mott transition*) at some critical value of the ratio t/U. Progress has been made in one dimension where an analytical solution to the Hubbard model at half filling can be found using the famous Bethe ansatz [34]. Such systems are

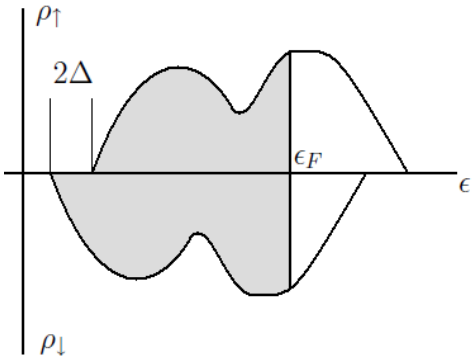

Figure 2.7: The density of states as a function of energy for up- and down-electrons in Stoner theory. Upon an itinerant system becoming magnetised, the bands of up- (occupying the shaded region above the horizontal axis) and down-electrons (below the axis) become split and a gap of 2Δ is opened. ϵ_F represents the Fermi energy.

insulators for any $U > 0$ and metallic when $U = 0$.

2.4.5 Stoner theory

The Stoner model of itinerant ferromagnetism can be arrived at by applying the well known Hartree-Fock approximation to the Hubbard model [35]. The Stoner model will be derived and analysed later in this thesis, here we discuss some general results.

The Stoner theory relies on a number of assumptions. Firstly, one assumes that the electrons in the model are those of a d-band and these must obviously obey Fermi statistics. Analogous to the treatment of localised moments by Weiss, Stoner assumed that these electrons are affected by some molecular field which incorporates the effects of exchange.

When such a system becomes magnetised by an amount M, the energy bands for up-spins and down-spins are split, see figure 2.7. This forces the total kinetic energy E_k of the system to go up and when the band splitting is small

$$E_k = \frac{1}{\rho\left(\epsilon_F\right)} M^2 + \frac{F_1}{4\rho\left(\epsilon_F\right)} M^4 + \cdots , \tag{2.34}$$

where $\rho\left(\epsilon_F\right)$ is the density of states of the unmagnetised system at the Fermi energy. Here F_1 is some function of $\rho\left(\epsilon_F\right)$ and its derivatives. Including the term which takes into account the

exchange energy I gives the total energy

$$E = \frac{1}{\rho(\epsilon_F)}\left(1 - I\rho(\epsilon_F)\right)M^2 + \frac{F_1}{4\rho(\epsilon_F)}M^4 + \cdots \tag{2.35}$$

The so-called *Stoner criterion* for ferromagnetism follows directly from equation 2.35 and is given by

$$I\rho(\epsilon_F) > 1. \tag{2.36}$$

The zero temperature magnetisation is given by

$$M = \rho(\epsilon_F)\sqrt{2\left(I\rho(\epsilon_F) - 1\right)/F_1}, \tag{2.37}$$

and the magnetic susceptibility by

$$\chi = \frac{\rho(\epsilon_F)}{2\left(1 - I\rho(\epsilon_F)\right)}, \tag{2.38}$$

which differs from the result of Pauli by the *Stoner enhancement factor* $1/\left(1 - I\rho(\epsilon_F)\right)$.

The incorporation of temperature into the model is possible and from there the temperature dependence of the magnetisation and susceptibility can be found, as well as an expression for the Curie temperature T_c. Crucially, the form of the temperature dependence of the susceptibility,

$$\chi^{-1}(T) \sim T^2, \tag{2.39}$$

disagrees with the Curie inverse-T law which is observed in almost all itinerant ferromagnets.

Further issues with finite temperature Stoner theory include the calculated values of T_c being too high and an incorrect observed temperature dependence of the magnetisation.

Solutions to the problems posed by Stoner theory do exist, notably the development of spin fluctuation theory. The analogous entity to a spin wave in localised systems does not exist in itinerant systems, however some other approach must be taken. It turns out that a suitable treatment might be to consider statistical fluctuations of the magnetic moment and this corrects

the Stoner model, bringing results in line with experiment. For a treatment of spin fluctuation theory see, among others, reference [36].

We will derive and consider Stoner theory in more detail later in this thesis. In particular we will concentrate on the zero-temperature phase diagram of the model.

2.5 Quantum criticality in itinerant systems

Here we discuss a final situation where non-Fermi-liquid behaviour has been observed, in itinerant magnetic systems which have a quantum-critical point [37].

There are a variety of tuning parameters used by workers on such systems. Here we consider the most regularly used parameters, for which there exists much experimental data, as well as considering systems whose quantum-critical point occurs naturally or with very little persuasion.

2.5.1 Doped systems

Historically, the first clear-cut example of non-Fermi-liquid character in an itinerant system with a quantum-critical point is arguably[4] the heavily doped system $U_{0.2}Y_{0.8}Pd_3$ [38] in the early 1990's. Figure 2.8 shows the specific heat coefficient $\gamma = C/T$ for the system which is doped to a region of the phase diagram far from the quantum-critical antiferromagnetic transition. This logarithmic behaviour is at odds with the Fermi-liquid prediction of a temperature independent γ. Figure 2.9 shows the magnetic susceptibility plot of the same system. In this case, measurements gives $\chi \sim T^{-1+\lambda}$ where $\lambda = 0.70$.

Other non-Fermi-liquid behaviours have been seen in the vicinity of many doped quantum-critical systems. For example, figure 2.9 shows magnetic susceptibility data from the material $U_{1-x}Th_xPd_2Al_3$ [39], doping to its quantum-critical point with $x = 0.4$. Here the susceptibility exponent $\lambda = 0.63$.

[4]Technically, the anomalous behaviour appears at a location in the phase diagram that is far from the quantum-critical point

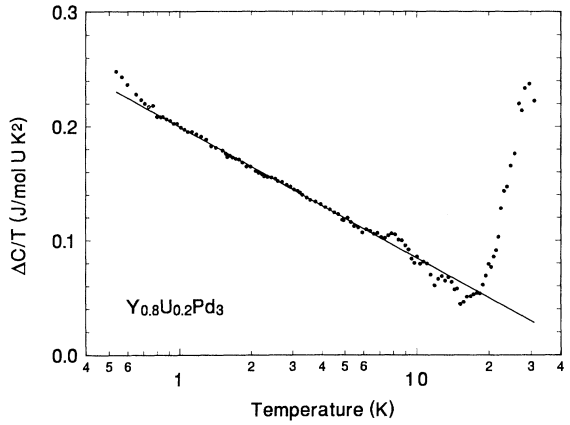

Figure 2.8: From [38]. The specific heat coefficient $\gamma = c/T$ of $U_{0.2}Y_{0.8}Pd_3$. $\gamma \sim -\ln T$ is behaviour that is not expected from a Fermi-liquid type argument (which predicts γ to be T-independent) and is to be found far from the quantum-critical point of the phase diagram of $U_xY_{1-x}Pd_3$.

2.5.2 Field induced systems and metamagnetism

Possibly the simplest quantum-critical points to access, where a tuning parameter is required, are those found via application of a magnetic field: experimentally a magnetic field that is not too substantial can be applied and varied straightforwardly. However, a downside of magnetic field is that they do break a symmetry. Indeed, there exist a number of systems that are magnetic field tuned.

The first example of magnetic field induced non-Fermi-liquid behaviour in a single crystal was in $CeCu_{5.2}Ag_{0.8}$ in the late 1990's [40, 41] – an easily achievable field of $B \approx 2.3$T suppressing antiferromagnetism and giving anomalous resistivity and specific heat behaviours.

Since then, many systems have been tuned using magnetic fields. Of particular note are those system that exhibit metamagnetism: a sudden jump in magnetisation of a sample as a critical magnetic field is reached. There are a few examples of systems to display such physics, notably $CeRu_2Si_2$ and UPt_3, and intense experimental investigation has revealed some interesting non-Fermi-liquid behaviour.

A further case of a metamagnetic system, with much experimental data, is $Sr_3Ru_2O_7$, a member of the ruthenate family. Samples display a metamagnetic jump for fields $B_{\text{crit}} \approx 5.5$T, see figure 2.10 [42] and in the vicinity of B_{crit} the resistivity obeys $\rho \sim T$. Further study of the resistivity exponent $\rho \sim T^{\alpha}$ illustrates the range over which anomalous behaviour is

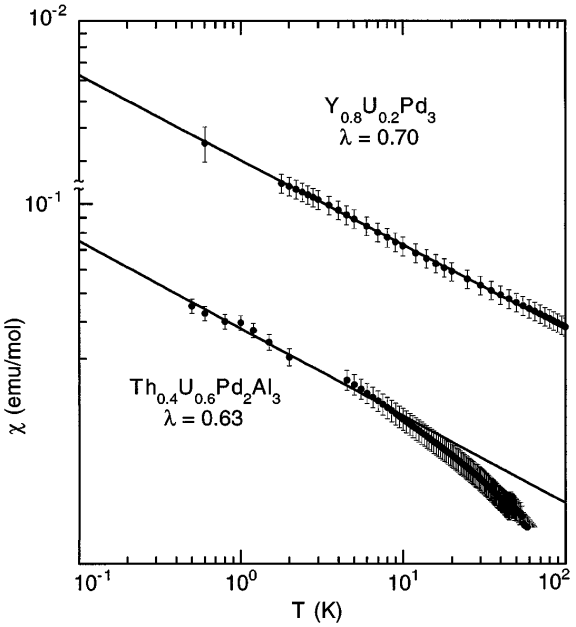

Figure 2.9: After [39]. Plots of the magnetic susceptibility dependence on temperature of $U_{0.2}Y_{0.8}Pd_3$ and $U_{0.6}Th_{0.4}Pd_2Al_3$. Both axes are on a logarithmic scale. Next to each plot is the susceptibility exponent λ, where $\chi \sim T^{-1+\lambda}$. Both materials shown exhibit non-Fermi-liquid behaviour (discussed in text).

associated with quantum criticality. Figure 2.12 shows the changes in the value of α across the temperature-magnetic field phase diagram. Not only does the non-Fermi-liquid $\rho \sim T$ (yellow in the figure) appear at the quantum critical point, but also at higher temperatures.

It is thought that Hertz-Millis theory, which we will consider in the next chapter, applies to the quantum-critical end-point of metamagnetic transitions in $Sr_3Ru_2O_7$ [43]. In the phase diagram, this is found at some critical values of the applied magnetic field and the angle it makes with the ab-plane [44]. This is shown in figure 2.11.

2.5.3 Pressure induced systems

The final tuning parameter that we consider is pressure which can be used to suppress magnetic order in both antiferromagnetic and ferromagnetic systems. Akin to using a magnetic field, pressure differs from doping in that disorder is not an issue. Furthermore, pressure can be applied very precisely, making it more attractive than doping. A downside is that it cannot be varied as straightforwardly as magnetic field can.

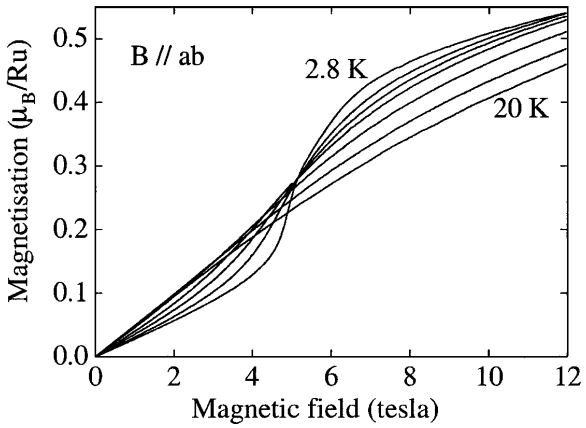

Figure 2.10: From [42]. The dependence of the magnetisation of $Sr_3Ru_2O_7$ on applied magnetic field for a range of temperatures. As the temperature tends towards the lowest reached experimentally, a metamagnetic transition – a discontinuously jump in magnetism as the field is increased – is observed at a magnetic field of $B_{\text{crit}} \approx 5.5$T.

Of particular note are those compounds which contain cerium and are antiferromagnets. All have their magnetism suppressed to a quantum critical point with pressure. For example, consider Ce_7Ni_3 which is a antiferromagnet at temperatures below $T = 1.8$K in ambient conditions. The magnetism disappears when a pressure of $p_c \sim 3.1$kbar is applied [46, 47]. At high pressures (of around 6kbar), this material displays the temperature dependences of resistivity, specific heat coefficient and magnetic susceptibility that might be expected of a Fermi-liquid. However, closer to the quantum critical point, these quantities have anomalous temperature dependences. To illustrate this consider the magnetic susceptibility: figure 2.13 displays a $\log\chi$-$\log T$ plot. For pressures near the quantum critical point (for example $p = 0.35$ GPa≈ 3.4 kbar), the susceptibility fails to obey $\chi \sim T^{\alpha}$ (the graph is not a straight line). However as pressure is increased, the plots become flatter, moving towards Fermi-liquid behaviour.

Turning our attention to itinerant ferromagnetic systems, two worthy of mention are MnSi and $ZrZn_2$. The latter example will be discussed at some length in Chapter Three, here we concentrate on MnSi (which, itself, we will revisit in Chapter Six).

MnSi becomes helimagnetic in ambient conditions below a temperature of approximately 30K. This magnetism is suppressed by a pressure of $p_c \approx 15$ kbar and studies show that this zero temperature transition is first-order in nature [48]. In the vicinity of this point, resistivity

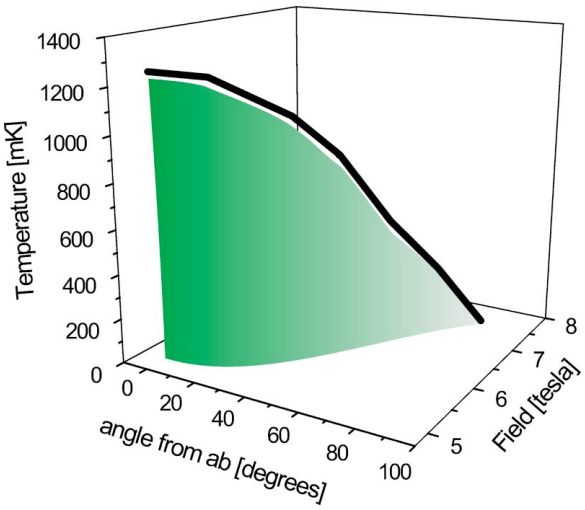

Figure 2.11: From [44]. The temperature-magnetic field-field angle phase diagram of $Sr_3Ru_2O_7$, inferred from measurements of the magnetic susceptibility. It is observed that a metamagnetic transition occurs in this material for some temperature dependent critical field, the shaded region. Varying the angle of the applied magnetic field from the ab-plane of a sample means the second-order endpoint of such transitions can be tuned to zero temperature. This, in turn, describes a line of similar endpoints (bold line), thus reaching a quantum-critical endpoint. In this case, the quantum-critical endpoint's (T, H, θ) coordinates are $(0, 7.5, 80)$.

measurements show non-Fermi-liquid behaviour: $\rho \sim T^{1.6-1.8}$ (depending on the exact pressure). Figure 2.14 shows the suppression of the Fermi-liquid $\rho \sim T^2$ behaviour as pressure is increased towards the quantum-critical point. However, strangely the magnetic susceptibility is temperature independent (that is, like a Fermi-liquid) in these same regions of the phase diagram [48].

2.5.4 Naturally quantum-critical systems

Finally, there do exist a handful of systems where little or no tuning parameter is required to reach a quantum-critical point. That is, the system is naturally quantum critical as temperature is lowered. For example, take $YbRh_2Si_2$ [49] which is tuned by a very moderate field and its resistivity measurements give $\rho \sim T$, see figure 2.15, instead of the expected Fermi-liquid $\rho \sim T^2$.

Finding a system that naturally lies close to its quantum-critical point is unlikely, but not impossible. In fact, the theoretical treatment we will discuss in the next chapter predicts non-

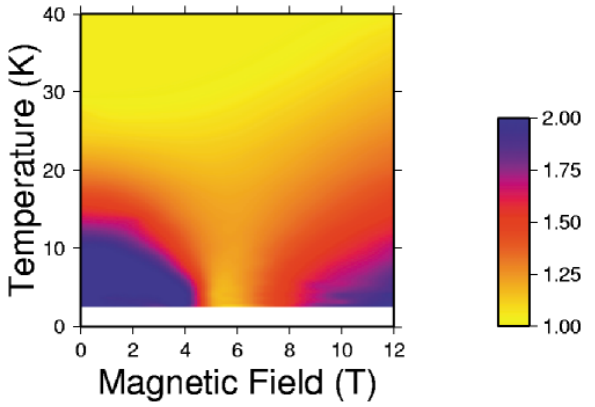

Figure 2.12: From [42]. Changes in the resistivity of $Sr_3Ru_2O_7$ as a function of temperature and magnetic field. Different colours represent different values of α, the resistivity exponent $\rho \sim T^{\alpha}$. Here blue represents $\alpha = 2$, normal Fermi-liquid behaviour. The yellow region is a region of anomalous behaviour $\rho \sim T$, which appears to have a quantum-critical point as its source and extends over a substantial amount of the phase diagram.

Fermi-liquid behaviour associated with quantum criticality in surprisingly large parts of the generic phase diagram, including quite large temperatures.

2.6 Summary

This chapter has acted as a primer to the rest of the thesis, introducing the background physics associated with the chapters to come.

We started in §2.2 with a treatment of Fermi-liquid theory, a standard model of the field that describes metallic behaviour in the limit of low temperatures. We discussed how metallic behaviour seems to indicate that we put aside intuitive thoughts about the individual electrons making up metallic behaviour, but rather to think about some new particle, linked to and somewhat similar to the original electrons, namely fermionic quasiparticles (see §2.2.3). It is the quasiparticles that are the collective excitations of metals. We proceeded to discuss some Fermi-liquid predictions (§2.2.5) and demonstrate that Fermi-liquids do indeed exist in nature (§2.2.7).

However, there do exist situations where Fermi-liquid theory is not a valid description of the low-temperature physics of some systems, §2.2.8 gave an overview of such cases. In particular

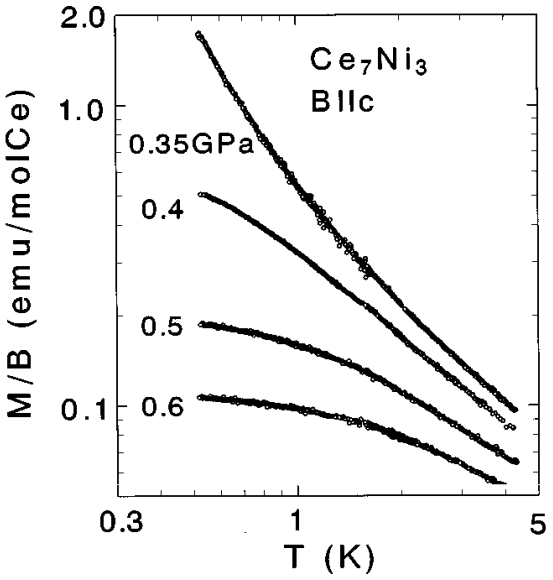

Figure 2.13: After [45]. Magnetic susceptibility measurements at various pressures of Ce_7Ni_3. The uppermost curve is nearest quantum criticality and displays non-Fermi-liquid behaviour. However, as pressure is incresed and the system is moved from its quantum critical point, the graphs flatten and Fermi-liquid behaviour is seen.

we concentrated on various types of superconductivity, such as conventional superconductivity – a state of matter where electrons attract each other, pairing up to form new particles called Cooper pairs – and high temperature superconductivity – a set of complex antiferromagnetic insulators whose superconductivity arises when doped and whose superconducting transition temperatures are huge compared with conventional superconductivity. Very little is known about these systems, not even a rigid explanation for a pairing mechanism exists. We also considered the possibility of metallic behaviour in one-dimension, arguing that the Fermi-liquid approach becomes invalid in such situations. However, a pair of excitations known as the holon and the spinon give rise to a one-dimensional analogue to Fermi-liquids, the Luttinger liquid.

But the non-Fermi liquid scenario of most interest to us in this thesis is the anomolous behaviour that appears in the vicinity of quantum critical points. After discussing classical criticality (sections 2.3.1 and 2.3.2) we introduced quantum criticality and pointed out the similarities and differences between the two cases (§2.3.2).

Before giving an overview of experiments which motivate the studies in the rest of the thesis, it was necessary to review itinerant ferromagnetism, this was done in §2.4. We discussed the

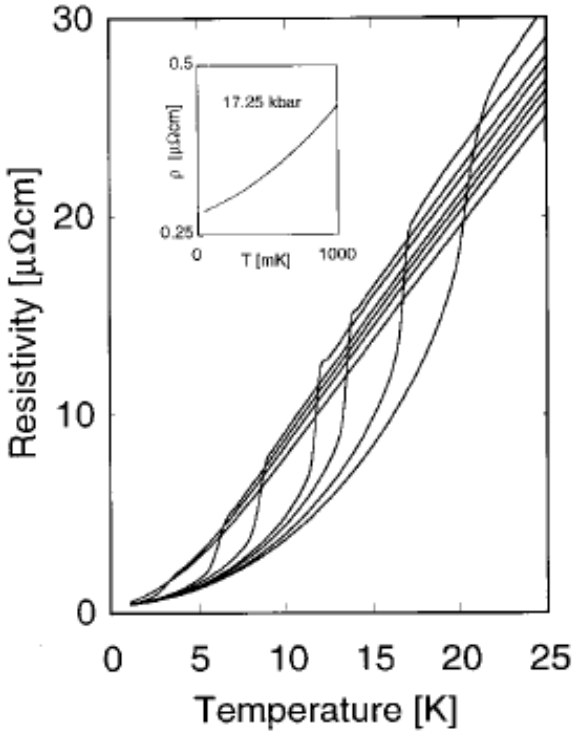

Figure 2.14: From [48]. Measurement of the resistivity versus temperature at various pressures in MnSi. The uppermost curve on the right is at 5.55 kbar and further measurement are taken up to a highest pressure of 15.50 kbar (lowest curve on the right). As the quantum critical point at a pressure $p_c = 14.6$ kbar is approached, the kink in resistivity moves lower and lower. For $p < p_c$, non-Fermi-liquid behaviour is seen. For example, the inset shows non-Fermi-liquid behaviour for $p = 17$ kbar at very low temperature.

historical story of magnetism, starting with the flawed – however influential – classical theories and then moving on to the quantum mechanical treatments introducing, along the way, the tight-binding, Hubbard and Stoner models.

Finally, in §2.5 we gave an insight into the many systems that appear to exhibit anomolous metallic behaviour near quantum criticality. We discussed a wide range of materials that show quantum criticality and introduced a range of tuning parameters, drawing examples from the many studies that have been performed by experimental workers.

We move on in the next chapter to consider an important theory of itinerant quantum criticality, Hertz-Millis theory.

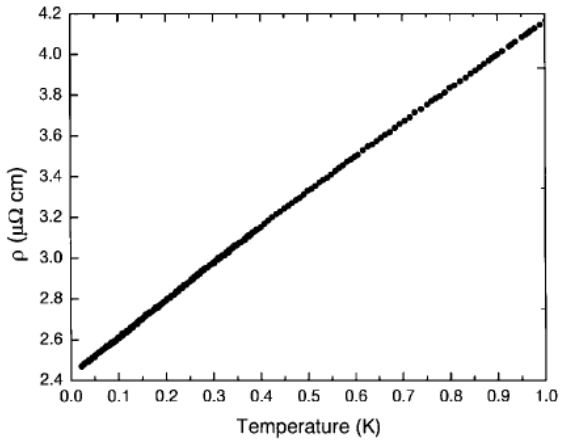

Figure 2.15: After [49]. Resistivity measurements of the material $YbRh_2Si_2$ show a linear relationship with temperature rather than the expected $\rho \sim T^2$ relationship of Fermi-liquid theory. $YbRh_2Si_2$ is special because it appears to naturally lie at a quantum critical point when temperature is lowered.

Chapter 3

Hertz-Millis theory

3.1 Introduction

We have introduced the concept of a zero-temperature (or quantum) phase transition and speculated on the effect of their presence on the properties of itinerant electron systems, in particular the appearance of non-Fermi-liquid behaviour in their vicinity [37]. In order to develop this further, we will spend some time in this chapter concentrating on the pioneering theory of the field, namely Hertz-Millis theory [27, 50, 51]. Hertz's [27] was the first work of note regarding quantum criticality in itinerant magnetic systems and, some twenty years later, the field was revisited and revived by Millis [50] whose results in the finite temperature regime differ from Hertz's.

We give the standard derivation of the Hertz-Millis action in §3.3. However, given the quantum-statistical nature of the problem in hand, it will be required that we work within the functional integral formalism [52]. For completeness we spend time initially developing this formalism (see §3.2), introducing the abstract algebra and calculus of Grassmann numbers beforehand [52, 53]. It is in terms of Grassmann numbers that the functional integral will be written.

To analyse the Hertz-Millis action, the primary tool we will employ is the renormalization group (RG) technique. Given the potential mathematical depth of RG and that a complete discussion necessarily requires more time and space than this thesis can facilitate, along with the fact that many suitable treatments exist in the literature already [25], some time will be spent in §3.4 motivating the concept and developing the bare formalism without being too rigorous.

We will follow RG's introduction by the direct application of renormalization group to the Hertz-Millis action in §3.5. We will derive, in the process, a set of flow equations (or renormalization group equations) that must be solved in (§3.6) order to compute the finite temperature phase diagram and furthermore to infer physical quantities of interest. It is in the next chapter that we will do such calculations in anger, but the final part of this chapter will be to derive the free energy and indicate which quantities can be extracted from it.

Throughout this chapter our considerations will be, as far as possible, general. This means that results presented here can be applied to systems of various itinerant magnetic nature and in

dimensions beyond those considered in of the rest of this thesis.

3.2 Fermionic functional integral formalism

Formulating quantum mechanical problems using a second quantized approach allows the treatment of multiple particles where the various particle exchange symmetries or anti-symmetries of the wavefunctions involved are taken care of by the inherent structure of the language itself [52, 53]. This, in principle, would allow the preparation of a quantum mechanical state and a subsequent investigation of possible outcomes of future measurements.

However, for any system containing a large number of particles, this approach becomes cumbersome and therefore the computation power required too great. In practice, a statistical approach is required: one might instead inquire about the probability that a system might be found in a certain state, a simpler question to answer.

To this end, we choose to write the partition function, the starting point of statistical physics considerations, as a trace over a set of over-complete states which span the fermionic Fock space. Due to the fact that particles are indistinguishable, **all** possible paths through imaginary time $t = i\beta$ taken by each of the system's particles must be taken into account.

Below we derive the many-fermion functional integral, but first we must introduce Grassmann numbers. These are required because the eigenfunctions of fermionic operators, coherent states, necessarily have anticommuting eigenvalues and the Grassmann numbers play this rôle. Aided by the fact that the coherent states are over-complete, *i.e.*, they span the fermionic Fock space, we are able to follow the standard derivation of functional integrals [52].

3.2.1 Grassmann numbers, algebra and calculus

Let us denote two objects which we will subsequently refer to as *Grassmann numbers* (or *Grassmann variables*, or simply *Grassmanns*) by ψ and η. It is important to note that they are not numbers in the usual sense of the word (they never take on an actual value), rather that the nature of Grassmanns is defined by the algebra and calculus dictating their manipulation. Here

we list those most fundamental rules and infer further properties.

The first, and most elemental, property is that **all** Grassmanns anti-commute with **all** other Grassmanns as well as **all** fermionic operators:

$$\{\psi, \eta\} \equiv \psi\eta + \eta\psi = 0, \tag{3.1}$$

$$\{\psi, \Psi\} = 0, \tag{3.2}$$

where Ψ is an arbitrary fermionic operator.

Setting $\psi = \eta$ in equation 3.1 immediately implies

$$\{\psi, \psi\} = 0 \Rightarrow \psi^2 = -\psi^2 \Rightarrow \psi^2 = 0, \tag{3.3}$$

and so any Grassmann multiplied by itself gives zero.

The property 3.3 instantly terminates, at first-order, the expansion of an arbitrary function of a Grassmann number:

$$f(\psi) = a + b\psi. \tag{3.4}$$

where generally a and b are complex numbers. A particularly important example of a function is the exponential $f(\psi) = e^{a\psi}$ which can straightforwardly be expanded to give

$$e^{a\psi} = 1 + a\psi. \tag{3.5}$$

Moving on to important calculus results, let us **define** Grassmann integration. It is easy to supply an exhaustive list of Grassmann integrals as there are merely two:

$$\int \psi d\psi = 1 \tag{3.6}$$

and

$$\int 1 d\psi = 0. \tag{3.7}$$

We are now in a position, therefore, to integrate all functions of Grassmanns.

Note that the entity $d\psi$ is itself a Grassmann and so

$$\int d\psi\psi = -\int \psi d\psi = -1. \tag{3.8}$$

Integration is a linear operation, the rule of thumb is that one must anti-commute Grassmanns until they are adjacent to their derivatives. For example, an important integral is

$$\int \bar{\psi}\psi d\psi d\bar{\psi} = -\int \psi\bar{\psi} d\psi d\bar{\psi} = +\int \psi d\psi\bar{\psi} d\bar{\psi} = 1. \tag{3.9}$$

3.2.2 Coherent states, the trace and the resolution of the identity

We now define the following state

$$|\psi\rangle = |0\rangle - \psi|1\rangle \tag{3.10}$$

which we will refer to as the *fermionic coherent state*. Here $|0\rangle$ and $|1\rangle$ are the usual fermionic states containing zero fermions and one fermion respectively. $|\psi\rangle$ is the right eigenstate of the fermionic annihilation operator with a Grassmann eigenvalue ψ, this is easy to show:

$$\begin{aligned} \Psi|\psi\rangle &= \Psi|0\rangle - \Psi\psi|1\rangle \\ &= 0 + \psi\Psi|1\rangle \\ &= \psi|0\rangle \\ &= \psi\left(|0\rangle - \psi|1\rangle\right). \end{aligned} \tag{3.11}$$

In a similar way

$$\langle\bar{\psi}|\Psi^\dagger = \langle\bar{\psi}|\bar{\psi} \tag{3.12}$$

where $\langle\bar{\psi}| = \langle 0| - \langle 1|\bar{\psi}$. It is important to note here that the coherent state vectors are not members of the usual complex vector space. Furthermore $\langle\bar{\psi}|$ is not the adjoint of $|\psi\rangle$ (and vice

versa) and ψ and $\bar{\psi}$ are not complex conjugate partners.

Finally, the quantity

$$\begin{aligned}\langle\bar{\psi}|\psi\rangle &= \left(\langle 0| - \langle 1|\bar{\psi}\right)\left(|0\rangle - \psi|1\rangle\right) \\ &= \langle 0|0\rangle + \bar{\psi}\psi\langle 1|1\rangle \\ &= 1 + \bar{\psi}\psi \equiv e^{\bar{\psi}\psi}\end{aligned} \tag{3.13}$$

is to be referred to as the *inner product* of the coherent states $\langle\bar{\psi}|$ and $|\psi\rangle$.

Before advancing to consider the functional integral, we require two more results. The first one is the trace of an operator constructed from an even number of fermionic operators. If we denote this operator as Ξ, it can be shown that

$$\text{Tr } \Xi = \int \langle -\bar{\psi}|\Xi|\psi\rangle e^{-\bar{\psi}\psi} d\bar{\psi} d\psi. \tag{3.14}$$

The second result is that of the identity, which we denote by $\hat{1}$. This is given by

$$\begin{aligned}\int |\psi\rangle\langle\bar{\psi}| e^{-\bar{\psi}\psi} d\bar{\psi} d\psi &= |0\rangle\langle 0| + |1\rangle\langle 1| \\ &\equiv \hat{1}.\end{aligned} \tag{3.15}$$

3.2.3 The functional integral

A quantity of interest in statistical physics is the partition function Z, which, for a Hamiltonian comprising of fermionic operators $H = H\left(\Psi^{+}, \Psi\right)$, is given to be:

$$Z = \text{Tr } e^{-\beta H}. \tag{3.16}$$

Here we assume that the Hamiltonian is *normal ordered*. This means that all creation operators apparent in the Hamiltonian lie to the left of all the annihilation operators. In such cases the creation operators are free to act on their eigenstates to the left and the annihilation operators

are free to act to the right on their eigenstates.

Using Grassmann variables, we can rewrite the trace following relation 3.2.2:

$$Z = \int \langle -\bar{\psi}|e^{-\beta H}|\psi\rangle e^{-\bar{\psi}\psi} d\bar{\psi} d\psi. \tag{3.17}$$

Furthermore, we can rewrite $e^{-\beta H}$ as a series in the following form

$$e^{-\beta H} = \lim_{n\to\infty} \left(e^{-\xi H}\right)^n, \tag{3.18}$$

where $\xi = \beta/n$ is taken to be infinitesimal.

Imagine writing n sets of $(1 - \xi H)$ adjacent to each other and **in between** each set inserting the resolution of the identity. It follows that the identity is inserted $n - 1$ times. This gives the partition function to be

$$\begin{aligned} Z = & \int \langle -\bar{\psi}_1| \left(1 - \xi H\right) |\psi_{n-1}\rangle e^{-\bar{\psi}_{n-1}\psi_{n-1}} \langle \bar{\psi}_{n-1}| \left(1 - \xi H\right) \\ & \times \cdots |\psi_2\rangle e^{-\bar{\psi}_2\psi_2} \langle \bar{\psi}_2| \left(1 - \xi H\right) |\psi_1\rangle e^{-\bar{\psi}_1\psi_1} d\bar{\psi}_{n-1} d\psi_{n-1} \cdots d\bar{\psi}_1 d\psi_1. \end{aligned} \tag{3.19}$$

Now, remembering that the Hamiltonian is normal ordered by construction, we make the replacement

$$\begin{aligned} \langle \bar{\psi}_{i+1}| \left(1 - \xi H\left(\Psi^+, \Psi\right)\right) |\psi_i\rangle &= \langle \bar{\psi}_{i+1}| \left(1 - \xi H\left(\bar{\psi}_{i+1}, \psi_i\right)\right) |\psi_i\rangle \\ &= e^{\bar{\psi}_{i+1}\psi_i} e^{-\xi H\left(\bar{\psi}_{i+1}, \psi_i\right)} \end{aligned} \tag{3.20}$$

everywhere throughout the partition function. This yields, where we define $\psi_N = -\psi_1$,

$$Z = \int \prod_{i=1}^{N-1} \exp\left(\frac{\bar{\psi}_{i+1} - \bar{\psi}_i}{\xi}\psi_i - H\left(\bar{\psi}_{i+1}, \psi_i\right)\right) \xi d\bar{\psi}_i d\psi_i. \tag{3.21}$$

Taking the limit $n \to \infty$ yields the fermionic functional integral.

$$Z \simeq \int \mathcal{D}\left(\psi, \bar{\psi}\right) e^{-S\left(\psi, \bar{\psi}\right)}, \tag{3.22}$$

where

$$S\left(\psi,\bar{\psi}\right)=\int_{0}^{\beta}\psi\left(\tau\right)\left(\frac{\partial}{\partial\tau}+\epsilon_{k}-\mu\right)\psi\left(\tau\right)d\tau. \tag{3.23}$$

Here ϵ_k is some dispersion and μ a chemical potential.

3.3 Derivation of the Hertz-Millis action

Let us begin by writing down the partition function Z in the standard functional integral representation [52]. The principal interaction we insert into our action S will be a spin-density interaction.

$$Z=\int\mathcal{D}\left(\psi,\bar{\psi}\right)e^{-S\left(\psi,\bar{\psi}\right)}, \tag{3.24}$$

where the action is given by

$$S\left(\psi,\bar{\psi}\right)=\int_{0}^{\hbar\beta}d\tau\sum_{k}\left[\bar{\psi}_{k}\left(\tau\right)\left(\frac{\partial}{\partial\tau}+\epsilon_{k}-\mu\right)\psi_{k}\left(\tau\right)-J\left(k\right)\mathbf{S}_{k}\left(\tau\right)\mathbf{S}_{-k}\left(\tau\right)\right]. \tag{3.25}$$

One can employ the standard Hubbard-Stratonovich [54, 55] transformation to decouple the interaction. This gives rise to a new Hubbard-Stratonovich field denoted by ϕ. Physically, ϕ is an order parameter of n components. In the case of ferromagnetism, ϕ represents the magnetisation and in the case of antiferromagnetism, ϕ represents the staggered magnetisation. The partition function now includes an integral over ϕ and becomes

$$Z=\int\mathcal{D}\left(\bar{\psi},\psi,\phi\right)e^{-S\left(\bar{\psi},\psi,\phi\right)}, \tag{3.26}$$

where

$$\begin{aligned} S\quad\left(\bar{\psi},\psi,\phi\right)&=\int_{0}^{\hbar\beta}d\tau\Bigg\{\sum_{k\alpha}\frac{1}{4J\left(k\right)\lambda^{2}}\phi_{k,\alpha}\phi_{-k,\alpha} \\ +\quad&\int d^{D}\mathbf{x}\psi_{\alpha}\left(\mathbf{x},\tau\right)\left[\delta_{\alpha\beta}\left(\frac{\partial}{\partial\tau}+\epsilon_{k}-\mu\right)+i\lambda\phi\left(\mathbf{x}\right)\cdot\sigma_{\alpha\beta}\right]\psi_{\beta}\left(\mathbf{x},\tau\right)\Bigg\}\end{aligned} \tag{3.27}$$

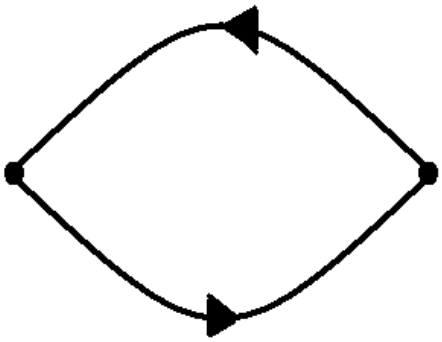

Figure 3.1: The diagram associated with the Lindhard function. Writing down the integral represented with this diagram gives us equation 3.31.

It should be clear that performing the integral over ϕ retrieves equations 3.24 and 3.25. The next step taken by both Hertz and Millis is to formally perform the integral over the Grassmann fields. Millis's claim [50] is that this step is justified for cases where the resulting action is an analytic function of the ordered fields. Later in this thesis, we will reconsider the assumption made here and concern ourselves with important situations where it is to be considered naïve. For the time being, we will follow the historical development of the theory and make the assumption too.

Integrating out the Grassmann variables leads to

$$Z = Z_0 \int \mathcal{D}\phi e^{-\tilde{S}(\phi)}, \tag{3.28}$$

with

$$\begin{aligned} \tilde{S} &= \int_0^{\hbar\beta} d\tau \Bigg\{ \sum_{k,\alpha} \frac{1}{4J\left(k\right)\lambda^2} \phi_{k,\alpha}\phi_{-k,\alpha} \\ &+ \int d^D\mathbf{x} \ln\det \left[\underbrace{\delta_{\alpha\beta}\left(\frac{\partial}{\partial\tau} + \epsilon_k - \mu\right)}_{\mathcal{G}^{-1}(k,i\omega_n)} + i\lambda\phi\left(\mathbf{x}\right)\cdot\sigma_{\alpha\beta} \right] \Bigg\}. \end{aligned} \tag{3.29}$$

Expanding the $\ln\det$ term allows us to write down an effective action whose foremost term

is the one of Gaussian order, $S_{\text{Gaussian}}(\phi)$:

$$S_{\text{Gaussian}}(\phi) = \sum_{\omega_n,k} \left(\frac{1}{4J(k)\lambda^2} + \frac{\lambda^2}{2}\chi(\mathbf{k},\omega) \right) \phi_{-\omega_n,-k}\phi_{\omega_n,k}, \tag{3.30}$$

where $\chi(\mathbf{k},\omega)$ is the Lindhard function [56]. This is represented by the diagram in figure 3.1 and given by

$$\chi(\mathbf{k},\omega) = -\frac{1}{\beta}\sum_{kn} \mathcal{G}(k,i\omega_n)\,\mathcal{G}(k+q,i\omega_n+\omega') \tag{3.31}$$

Here $\mathcal{G}$ is defined in equation 3.29.

Expansion of the Lindhard function itself, and absorption of uninteresting constants into the ϕ's, leads to the Gaussian term of the effective action taking the form

$$S^{\text{FM}}_{\text{Gaussian}}(\phi) = \beta V \sum_n \int \frac{d^D k}{(2\pi)^2} \left(r + \xi^2 k^2 + \frac{|\omega_n|}{k} \right) \phi_n(k)\,\phi_{-n}(-k) \tag{3.32}$$

for a system exhibiting a ferromagnetic transition, and

$$S^{\text{AFM}}_{\text{Gaussian}}(\phi) = \beta V \sum_n \int \frac{d^D k}{(2\pi)^2} \left(r + \xi^2 k^2 + |\omega_n| \right) \phi_n(k)\,\phi_{-n}(-k) \tag{3.33}$$

for a system of antiferromagnetic nature. The next term in the action looks like

$$S_{\text{self-interaction}} = u \int d\tau \int d^D\mathbf{x} \left[\phi(\mathbf{x},\tau)^2 \right]^2 \tag{3.34}$$

where we assume that the leading term of the coefficient of the quartic part of the action is a constant u, although in general this coefficient would have a dependence on wavevector and frequency. Finally, a term accounting for the application of a conjugate magnetic field (which is uniform in ferromagnetic cases and staggered in anti-ferromagnet cases) is given by

$$S_h = \frac{1}{\beta V}\sum_{kn} h_{k\omega_n} \cdot \phi_{-k,-\omega_n}. \tag{3.35}$$

We therefore use equations 3.34 and 3.35 along with either equation 3.32 or equation 3.33

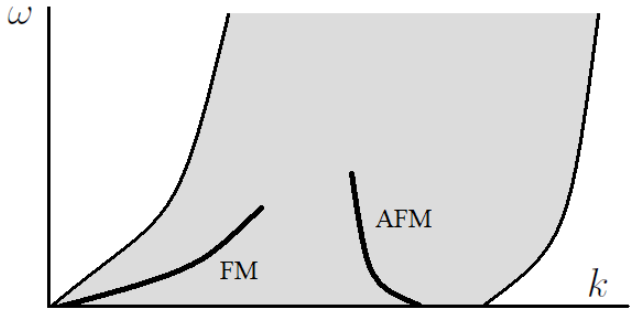

Figure 3.2: Plot in (k, ω)-space showing the allowed particle-hole excitations (shaded region) as well as typical critical fluctuations (solid lines) for the ferromagnetic and antiferromagnetic cases. For both of these cases, the fact that these lines lie inside the continuum implies that such scenarios are overdamped and the dynamic exponent $z > 1$.

to write down the Hertz-Millis action:

$$S_{\text{HM}}(\phi) = S_h + S_{\text{Gaussian}} + S_{\text{self-interaction}} + \cdots . \tag{3.36}$$

Except for the dependence on frequency, the Hertz-Millis action resembles the actions found in the classical critical Landau-Ginzburg-Wilson theory. It is important to discuss the form of the term involving frequency in each of the two magnetic cases, equations 3.32 and 3.33. These terms account for the damping of the spin fluctuations that occur due to electron-hole excitations across the Fermi-surface of the systems of interest. This is *Landau damping*.

Figure 3.2 shows a (k, ω)-plot of allowed particle-hole excitations [50]. Also shown are typical critical fluctuations for ferromagnetic and antiferromagnetic systems. Both cases lie inside the continuum and are therefore said to be overdamped, giving rise to values of the dynamic exponent $z > 1$.

3.4 The renormalization group procedure

The roots of the renormalization group (RG) technique are to be found in the field of quantum electrodynamics. Before the advent of RG (initial concepts can be traced to work published by Stuckelberg and Petermann [57]) certain calculations resulted in infinite valued answers where

experiment suggested this should not be the case. The issues were born out of the fact that certain integrals over, for example, momenta diverged because a particle's allowed momentum can be infinite. RG's solution to these problems involved the introduction of a finite cutoff on momenta, a recalculation of the previously divergent quantities and then an investigation into the answers' various dependences on the cutoff. It was found that certain *renormalizable* theories could be massaged such that final results remained finite for values of momentum much less than the cutoff which is finally re-set to infinity.

A more physical viewpoint of RG came from workers, most notably Kadanoff [58] and Wilson [59], in the field of condensed matter. Perversely, it became apparent that RG had an application in theories where natural cutoffs, and no divergences of quantities such as momentum that gave rise to its formulation, already existed. An example of such a cutoff might be inverse lattice spacing.

The aim here is to introduce the RG procedure, which we will need later on in this chapter and the next. We will see that this procedure is made up of three steps and will allow us to define a transformation of an action S defined in some space of coupling constants to another equivalent action S' where we have "integrated out" any unwanted modes, *e.g.* we might be interested only in correlations within our system that take place over long distances in real space (or, equivalently, small momenta in reciprocal space).

Our use of RG to analyse Hertz-Millis theory will allow us to take the Hertz-Millis action which thus far comprises of an infinite number of terms, renormalize it and end up with an effective Gaussian action which can be used much more easily for calculations.

3.4.1 The three-step RG recipe

Let us now describe the three stages of the RG process, these stages are shown schematically in figure 3.3. Imagine that a theory of interest is described by an action $S(\phi)$, where its modes, that is the ϕ's, are functions of momenta. Our system, it is imagined, has its own natural cutoff on momenta which we will label Λ. Interest in only long-range modes leads us to impose a further cutoff on momenta: the separation of those modes we are interested in, referred to as

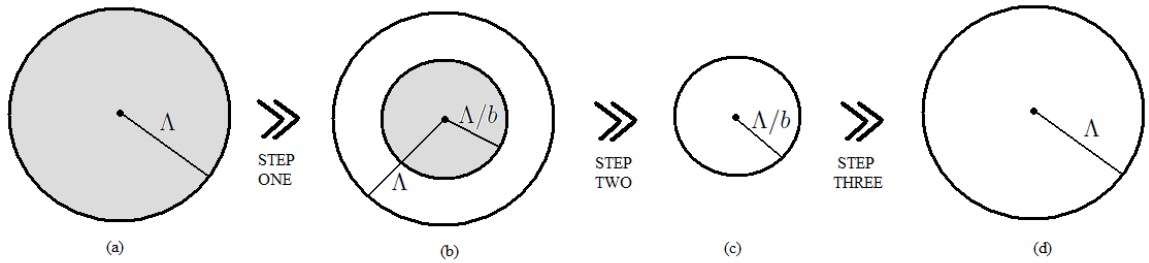

Figure 3.3: The three stages of the renormalization group recipe. The first step is to take a system whose natural cutoff on momenta is Λ, picture (a). Then let us impose some cutoff on the momenta of our system, $\Lambda \to \Lambda/b$, where $b > 1$. This defines a set of slow modes (the shaded region of picture (b)) having momenta $k < \Lambda/b$, and fast modes (the unshaded region of picture (b)) with momenta $\Lambda/b < k < \Lambda$. The second stage is to completely remove the fast modes, picture (c), before rescaling momenta to fit a new kinematic region $k/b \to k'$. Note that the new kinematic region, picture (d), has the same cutoff as originally shown in (a).

slow-modes and labelled by $\phi_<$, and those we are not, referred to as *fast modes* and labelled by $\phi_>$. We write that the momentum cutoff is at some value Λ/b where $b > 1$. We can therefore rewrite our action as the sum of a part containing solely slow modes, a part containing solely fast modes and a part which is a mixture of both slow and fast modes:

$$S(\phi) = S_<(\phi_<) + S_>(\phi_>) + S_{<,>}(\phi_<, \phi_>). \tag{3.37}$$

As such, we can rewrite the partition function as

$$Z = \int [d\phi_<]\, e^{S_<(\phi_<)} \int [d\phi_>]\, e^{S_>(\phi_>)} e^{S_{<,>}(\phi_<, \phi_>)} \tag{3.38}$$

and define an effective action $S'(\phi_<)$ consisting of slow modes. In this case

$$Z = \int [d\phi_<]\, e^{S'(\phi_<)}, \tag{3.39}$$

where

$$e^{S'(\phi_<)} = e^{S_<(\phi_<)} \int [d\phi_>]\, e^{S_>(\phi_>)} e^{S_{<,>}(\phi_<, \phi_>)}. \tag{3.40}$$

Multiplying the top and bottom of this expression by

$$Z_> \equiv \int [d\phi_>]\, e^{S_>(\phi_>)}, \tag{3.41}$$

allows us to write

$$e^{S'(\phi_<)} = Z_> e^{S_<(\phi_<)} \langle e^{S_{<,>}(\phi_<,\phi_>)} \rangle_> \tag{3.42}$$

where the angled bracketed expression is an average over the fast modes of the system. To deal with this average, we approximate by making use of the cumulant expansion which, in practice, involves making the replacement

$$\langle e^{S_{<,>}(\phi_<,\phi_>)} \rangle_> \approx e^{\langle S_{<,>}(\phi_<,\phi_>) \rangle_>}. \tag{3.43}$$

To investigate how we integrate over the fast modes, let us consider a (schematic) fourth order interaction term of our action:

$$S_4 = u \int_{k<\Lambda} d^D k \phi_1^* \phi_2^* \phi_3 \phi_4, \tag{3.44}$$

which can be rewritten in terms of the fast and slow modes and averaged over the fast modes

$$\langle S_4 \rangle = \left\langle u \int_{k<\Lambda} d^D k\, (\phi_< + \phi_>)_1^* (\phi_< + \phi_>)_2^* (\phi_< + \phi_>)_3 (\phi_< + \phi_>)_4 \right\rangle_> . \tag{3.45}$$

Multiplying out all the modes gives sixteen different terms. One term contains all slow modes and this can be found by directly setting $\phi = \phi_<$ in equation 3.44. We refer to such quantities as *tree-level* terms. There is one term containing all fast modes (this becomes a constant once the fast modes are integrated over and will be dropped from our considerations), eight terms containing either one or three fast modes (these disappear due to symmetry reasons and won't be considered from now on) and six terms that contain two slow and two fast modes. Integrating such terms over the fast modes yields a correction to the tree-level term of the part of the action that involves two fewer powers of ϕ than the term being considered. In this case, the fourth

order term adds a correction, or renormalizes, the Gaussian term. Higher order terms can be constructed in a similar way.

In practice, diagrams can be used to represent these corrections [60]. These are formed by drawing a vertex comprising of the same number of prongs as there are fields in the term under consideration and joining up these prongs to form loops which represent integration over fast fields. In general one approximates and works to a specific number of loops, for example, in this thesis we will only work to one-loop order.

After having performed elimination of the fast modes, the final two steps of the RG process must be undertaken. Because we have essentially redefined a new kinematic region, $\Lambda \to \Lambda/b$, we must rescale all other quantities appearing in the action beginning with introducing a new momentum $k' = k/b$ and following with any other parameters such as coupling constants.

The third and final step is to rewrite the action in terms of

$$\phi'(k') = \rho\phi_<(k), \tag{3.46}$$

a new set of rescaled fields.

Having discussed the RG procedure, let us now show off its power by considering an example of relevance to this thesis, namely its application to the Hertz-Millis action derived above.

3.5 RG application to the Hertz-Millis action

Having derived the Hertz-Millis action, and having discussed the concept of the renormalization group, we proceed to reproduce some key results of Hertz-Millis theory. For the time being we will keep considerations as general as possible, meaning our findings will be applicable to itinerant systems of varying magnetic nature in arbitrary dimensions. Recall the system's nature enters the theory via the quantity z, known as the dynamic exponent, and that the dimension is denoted by D.

3.5.1 Tree-level scaling equations

Let us write down the Hertz-Millis action, terminating at the term of sixth order:

$$S(\phi) = S_2 + S_4 + S_6 + \cdots + S_h, \tag{3.47}$$

where

$$S_2 = \int^{\Lambda} d^D k d\omega \left[r + \xi^2 k^2 + \frac{|\omega_n|}{k^{z-2}} \right] \phi^2, \tag{3.48}$$

$$S_4 = u \int^{\Lambda} \left(d^D k d\omega \right)^3 \phi^4, \tag{3.49}$$

$$S_6 = v \int^{\Lambda} \left(d^D k d\omega \right)^5 \phi^6, \tag{3.50}$$

and

$$S_h = h\phi. \tag{3.51}$$

Following the standard three-stage renormalization group procedure, discussed in the previous section, we are able to quite trivially write down the scaling equations of the quantities appearing in the action at tree-level. This is, in practise, no more than dimensional analysis.

As dictated by the renormalization prescription, we must reduce the cutoff in momentum space like $\Lambda_k \rightarrow \Lambda_k / b$ where $b > 1$. It follows instantly that the frequency cutoff must be reduced via $\Lambda_\omega \rightarrow \Lambda_\omega / b^z$. In the action we should therefore rescale momenta and frequencies via the relations $k \rightarrow k/b$ and $\omega \rightarrow \omega / b^z$.

From the Gaussian term of the action S_2, one concludes that the scaling of the parameter r is $r \rightarrow r b^2$. Absorbing all factors of b from the terms in parenthesis, as well as those arising from the differentials, forces the fields to scale as $\phi \rightarrow \phi b^{-(D+z+2)/2}$.

The final parameters seen in the action for which tree-level scaling equations can be written down are u, v and the magnetic field h. From the scaling relations of the preceding two paragraphs, and from the fourth order term of the action S_4, one infers $u \rightarrow u b^{-(4-(D+z))}$. From the sixth order term S_6 one notices $v \rightarrow v b^{(6-2(D+z))}$ and from the magnetic field term S_h, $h \rightarrow h b^{(D+z+2)/2}$.

Rewriting $b = e^{\lambda}$, we can proceed to list the tree-level renormalization group equations of every quantity appearing in the action. To begin with, those involved in the definition of the renormalization group process:

$$\frac{\partial k}{\partial \lambda} = k \tag{3.52}$$

and

$$\frac{\partial \omega}{\partial \lambda} = z\omega, \tag{3.53}$$

and those inferred from dimensional analysis of the action:

$$\frac{\partial r}{\partial \lambda} = 2r, \tag{3.54}$$

$$\frac{\partial \phi}{\partial \lambda} = \frac{(D + z + 2)}{2}\phi, \tag{3.55}$$

$$\frac{\partial u}{\partial \lambda} = (4 - (D + z))\, u, \tag{3.56}$$

$$\frac{\partial v}{\partial \lambda} = (6 - 2\,(D + z))\, v \tag{3.57}$$

and

$$\frac{\partial h}{\partial \lambda} = \frac{(D + z + 2)}{2}h. \tag{3.58}$$

At this point, let us consider the flow equation for the quartic coupling, equation 3.56. We are interested in the case where the coupling constant u becomes smaller along the renormalization group flow, that is when u becomes an irrelevant quantity. The significance of this is that the renormalization group process takes the Hertz-Millis action and transforms it into one where all coupling constants of terms of higher order than the Gaussian term become negligible compared to the Gaussian term. An interacting action has been mapped onto a non-interacting one. A schematic picture of this idea is given in figure 3.4.

From equation 3.56, it is apparent that we require $4 - (D + z) < 0$, which gives the condition, first pointed out by Hertz, for the behaviour at criticality to be that of a Gaussian model. This is, of course, the definition of the upper critical dimension D_c^+ and for the cases considered

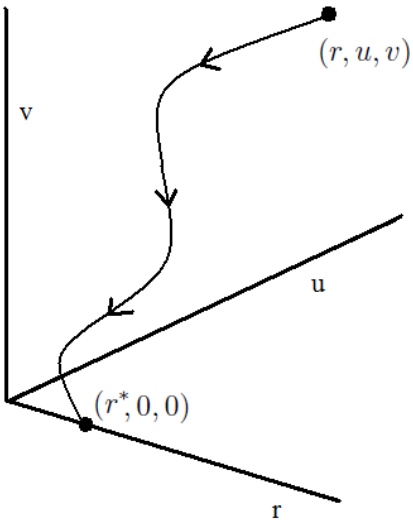

Figure 3.4: Schematic diagram representing the point of performing a renormalization group procedure. Imagine starting with some point in coupling constant space which is the description of some system of interest. This is the point denoted by (r, u, v). The RG procedure takes these coupling constants and renormalizes them, creating some flow through parameter space of equivalent actions. So long as the renormalization of u and v makes them smaller, we stop at some new point in coupling constant space, $(r^*, 0, 0)$ – therefore having reached a completely Gaussian, nonetheless equivalent, action.

here,

$$D_c^+ = 4 - z. \tag{3.59}$$

It follows that both three-dimensional itinerant antiferromagnetic ($z = 2$) and three-dimensional itinerant ferromagnetic ($z = 3$) systems are above their upper critical dimension. So too are two-dimensional ferromagnets ($D + z = 5$), whereas the two -dimensional anti-ferromagnetic case ($D + z = 4$) is marginal and requires further treatment which we won't discuss here.

Aspects of the critical behaviour of the Gaussian model will be considered shortly in this chapter.

3.5.2 One-loop corrections to the tree-level scaling equations

Having derived the tree-level scaling equations for quantities appearing in the action, we move on to perturbatively add in their corrections at the level of one-loop. This will involve performing a frequency summation and an integral over momenta on the inverse propagator $\mathcal{G}^{-1}_{\mathbf{k}n}$. The

relevant diagrams are shown in figure 3.5. Let us denote the loop by L where:

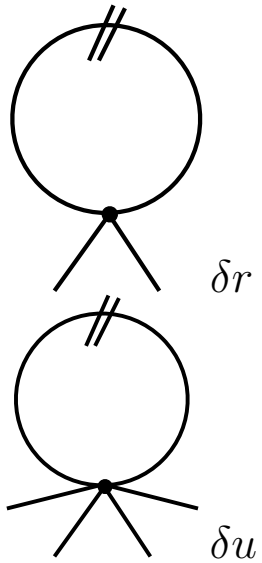

Figure 3.5: The two one-loop diagrams, δr and δu that renormalize the Gaussian and fourth-order terms in the Hertz-Millis action respectively. These represent averaging over two fast modes (denoted by bars through the loops) of the ϕ^4 and ϕ^6 terms in the action.

$$\begin{aligned} L &= \int_{\Lambda/b}^{\Lambda} \frac{d^D k}{(2\pi)^D} \frac{1}{\beta} \sum_{n'} \mathcal{G}_{\mathbf{k}n}^{-1} \\ &= \int_{\Lambda/b}^{\Lambda} \frac{d^D k}{(2\pi)^D} \frac{1}{\beta} \sum_{n'} \frac{1}{r + \xi^2 k^2 + |\omega_n|/\Gamma_k}. \end{aligned} \tag{3.60}$$

Here the prime denotes summation over fast modes and $\beta = 1/T$ is the inverse of temperature in units such that Boltzmann's constant is unity.

One can use standard techniques [61] to convert the frequency summation into an integral. Thus we obtain

$$L\left(T, r\right) = \int_{\Lambda_k/b}^{\Lambda_k} \frac{k^{D-1}}{2\pi^D} dk \int_{\Lambda_\omega/b^z}^{\Lambda_\omega} \frac{d\omega}{\pi} \coth\left(\frac{\beta\omega}{2}\right) \frac{\omega/\Gamma_k}{\left(r + \xi^2 k^2\right)^2 + \left(\omega/\Gamma_k\right)^2}, \tag{3.61}$$

in two- or three-dimensions. Notice the dependence of L on temperature and the distance from criticality r.

The integrals are performed over the fast modes, these are the modes in between momentum values Λ/b and Λ and, it follows from the relation of frequency and momentum, frequency

values Λ_ω/b^z and Λ_ω. It can be shown that the evaluation of the loop results in it having two terms: one dependent on and one independent of temperature.

$$L\left(T,r;D,z\right)=L_T\left(T;D,z\right)+L_0\left(D,z\right), \tag{3.62}$$

where, setting $r=0$, *i.e.*, close to criticality,

$$L_T\left(T;D,z\right)=\frac{1}{2\pi^D}\int_0^1 dx n_B\left(\frac{x^{z-2}}{T}\right)\left(\frac{x}{x^2+1}+2\frac{x^{D+z-3}}{x^4+1}\right) \tag{3.63}$$

and

$$L_0\left(D,z\right)=\frac{1}{2\pi^D}\int_0^1 dx\left(\frac{x}{x^2+1}+2\frac{x^{D+z-3}}{x^4+1}\right). \tag{3.64}$$

The second, temperature independent, term can be thought of as arising from quantum effects and is merely a constant which is dependent on z and D. The first term provides this theory's temperature dependence. Of particular interest is its low temperature form and in the limit where $T\rightarrow 0$ progress can be made in doing the integral by approximating the Bose function by an exponential and integrating by parts. To leading order in T one obtains

$$L\left(T,0\right)=A+BT^2. \tag{3.65}$$

Furthermore, at high temperatures

$$L\left(T,0\right)\sim T. \tag{3.66}$$

We can now move on to writing down the renormalization group equations for r and u which now include one-loop corrections. r is corrected by u which itself is corrected by v. The renormalization group equations for other quantities, derived above, remain the same.

$$\frac{dr}{d\lambda}=2r+\frac{n+2}{2}u\left(\lambda\right)L\left(T,0\right), \tag{3.67}$$

$$\frac{du}{d\lambda}=\left(4-\left(D+z\right)\right)u+\frac{n+4}{2}v\left(\lambda\right)L\left(T,0\right). \tag{3.68}$$

In the next section we will discuss the solutions of the renormalization group equations that we have written down.

3.6 Solving the renormalization group equations

The aim here is to integrate and solve the renormalization group equations that we have derived. Doing this will allow us to derive not only the temperature-control parameter phase diagram in the vicinity of a quantum critical point, but also the form of a range of experimental observables in the phase diagram's various regimes. We'll consider only cases where $D + z > 4$ and hence the systems are above their upper critical dimension. The marginal case of $D + z = 4$ (two-dimensional anti-ferromagnet) is slightly more complicated with additional logarithms appearing, we won't discuss this case here.

3.6.1 Integrating the flow equations

Imagine that we begin the renormalization flow with an initial set of parameter values: r_0, u_0, v_0, T_0. Integrating the equations for $v(\lambda)$ and $T(\lambda)$, subject to these initial conditions, gives

$$v(\lambda) = v_0 e^{(6-2(D+z))\lambda} \tag{3.69}$$

and

$$T(\lambda) = T_0 e^{z\lambda}. \tag{3.70}$$

We can now substitute equation 3.69 into equation 3.68 and integrate subject to the initial condition $u(0) = u_0$ to find

$$u(\lambda) = e^{-\lambda(D+z-4)} \left(u_0 + \frac{n+4}{2} v_0 \int_0^\lambda dp e^{-p(D+z-2)} L\left(T_0 e^{zp}, 0\right) \right). \tag{3.71}$$

Finally, equation 3.71 can be inserted into equation 3.67 and this, in turn, can be solved sub-

jected to the initial condition $r(0) = r_0$ to give the equation for the flow of the quantity r:

$$r(\lambda) = e^{2\lambda}\left(r_0 + \frac{n+2}{2}\int_0^\lambda ds e^{-2s} L\left(T_0 e^{zs}, 0\right) u(s)\right). \tag{3.72}$$

To solve the RG equations we enforce the condition, essentially an arbitrary normalization we will use, that the flow stops at some value of the flow parameter $\lambda = \lambda_0$ where the condition $r(\lambda_0) = 1$ is satisfied. We then proceed to use all quantities at the scale $\lambda = \lambda_0$.

3.6.2 Phase diagram for $D + z > 4$

We are now in a position to extract some physical results from the theory we have set-up. It will suffice at this juncture to set $v_0 = 0$ in all RG equations, we therefore renormalize only from the quartic term to the Gaussian term in the action. Our RG equations for the parameters r and u reduce to

$$u(\lambda) = u_0 e^{-\lambda(D+z-4)} \tag{3.73}$$

and

$$r(\lambda) = e^{2\lambda}\left(r_0 + \frac{n+2}{2}\int_0^\lambda ds e^{-2s} L\left(T_0 e^{zs}, 0\right) u(s)\right) \tag{3.74}$$

Let us consider the so-called *quantum disordered regime* which was first considered by Hertz. This regime is the region of the phase diagram at low temperatures and $r > 0$. To ensure we are in this regime, we require that the temperature does not become large when we reach scale λ_0. To find a condition for this, let us firstly set $T_0 e^{zs} = 0$ in equation 3.74 and use the low temperature form of the loop, *i.e.*, equation 3.65:

$$r(\lambda) = e^{2\lambda}\left(r_0 + \bar{A}\int_0^\lambda e^{-s(D+z-2)} ds\right), \tag{3.75}$$

where $\bar{A}$ is some constant. Enforcing $r(\lambda_0) = 1$ and solving for λ_0 allows us to find the quantum disordered region of the phase diagram when we further enforce that the renormalized

temperature $T(\lambda_0) \ll 1$. We obtain:

$$T_0 \ll \left| r_0 + \frac{\bar{A}}{D+z-2} \right|^{\frac{z}{2}} \equiv |r'|^{\frac{z}{2}} . \tag{3.76}$$

The line in the phase diagram where $T_0 \sim |r'|^{\frac{z}{2}}$ marks the crossover from the quantum disordered regime to the so-called *quantum critical regime*. We will consider this region of the phase diagram now.

Aspects of the phase diagram at higher temperatures can be inferred from the RG equations by enforcing that at a scale $\lambda = \lambda_0$, $T(\lambda_0) \gg 1$. Starting from a scale $T(\lambda) \sim 1$, defining a new variable $w = uT$ and employing equation 3.66 yields, for dimensions $D = 2$ and $D = 3$ and at the scale $r(\lambda_0) = 1$,

$$r(\lambda) = \lambda^2 \left(r' + E u_0 T^{1/\psi} \right), \tag{3.77}$$

with ψ being the *shift exponent*

$$\psi = \frac{z}{D+z-2}. \tag{3.78}$$

Physically, ψ describes the position of the finite-temperature phase transition T_c

$$T_c \sim (-r')^{\psi} \tag{3.79}$$

If at the scale $\lambda = \lambda_0$ $w(\lambda_0) \ll 1$, the Gaussian approximation holds true – this is the *Ginzburg criterion* [62]. At a scale $w(\lambda_0) \sim 1$ the approximation is invalid. This means that the line in the phase diagram $w(\lambda_0) = 1$ describes a region of classical criticality surrounding the finite temperature phase transition. This region becomes smaller as $T \to 0$ and only actually disappears at $T = 0$ implying that the actual phase transition is classical at **all** finite temperatures.

Finally, we consider the form of the correlation length ξ in various regions of the phase diagram. In the quantum disordered regime, using equation 3.65

$$\xi \sim |r'|^{-1/2}, \tag{3.80}$$

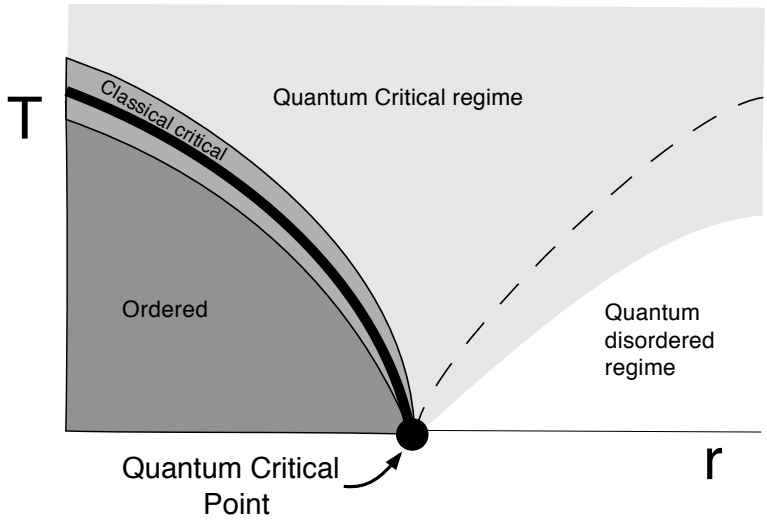

Figure 3.6: The phase diagram inferred from the solutions of the RG equations (discussed in the text) associated with Hertz-Millis theory in systems where $D+z>4$. The darkest region is the ordered phase and the other, lighter regions are characterised by differing solutions of the relevant equations. The dotted line through the quantum critical region represents a crossover in the behaviour of the correlation length.

and in the quantum critical regime, using equation 3.77

$$\xi \sim \frac{1}{\sqrt{r' + Eu_0 T^{1/\psi}}}. \tag{3.81}$$

The two terms in the argument of the square root of equation 3.81 can individually dominate in different areas of the quantum critical regime. This means the correlation length takes two differing forms in this regime: one high temperature form above the quantum critical point ($r \sim 0$) and another low temperature form away from it ($r \gg 0$) adjacent to the quantum disordered region.

The results from this section imply a generic phase diagram which is shown in figure 3.6

3.6.3 The free energy

The path of statistical mechanics begins with the partition function Z. From the partition function, through the free energy and its various derivatives, one can derive thermodynamic quantities of interest. We can write down the free energy of the Gaussian part of the action $S_G(\phi)$ in

terms of Z:

$$\beta F = -\ln Z, \tag{3.82}$$

where β is the usual inverse temperature and Z is given by the functional integral

$$Z = Z_0 \int \mathcal{D}\phi e^{-S_G(\phi)}. \tag{3.83}$$

Performing the Gaussian functional integral is straightforward:

$$Z = Z_0 \prod_{n,k} \mathcal{G}^{-1}_{\mathbf{k}n}, \tag{3.84}$$

as is writing down the free energy

$$F = F_0 + \frac{V}{\beta} \int \frac{d^D k}{(2\pi)^D} \ln \mathcal{G}_{\mathbf{k}n}. \tag{3.85}$$

Standard techniques [61] can turn the Matsubara summation into an integral. Thus, we obtain the Gaussian free energy density, let us call it F_G which takes the form

$$F_G = -\int_0^{\Lambda_k} \frac{d^D k}{(2\pi)^D} \int_0^{\Lambda_\omega} \frac{d\omega}{\pi} \coth\left(\frac{\omega\beta}{2}\right) \tan^{-1}\left(\frac{\omega/\Gamma_k}{r+\xi^2 k^2}\right). \tag{3.86}$$

In a similar way to above, one can find tree-level scaling equations for the free energy per unit volume. It is straightforward to see, given that only the differentials and not the arguments of the functions appearing in the free energy can rescale, that the RG flow equation must look like

$$\frac{dF}{d\lambda} = (D+z)\, F. \tag{3.87}$$

Corrections to equation 3.87 [50] give

$$\frac{dF_G}{d\lambda} = (D+z)\, F_G - f\,(T,r)\,, \tag{3.88}$$

where for low temperatures, and close to criticality ($r = 0$),

$$f\left(T,0\right) = f\left(0,0\right) + \gamma T^2 + \delta T^4, \tag{3.89}$$

with γ and δ constants, and for high temperatures above criticality ($r = 0$)

$$f\left(T,0\right) \sim T. \tag{3.90}$$

3.6.4 Thermodynamics

From the free energy, using a handful of simple relations, one can derive the properties of a number of thermodynamic quantities. Here we simply list the results of Hertz-Millis theory. No attempt is made to be rigorous, merely the leading order dependences are given. The results shown here are for the quantum disordered and quantum critical regimes of the generic phase diagram seen in figure 3.6.

The first quantity derived from the free energy F is the entropy S. Their relation is expressed via

$$S = -\frac{\partial F}{\partial T}. \tag{3.91}$$

The second temperature derivative of the free energy is the specific heat coefficient

$$\gamma = \frac{C}{T} \equiv \frac{\partial S}{\partial T} = -\frac{\partial^2 F}{\partial T^2} \tag{3.92}$$

where C is the specific heat.

An entity which is an experimental observable is $\alpha = \partial S/\partial r$. For quantum phase transitions where the control parameter is pressure p, α plays the rôle of the thermal expansion:

$$\alpha = \frac{\partial S}{\partial p}, \tag{3.93}$$

Table 3.1: Dependences of the specific heat coefficient, thermal expansion and Grüneisen parameter on temperature T and non-thermal control parameter r in the quantum disordered regime.

	$d = 2,\ z = 3$	$d = 3,\ z = 2$	$d = 3,\ z = 3$
γ	$r^{-1/2}$	$r^{1/2}$	$\ln \frac{1}{r}$
α	$Tr^{-3/2}$	$Tr^{-1/2}$	Tr^{-1}
Γ	r^{-1}	r^{-1}	$r^{-1} \left(\ln \frac{1}{r}\right)^{-1}$

and finally the quantity

$$\Gamma = \frac{\alpha}{C} \tag{3.94}$$

is known as the Grüneisen parameter [63].

Armed with the various thermodynamic relations, we can now proceed to consider the free energy in both the quantum disordered and the quantum critical regimes of the phase diagram for various values of D and z (for cases where $D+z > 4$) and produce a table listing the various leading order dependences. Firstly in the quantum disordered regime, see table 3.1:

In the high temperature quantum critical regime, table 3.2 lists the leading order low temperature behaviours of the quantities introduced above.

Table 3.2: Lowest order temperature dependences of the specific heat coefficient, thermal expansion and Grüneisen parameter in the quantum critical regime.

	$d = 2,\ z = 3$	$d = 3,\ z = 2$	$d = 3,\ z = 3$
γ	$T^{-1/3}$	$T^{1/2}$	$\ln \frac{1}{T}$
α	$\ln \frac{1}{T}$	$T^{1/2}$	$T^{1/3}$
Γ	$T^{-2/3} \ln \frac{1}{T}$	T^{-1}	$\left(T^{2/3} \ln \frac{1}{T}\right)^{-1}$

3.7 Summary

This chapter has been concerned with Hertz-Millis theory, the theory associated with the impact on the temperature-r phase diagram (where r tunes the quantum phase transition at zero temperature) due to the existence of quantum criticality in itinerant magnetic systems.

To begin with, it was necessary to introduce and discuss the fermionic functional integral

formalism (see §3.2), and the mathematics of Grassmann variables (§3.2.1) on which the formalism depends, which provides a method for writing down the many-particle partition function, a key quantity in statistical physics.

Aided with the partition function we proceeded to derive the Hertz-Millis action in §3.5, via a Hubbard-Stratonovich decoupling of the interaction and an expansion of the Lindhard function, which takes the form of an expansion in terms of the order parameter. Thus we arrived at equation 3.36.

In order to analyse the critical behaviour of the Hertz-Millis action (see §3.5), we employed the renormalization group (RG) technique (§3.4). As such, we introduced the three-step RG recipe which allowed us to derive a set of RG flow equations at the tree-level for all parameters of the action. The analysis of these equations (see §3.6) indicated that the upper critical dimension (usually given by $d_c^+ = 4$ in classical criticality) is reduced in quantum critical systems. This is one of the key results of the theory.

The tree-level RG flow equations were corrected at the level of one-loop diagrams (§3.5.2) and the solutions of the resulting equations, for various regions in the $T - r$ phase diagram (see figure 3.6 and §3.6.2), give rise to new sets of critical exponents (sections 3.6.3 and 3.6.4), which in general differ from those seen in classical critical systems. These critical exponents are given by tables 3.1 and 3.2.

We now turn to an application of this theory. In the next chapter we will consider the quantum critical behaviour of a three-dimensional itinerant ferromagnet's quantum-critical endpoint. We speculate on the theory's application to the material $ZrZn_2$.

Chapter 4

Hertz-Millis theory at a quantum-critical end-point

4.1 Introduction

In the previous chapter we discussed the Hertz-Millis treatment of quantum criticality in itinerant magnetic systems. Our discussion introduced nothing new and was kept general in terms of type of magnetic behaviour and the spatial dimension. In this chapter we will apply the theory to a quantum-critical end-point in a clean three-dimensional ferromagnetic system. This has previously been done in two-dimensions [43].

In §4.2 we will discuss how the RG equations, derived in the previous chapter, are to be solved for the case in hand. We pedagogically show how to compute the magnetic susceptibility, the free energy and the specific heat capacity in the vicinity of criticality.

One possible application of this analysis might be to the three-dimensional itinerant ferromagnet $ZrZn_2$, in §4.4 we review its properties. $ZrZn_2$ displays a first-order transition at low temperatures [64] and we assume this first-order nature can be suppressed to a quantum-critical end-point via the application of a magnetic field. In §4.5 we discuss the simplest mean-field theory to capture the phase diagram in question and use it to predict the experimental conditions under which the hitherto unreached quantum-critical end-point might be found.

4.2 Solving the RG equations

As described in Chapter Three, the RG flow equations are to be solved as followed: we start with an initial set of parameters, which have been set above by the mean-field analysis, and enforce that $r(\lambda) = 1$ in equation 3.72 to find a scale for λ. All quantities are to be calculated at this scale.

After finding λ, one can compute various quantities of interest and the method for doing this is described below. The process is performed numerically.

4.2.1 In the vicinity of criticality

Performing a mean-field analysis (see later in this chapter) gives rise to an expression for the magnetisation at the quantum-critical end-point, denoted m_c, and an expression for the required

magnetic field to be at that point, denoted h_c. We wish to explore the region around this point and so we can expand around around m_c. The result of doing this [43] is to replace the bare mass in the Gaussian term r with a new mass term which is given by

$$\delta = \left(\frac{4r}{m_c^2}\right)^{1/3} (3\delta h)^{2/3}, \tag{4.1}$$

where δh measures the applied magnetic field relative to the critical field

$$\delta h = \frac{h - h_c}{h_c}. \tag{4.2}$$

4.3 Computation and results

Having established the renormalization group equations to deal with the physics in the vicinity of quantum criticality in a three-dimensional, clean itinerant ferromagnet, we wish to move on to pedagogically discuss the computation of various physical observables. Here we describe the calculation of the magnetic susceptibility χ, the free energy F and specific heat capacity γ.

4.3.1 The susceptibility

We define the magnetic susceptibility to be the increase in magnetisation of a sample per unit applied magnetic field H.

$$m = \langle\phi\rangle = \chi H, \tag{4.3}$$

where $\langle\phi\rangle$ is the average magnetic moment of the sample. The average of any quantity x is computed via

$$\langle x\rangle = \frac{1}{Z}\int [\mathcal{D}\phi_k]\, x e^{\sum_k(-S(\phi_k))}, \tag{4.4}$$

where S is our renormalized action, containing our new theory's parameters. For our purposes we will use only the Gaussian term - all other coupling coefficients are irrelevant because of the RG process. Now, computing the average magnetic moment on a site means computing the

quantity $\langle\phi\rangle$:

$$\begin{aligned}\langle\phi\rangle &= \frac{1}{Z}\int [\mathcal{D}\phi_k]\,\phi_k e^{-\sum_k \phi_k\left(r+\xi^2k^2+\frac{\omega_k}{k}\right)\phi_k+h\phi_k} \\ &\approx \frac{1}{Z}\int [\mathcal{D}\phi_k]\,\phi_k\left(e^{-\sum_k \phi_k\left(r+\xi^2k^2+\frac{\omega_k}{k}\right)\phi_k}+h\phi_k e^{-\sum_k \phi_k\left(r+\xi^2k^2+\frac{\omega_k}{k}\right)\phi_k}\right) \end{aligned} \quad (4.5)$$

Computing the $k=\omega_k=0$ magnetic susceptibility amounts to calculating

$$\begin{aligned}\langle\phi_{k=0}\rangle &= \frac{1}{Z}\int [\mathcal{D}\phi]\,\phi\left(e^{-\phi r\phi}+h\phi e^{-\phi r\phi}\right) \\ &= \frac{1}{Z}\int [\mathcal{D}\phi]\,\phi e^{-\phi r\phi}+h\frac{1}{Z}\int [\mathcal{D}\phi]\,\phi^2 e^{-\phi r\phi} \end{aligned} \quad (4.6)$$

The first integral in equation 4.6 is zero. The second integral is the applied magnetic field

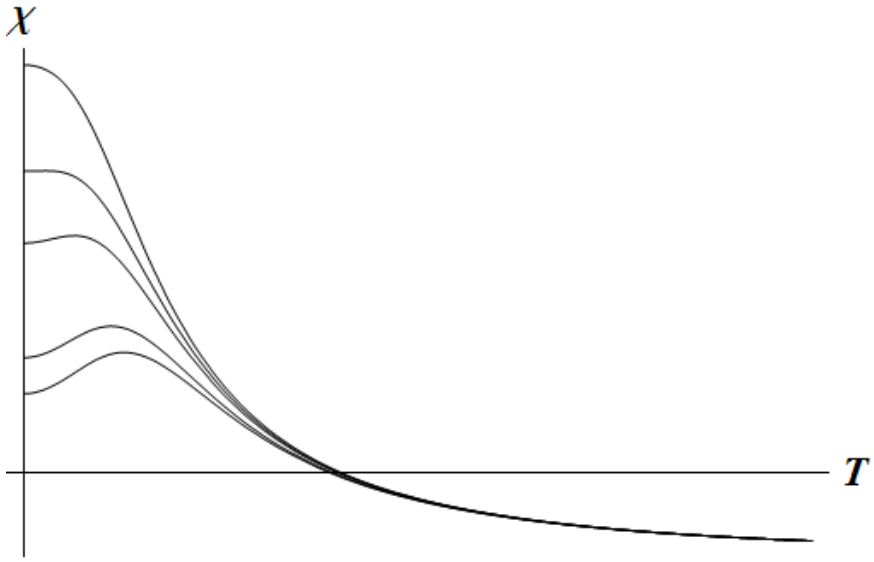

Figure 4.1: The temperature dependence of the magnetic susceptibility χ near a three-dimensional quantum-critical end-point. The uppermost curve is the result for an applied magnetic field close to the critical field whereas the lower curves are for fields away from criticality. Note that units are arbitrary.

multiplied by the average value of ϕ^2. We can calculate this integral and furthermore write down the susceptibility:

$$\chi = \frac{1}{Z}\int [\mathcal{D}\phi]\,\phi^2 e^{-\phi r\phi} \quad (4.7)$$

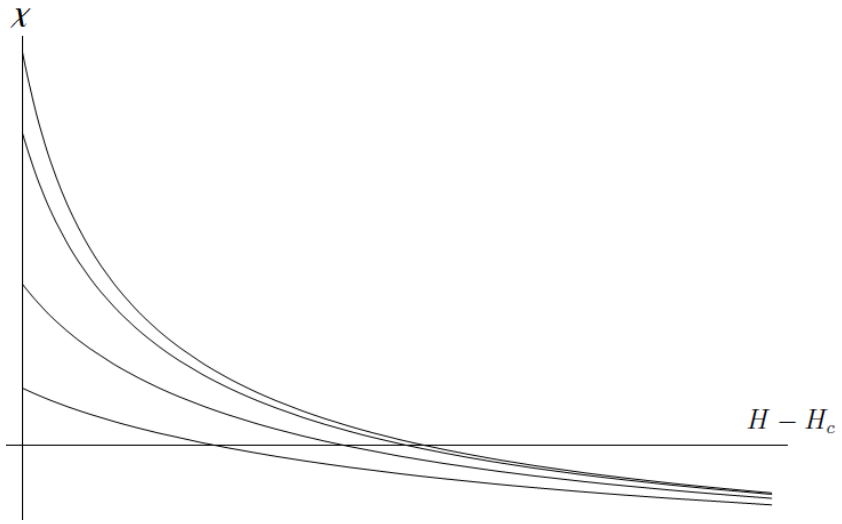

Figure 4.2: The dependence of the magnetic susceptibility χ on magnetic field (measured relative to the magnetic field to be at criticality) for a range of temperatures. The uppermost curve is the lowest temperature and as temperature is increased the curves flatten. Note that units are arbitrary.

Performing the functional integral is simple as it is Gaussian, therefore

$$\chi = r^{-1}. \tag{4.8}$$

Now by construction

$$1 = r(\lambda) \equiv re^{2\lambda} \tag{4.9}$$

and so we have that the susceptibility is given by

$$\chi(T, H) = e^{2\lambda}. \tag{4.10}$$

Depending on the temperature and applied magnetic field, the λ where $r(\lambda) = 1$ will vary, giving the susceptibility a temperature and magnetic field dependence.

Results for the magnetic susceptibility are shown in figures 4.1 and 4.2. Figure 4.1 shows the dependence on temperature for a variety of fields, beginning close to criticality (uppermost curve) and ending far from criticality (lowest curve). In a similar vein, figure 4.2 shows the magnetic field dependence of the magnetic susceptibility at a range of temperatures. The uppermost curve corresponds to the lowest temperature, for higher temperatures the curves flatten.

4.3.2 The specific heat capacity

We wish to determine a relation for the free energy associated with the Gaussian term in the action [50]. We write the Gaussian term as S_G

$$S_G = \int^{\Lambda} \int^{\Gamma} d^3k d\omega \left[\delta + \xi^2 k^2 + \frac{\omega_n}{k}\right] \phi^2, \tag{4.11}$$

where Λ and Γ are cuttoffs in momenta and frequency respectively, δ is mass term found above and is given by equation 4.1. We can now write down the simple statistical relation between the Gaussian free energy, F_G and the partition function associated with the Gaussian part of the action $\mathcal{Z}_G$:

$$\beta F_G = -\ln \mathcal{Z}_G. \tag{4.12}$$

Now we can write down the partition function, $\mathcal{Z}_G$, written as a functional integral:

$$\mathcal{Z}_G = \mathcal{Z}_0 \int \mathcal{D}\phi e^{S_G(\phi)}. \tag{4.13}$$

Due to the construction of S_G (we have only used the Gaussian part of the action) we can perform the path integral easily. This path integral is standard and its general form is given by

$$\int \mathcal{D}\phi e^{\mathcal{G}_{\mathbf{k}n}^{-1}\phi^2} = \prod_{n,k} \mathcal{G}_{\mathbf{k}n}, \tag{4.14}$$

and thus we have that

$$\mathcal{Z}_G = \mathcal{Z}_0 \prod_{n,k} \frac{1}{\delta + \xi^2 k^2 + \frac{\omega_n}{k}}. \tag{4.15}$$

So we can substitute equation 4.15 into equation 4.12 to find an expression for the Gaussian free energy:

$$\begin{aligned} F_G &= -\frac{1}{\beta}\ln \mathcal{Z}_0 \prod_{n,k} \frac{1}{\delta + \xi^2 k^2 + \frac{\omega_n}{k}} \\ &= -\frac{1}{\beta}\left(\ln \mathcal{Z}_0 + \ln \prod_{n,k} \frac{1}{\delta + \xi^2 k^2 + \frac{\omega_n}{k}}\right) \\ &= -\frac{1}{\beta}\ln \mathcal{Z}_0 - \frac{1}{\beta}\ln \prod_{n,k} \frac{1}{\delta + \xi^2 k^2 + \frac{\omega_n}{k}} \\ &\equiv F_0 - \frac{1}{\beta}\ln \prod_{n,k} \frac{1}{\delta + \xi^2 k^2 + \frac{\omega_n}{k}} \end{aligned} \tag{4.16}$$

Here we note that we treat momenta as being continuous and treat frequencies as discrete entities, each having a separate label n. We can move the logarithm into the product and replace the product sign with a summation sign to get

$$F_G = F_0 - \frac{V}{\beta}\int_0^\Lambda \frac{d^3k}{(2\pi)^3} \sum_n \ln\left(\frac{1}{\delta + \xi^2 k^2 + \frac{\omega_n}{k}}\right) \tag{4.17}$$

where V is the volume of the system. Performing the Matsubara summation [61]

$$\sum_n \ln\left(\delta + \xi^2 k^2 + \frac{\omega_n}{k}\right) \tag{4.18}$$

yields

$$\beta \int_{-k}^{k} \frac{d\omega}{\pi} n_B(\omega) \tan^{-1}\left(\frac{\omega/k}{\delta + \xi^2 k^2}\right), \tag{4.19}$$

which, when substituted into equation 4.17 gives

$$F_G = -V\int_0^\Lambda \frac{d^3k}{(2\pi)^3}\int_{-k}^{k} \frac{d\omega}{\pi} n_B(\omega) \tan^{-1}\left(\frac{\omega/k}{\delta + \xi^2 k^2}\right) \tag{4.20}$$

Note here that we have dropped F_0. To simplify the integration we can split the boson distribution function up into its odd and even parts. We do this via the relation

$$n_B(\omega) = \frac{1}{2}\left(\coth\left(\frac{\beta\omega}{2}\right) - 1\right) \tag{4.21}$$

The inverse tangent function is odd and so when we perform the frequency integral, over the even part of the Bose factor times the inverse tangent, we get zero. This leaves the odd part of the Bose function times the inverse tangent, which is even. Therefore we can halve the region of frequency integration and remove the factor of one half. We can write down the free energy associated with the Gaussian term of the action as

$$F_G = -V\int_0^{\Lambda}\frac{d^3k}{(2\pi)^3}\int_0^{k}\frac{d\omega}{\pi}\coth\left(\frac{\beta\omega}{2}\right)\tan^{-1}\left(\frac{\omega/k}{\delta+\xi^2k^2}\right). \tag{4.22}$$

This is the three-dimensional equivalent of equation A1 in reference [50].

The evaluation of the specific heat capacity follows straightforwardly from the usual statistical relation, *i.e.*, the second temperature derivative of equation 4.22.

$$\gamma = \frac{C}{T} = -\frac{\partial^2 F_G}{\partial T^2}. \tag{4.23}$$

Figure 4.3 shows the specific heat capacity for a variety of fields at the pressure required to be at the quantum-critical end-point. In these cases $\delta h = 0.00001, 0.001, 0.005$ and 0.01. δh is defined by equation 4.2.

4.3.3 Experimental application

Unfortunately very few systems exist that could provide a clear test of the theory developed above. Currently, the best candidate is the three-dimensional itinerant ferromagnet $ZrZn_2$. However, its quantum-critical end-point has never been found experimentally. In the next section we will discuss this material in some detail and speculate on the conditions for reaching quantum criticality.

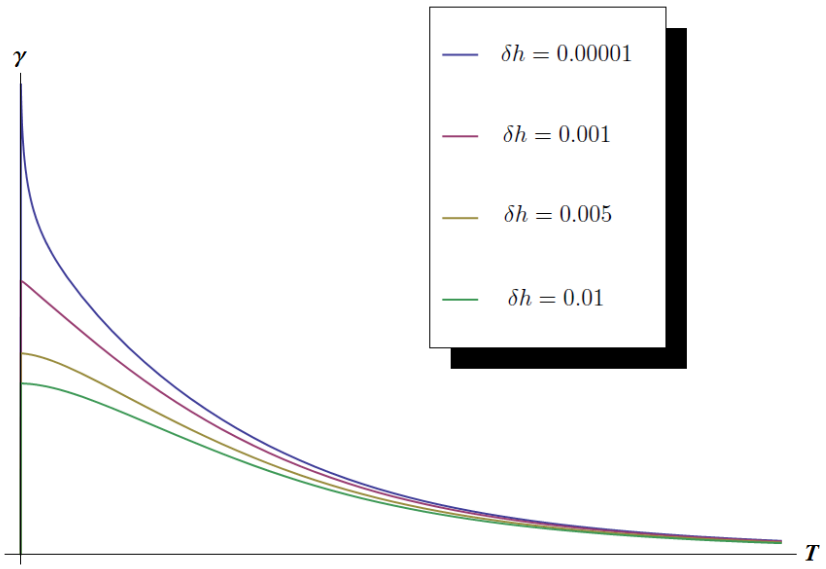

Figure 4.3: Plots of the dependence on magnetic field of the specific heat capacity versus temperature. The plots are taken at a number of values of δh (discussed in text) ranging from 0.00001, *i.e.*, close to criticality (this is the uppermost curve), to 0.01, *i.e.*, far from criticality (this is the lowest curve).

4.4 An overview of $ZrZn_2$

The itinerant ferromagnet $ZrZn_2$ was discovered in the late 1950's [66] and crystallises into the C15 Laves structure, see figure 4.4, with a lattice constant of $a \approx 7.4$Å. Both elemental zirconium and zinc fail to exhibit magnetic order making this compound out of the ordinary. Within the compound the zirconium atoms form a diamond structure and it is the existence of the overlap of their 4d orbitals which gives rise to the observed ordered magnetic moment of $\mu_0 = 0.17\mu_B$ per zirconium atom which extends across a sample.

Given its relatively low Curie temperature (Arrott plots give $T_C = 27.5$K [65]) and the fact its magnetic moment is far from saturation, even as far as fields of 35 T [64], one would classify $ZrZn_2$ as a weak itinerant ferromagnet. In ambient conditions, the observed disappearance of ferromagnetism is continuous, see the inset of the uppermost pane of figure 4.5.

In addition to temperature, it is an experimental observation that the ferromagnetism seen in $ZrZn_2$ is susceptible to pressure, its effect being to lower T_C, see middle pane (pane **b**) of figure 4.5. Initial studies indicated that subjecting $ZrZn_2$ to pressure, and for temperatures $T < T_C$, forced the system to undergo a second-order transition. However, with the advent of cleaner

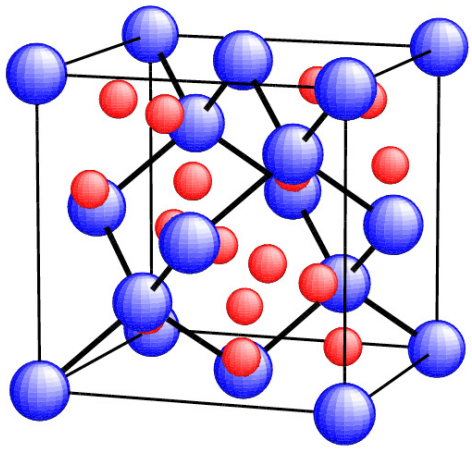

Figure 4.4: From [65]. Zirconium atoms (the larger spheres) form a diamond structure. The smaller spheres are zinc atoms. Together they form the C15 Laves structure in the compound $ZrZn_2$.

samples (residual resistivity ratio ≈ 100), studies of the order parameter [64] have shown that for low temperatures ($T < 5$K) the disappearance of the ordered moment is first-order in nature as the pressure on the system is passed through some critical value $p_1 \approx 16.7$kbar. This is illustrated in the topmost pane of figure 4.5. As such a second-order critical end-point separates the lines of first- and second-order transitions. It is the application of a magnetic field, in addition to further pressure, which drives this critical end-point to zero temperature. Thus we reach a quantum-critical end-point at a unique location in the zero-temperature phase diagram whose coordinates we denote with (p_c, h_c). A line of metamagnetic transitions links the zero-field, zero temperature transition at $p = p_1$ and the (hitherto unreached) quantum-critical-end-point, see lowest pane of figure 4.5. It is in the vicinity of this quantum-critical end-point that we take an interest. This paragraph is summarised in the phase diagram in figure 4.7.

Finally we discuss properties of the density of states inferred from angle-resolved de Haas-van Alphen studies [70]. In comparison with other d-band weak itinerant ferromagnets, such as iron or nickel, paramagnetic $ZrZn_2$ has its Fermi level situated in a region of large density of states and this situation in not changed upon transition into the ferromagnetic state owing to a small exchange splitting. This is illustrated in the density of states shown in figure 4.8. Usually, if there exists a high density of states at the Fermi energy then one might expect the system to superconduct. Despite initial reports claiming that this is the case for this material [71], the

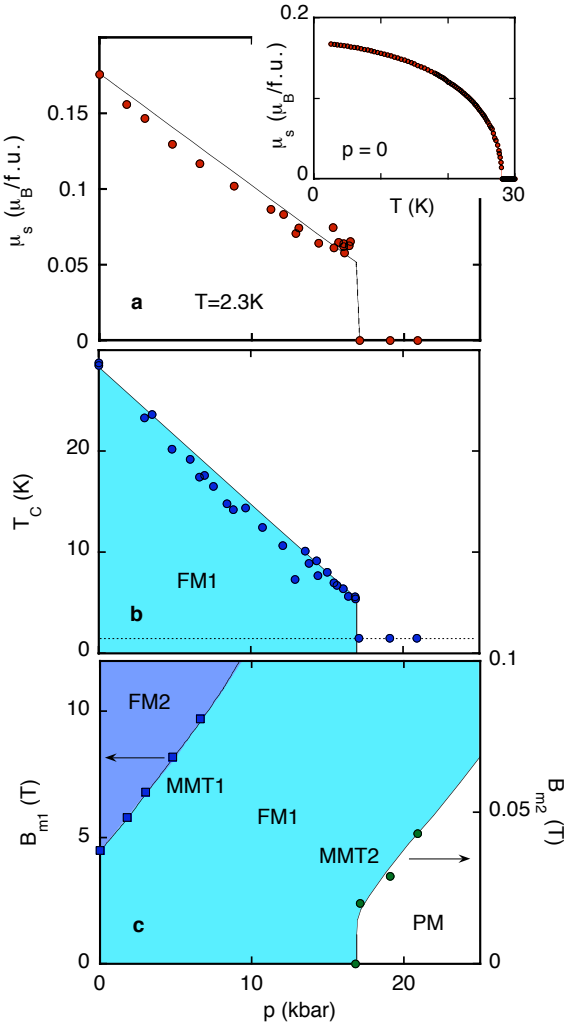

Figure 4.5: Experimental data on $ZrZn_2$ [64]. Pane **a** shows the abrupt disappearance of the magnetic moment at low temperature - a fist-order transition. Compare to the inset which shows a continuous transition at ambient pressure. Pane **b** shows the transition temperature as a function of the applied pressure and pane **c** shows the inferred zero-temperature pressure-magnetic field phase diagram.

observed superconductivity was later found to not exist [72].

4.5 Mean-field analysis, Landau theory

Here we put Hertz-Millis theory to one side and attempt to model $ZrZn_2$ via a simple Landau mean-field theory. Our intention is to use this theory to find some numerical values of parameters which could be inserted into the Hertz-Millis theory we have discussed. The most

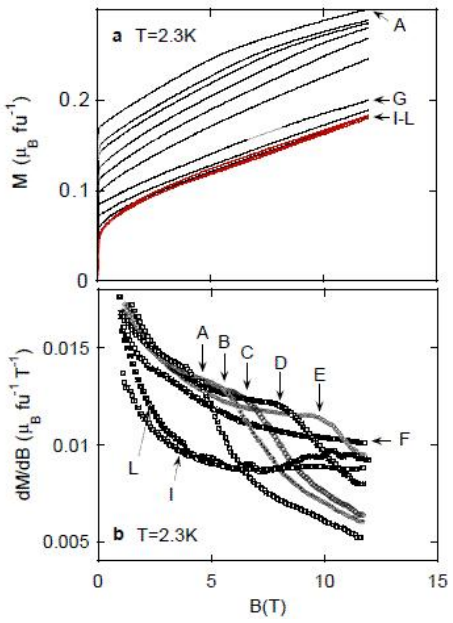

Figure 4.6: Experimental data from [64]. Pane **a** shows the low temperature dependence of the magnetisation as a function of the applied magnetic field for a range of pressures ranging from low (A) to high (L). For the same range of pressures, pane **b** shows the differential susceptibility at low temperatures.

elementary model one can write down[1], one that gives (at least) crude qualitative agreement with the zero temperature phase diagram, is a free energy within Landau theory:

$$F\left(m;p,h\right)=\frac{1}{2}r\left(p\right)m^{2}+\frac{1}{4}um^{4}+\frac{1}{6}vm^{6}-hm, \tag{4.24}$$

where dependence on pressure enters only via $r\left(p\right)$, u and v are constants which are to be found in what follows. h is the applied magnetic field. m is the order parameter and physically corresponds to the average magnetic moment $m\equiv\left\langle s_{z}\right\rangle$. As usual in Landau theory, the terms written down are only those which obey the symmetries of itinerant ferromagnetic systems and the physical state of the system is defined via the order parameter which is the global minimum of the free energy.

[1]Technically, this model is included in Hertz-Millis theory and is found by suppressing the order parameter's dependence on both space and imaginary time.

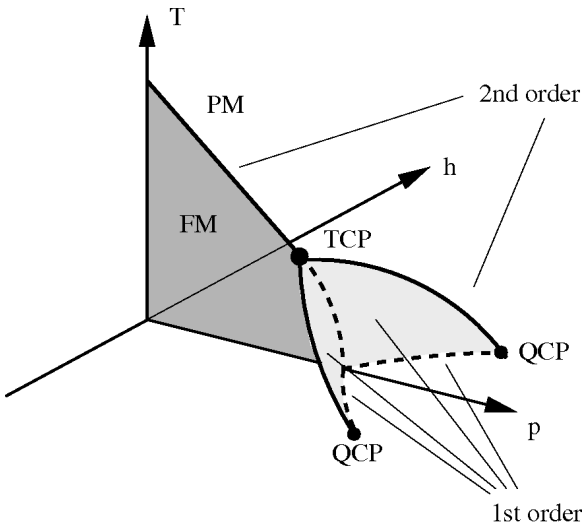

Figure 4.7: From [67]. The "fish-tail" phase diagram [68, 69] of $ZrZn_2$. At high temperatures the transition from a paramagnetic phase (PM) to ferromagnetic phase (FM) is second-order in nature. The situation is changed at low temperatures as the transition becomes first-order as pressure is varied. A tricritical point (TCP) separates the two different natures of transition. Application of a magnetic field (h) drives the TCP to the quantum-critical end-point (QCP) describing, in the process, two "wings" of first-order nature (lightly shaded areas) whose edges are a set of end-points.

4.5.1 The first-order transition

In zero applied magnetic field, one can cause a first-order (metamagnetic) transition by varying pressure alone, see figure 4.9. The condition for a first-order transition to occur must be $F = \frac{\partial F}{\partial m} = 0$ with $m \neq 0$. It can be shown straightforwardly [43] that this occurs if the parameters r, u and v satisfy

$$\frac{rv}{u^2} = \frac{3}{16}, \tag{4.25}$$

and that the magnetisation jump is given by

$$m = \sqrt{-\frac{4r}{u}}. \tag{4.26}$$

4.5.2 The quantum-critical end-point of transitions, $h \neq 0$

Application of a magnetic field means that the first-order nature of the transition is suppressed and with increasing field will eventually end up being continuous, see figure 4.10. The point at which the first-order transition becomes continuous is the quantum-critical end-point of first-

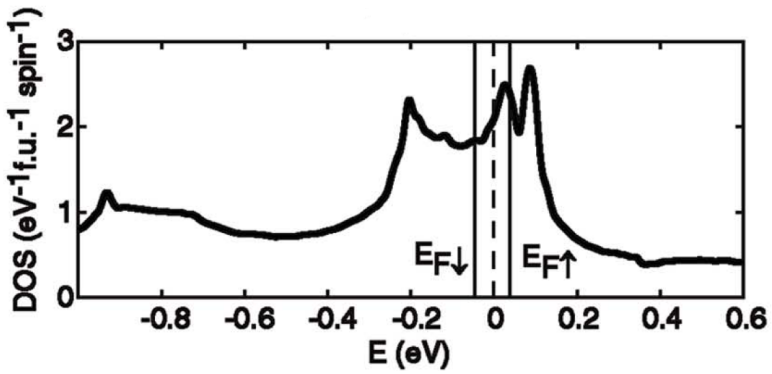

Figure 4.8: From [70]. Computed density of states of $ZrZn_2$ showing the Fermi-level (denoted by a dotted line) and its small shift when a transition to an ordered state takes place.

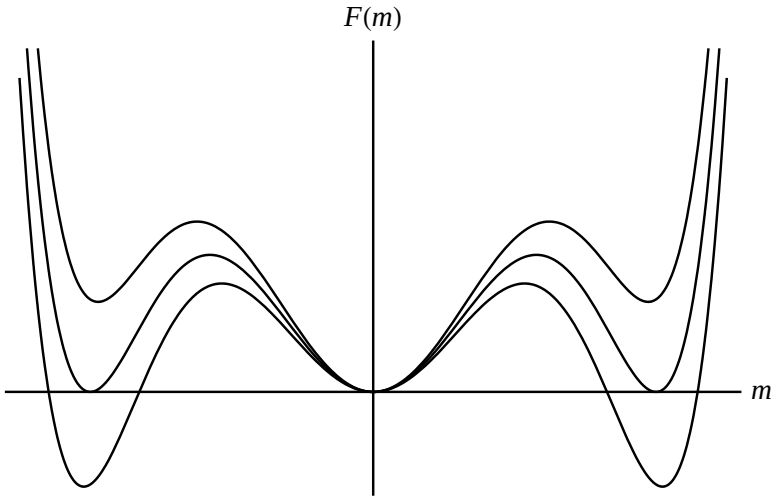

Figure 4.9: A graphical illustration of the first-order transition of the mean-field model given by equation 4.24. Lessening the pressure p via the parameter $r\,(p)$ allows the free energy curve's minimum, which is situated at $m = 0$ for high pressures (uppermost curve), to jump to some non-negative value as the curve passes through the horizontal axis.

order transitions. The point that this occurs at is when $\frac{\partial F}{\partial m} = \frac{\partial^2 F}{\partial m^2} = \frac{\partial^3 F}{\partial m^3} = 0$. From the third derivative of the free energy, one finds the magnetisation at the critical end-point m_c to be

$$m_c = \sqrt{-\frac{3u}{10v}}, \tag{4.27}$$

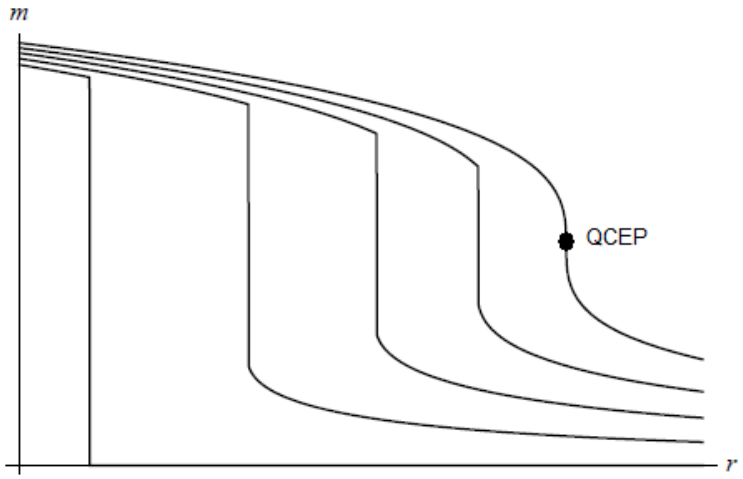

Figure 4.10: Graphical demonstration of the change of the order parameter m with variation of pressure via the parameter r. For zero applied magnetic field and fields $h < h_c$, varying pressure results in a first-order jump in order parameter magnitude. For $h = h_c$ (rightmost curve), the jump becomes continuous. This is a second-order end-point of first-order transitions.

and from the second derivative one finds the relationship between r, u and v required so that the system is at its the critical end-point to be

$$\frac{rv}{u^2} = \frac{9}{20}. \tag{4.28}$$

Finally, one can find the critical magnetic field from the first derivative of the free energy:

$$h_c = \frac{6}{25}\frac{u^2}{v}m_c = \frac{6}{25}\frac{u^2}{v}\sqrt{-\frac{3u}{10v}}. \tag{4.29}$$

4.5.3 Application to $ZrZn_2$

We can insert susceptibility and magnetisation data from experiment [64] into the mean-field theory discussed to predict the location in the zero temperature phase diagram of the quantum-critical end-point. Figure 4.6 would imply an estimate of $\chi \approx 0.01\mu_{\mathrm{B}}\mathrm{T}^{-1}$ and therefore

$$\chi^{-1} \approx 100\mathrm{T}\mu_{\mathrm{B}}^{-1}. \tag{4.30}$$

The magnetisation jump, given in plate **a** of figure 4.5, across the first-order transition is

$m \approx 0.05\mu_B$. Therefore, from equation 4.26 one finds

$$u = -40000\mu_{\mathrm{B}}^{-4}, \tag{4.31}$$

and from equation 4.25

$$v = 12 \times 10^6 \mu_{\mathrm{B}}^{-6}. \tag{4.32}$$

It follows that the values of r (in the units used here) at the first-order transition and at the quantum-critical end-point are $r_F = 25\mu_{\mathrm{B}}^{-2}$ and $r_Q = 60\mu_{\mathrm{B}}^{-2}$ respectively. Given that the first-order transition is experimentally observed at a pressure of 16.5kbar, it follows that the quantum-critical end-point will lie at extremely high pressures, giving a possible explanation for the fact it has yet to be reached experimentally. Finally, from equation 4.29 one can predict that the magnetic field required to tune $ZrZn_2$ to its quantum-critical end-point is

$$h_c \approx 1\mathrm{T}. \tag{4.33}$$

Unfortunately, despite the fact only a moderate field is required, it appears that very high pressures are needed to access the quantum-critical end-point. It has yet to be accessed experimentally.

4.6 Summary

In this chapter we have applied Hertz-Millis theory (which was discussed and developed in the previous chapter) to a clean, three-dimensional quantum-critical end-point in an itinerant ferromagnetic system. We followed this with a discussion of a potential test of the theory, the material $ZrZn_2$.

In §4.2 we briefly described how to solve the relevant renormalization group equations in the vicinity of quantum criticality. It was in §4.3 that we computed some experimental quantities and we took time to explain how to find the magnetic susceptibility (§4.3.1), the free energy and the specific heat capacity (§4.3.2). This has only been done for the two-dimensional case

before and hence our results, illustrated in figures 4.1, 4.2 and 4.3, are original.

In §4.4 we reviewed the material $ZrZn_2$ which is the best example of a three-dimensional system with a relevant quantum-critical end-point currently known. However, the quantum-critical end-point has yet to be reached experimentally. We introduced the experimental data relevant to discussions later in the chapter and, indeed, the rest of this thesis.

In order to describe $ZrZn_2$, we wrote down the simplest mean-field theory which incorporates its phase diagram: the appearance of a first-order transition (§4.5.1) and the quantum-critical end-point (§4.5.2). We applied this theory to $ZrZn_2$ and speculated on the conditions under which the quantum-critical end-point might be accessed (§4.5.3). We concluded that, despite requiring only a moderate applied field of approximately 1 T, the pressure required is very substantial. This possibly explains why the quantum-critical end-point has yet to be reached.

In the next chapter we will move away from this quantum-critical end-point and concentrate on the appearance of the first-order transition.

Chapter 5

First-order magnetic transitions in metals

5.1 Introduction

Thus far, this thesis has considered Hertz-Millis theory which treats the physics of metallic systems tuned to the vicinity of a magnetic quantum critical point.

Hertz-Millis theory assumed, from the outset, that the quantum phase transition involved is second-order in nature. As such, any application of the theory must **not** be to any system which displays first-order behaviour. An example of a system exhibiting a first-order transition, namely $ZrZn_2$, was discussed in the previous chapter.

The aim of this chapter is to discuss the appearance of this first-order transition. In order to do so we will concentrate on two separate theories, both purport to explain the phenomenon in question: one is a theory which incorporates soft-modes that were previously neglected in the Hertz-Millis treatment [67] and the other is an argument based on features of the density of states [73].

In §5.2 we discuss how the Lindhard function seen in Hertz-Millis theory must be corrected in order to include certain important modes that were previously integrated out. We will derive a new mean-field free energy which, it is claimed, correctly describes the physics on show. We show how it does give the correct phase diagram and check its conforms to the Clausius-Clapeyron condition. Finally we will apply the theory to $ZrZn_2$ (introduced in the previous chapter) and question its applicability to the material.

The second theory of the appearance of first-order transitions, one which uses features of the density of states, is discussed in §5.3. We will derive and analyse Stoner theory and investigate a variety of density of states features that may or may not give rise to a first-order transition. Once again we will comment on the applicability of this theory to $ZrZn_2$.

5.2 Non-existence of an expansion of the order-parameter

A conventional treatment of quantum-phase transitions would not differentiate them from classical transitions. One might construct a Landau-style free energy which is dependent on both

temperature T and some non-thermal parameter x,

$$F\left(T,x;m\right)=t\left(T,x\right)m^{2}+um^{4}-hm \tag{5.1}$$

and realise that regardless of the way one approaches the transition in $T-x$ space, the Landau exponents are always the same.

Furthermore, the basic premise of mean-field theory - *i.e.*, the assumption that the order-parameter's fluctuations are small and one is free to replace it with some average value m - becomes invalid in dimensions below the so-called *upper critical dimension* d_{c}^{+}. However, the scaling analysis in Chapter Three demonstrated that for a quantum phase transition the upper critical dimension is reduced by a factor z due to the necessary mixing of statics and dynamics. For a ferromagnetic system $z=3$ and hence both two- and three-dimensional systems are, it is claimed, described suitably by mean-field theory. However, as we will now see, the situation is not quite as straightforward as this reasoning would imply [51, 74, 67] and certain attempts to pursue the issue lead to a logarithmic correction term in equation 5.1.

5.2.1 Crucial soft modes

We approach the issue by reconsidering an assumption made in developing Hertz-Millis theory [27, 50]. The standard treatment, as a consequence of the nonchalant integrating out of the fermionic Grassmann fields, neglects the coupling of the order parameter to critical soft-modes in the system. These soft modes are particle-hole excitations in the spin-triplet channel. From a mathematical point of view, the coefficients of a canonical Landau-Ginzburg-Wilson free energy (which are simply numbers should this coupling be neglected, thus meaning the only modes considered are those associated with the order parameter [27]) will, in general, be given by divergent integrals. These divergences arise due to an effective long-range order parameter interaction in real-space. Evaluations of the coefficients using a diagrammatic approach [75] correct at second order in perturbation theory the usual Lindhard function as used by Hertz-Millis theory. One can write a corrected spin susceptibility down in terms of the Lindhard

function $\chi_0(\mathbf{k})$ and seven corrections

$$\begin{aligned}\chi(\mathbf{k}) &= \chi_0(\mathbf{k}) + \delta\chi(\mathbf{k}) \\ &= \chi_0(\mathbf{k}) + \sum_{m=1}^{7} \chi^{(m)}\end{aligned} \tag{5.2}$$

where the $\chi^{(m)}$'s are given by seven second order diagrams which are shown in figure 5.1. Performing these integrals gives the leading non-analytic term in three-dimensions, this takes

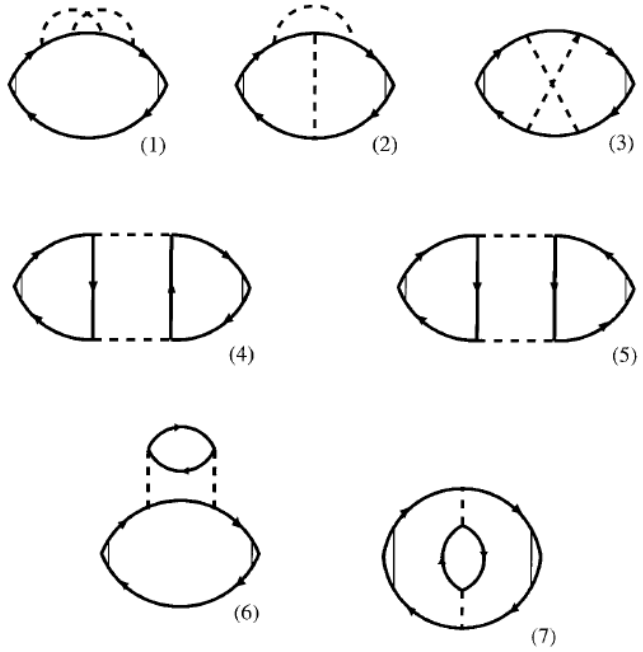

Figure 5.1: From [75]. The seven diagrams representing corrections to the Lindhard function. See equation 5.2.

the form

$$\delta\chi(\mathbf{k}) \sim \mathbf{k}^2 \ln\left(2k_f/|\mathbf{k}|\right), \tag{5.3}$$

where k_f is the Fermi momentum.

Furthermore, higher order terms too diverge, thus making the legality of an expansion in powers of the order parameter dubious.

5.2.2 Mean-field theory

So as not to leave out some potentially important physics, any theory must take into account the previously overlooked fermionic modes. To this end, one might begin with the partition function

$$Z = \int D\left[\mathbf{M}, q\right] e^{-\mathcal{A}(\mathbf{M},q)}, \tag{5.4}$$

where $\mathbf{M}$ is the field associated with fluctuations of the order parameter and q is the field describing the soft fermionic modes. The action takes the form

$$\mathcal{A}\left(\mathbf{M}, q\right) = \mathcal{A}_M\left(\mathbf{M}\right) + \mathcal{A}_q\left(q\right) + \mathcal{A}_{M,q}\left(\mathbf{M}, q\right), \tag{5.5}$$

where the terms are, respectively, that part of the action solely associated with the magnetisation, that part of the action solely associated with fermionic modes and that part which links the two. $\mathcal{A}_M\left(\mathbf{M}\right)$ is given by

$$\mathcal{A}_M\left(\mathbf{M}\right) = \int dx \left[\mathbf{M}\left(x\right)\left(t_0 - \nabla^2\right)\mathbf{M}\left(x\right) + s\mathbf{M}^4\left(x\right)\right] \tag{5.6}$$

and the **schematic** forms of the other two terms are

$$\mathcal{A}_q\left(q\right) = \int dxdy\Gamma\left(x - y\right) q\left(x\right) q\left(y\right) \tag{5.7}$$

and

$$\mathcal{A}_{\mathbf{M},q}\left(\mathbf{M}, q\right) = \int dx\mathbf{M}\left(x\right) q\left(x\right) + \mathbf{M}\left(x\right) q^2\left(x\right) + \cdots \tag{5.8}$$

It is possible to derive a resulting mean-field free energy which is given by

$$F\left(\mathbf{M}\right) = t\mathbf{M}^2 + u\mathbf{M}^4 \ln \mathbf{M}^2 + v\mathbf{M}^4, \tag{5.9}$$

where $\mathbf{M}$ is measured relative to some scale $\mathbf{M}_0$. As usual, the physical value of the order parameter $\mathbf{M}$ chosen by any system under scrutiny is that which minimises equation 5.9. The

appearance of the logarithmic term is a direct consequence of the modes previously neglected. Addition of a dependence on temperature T yields

$$F(\mathbf{M}) = t\mathbf{M}^2 + u\mathbf{M}^4 \ln\left(\mathbf{M}^2 + \frac{T^2}{T_0^2}\right) + v\mathbf{M}^4, \tag{5.10}$$

where temperature is measured relative to some microscopic temperature scale T_0 which we set to unity in what follows.

In the next part of this chapter we discuss the implications of this new mean-field theory.

5.2.3 General discussion of the phase diagram

Before an application of the mean-field free energy derived above, we briefly consider some of its features. It is clear that equation 5.10 differs from usual Landau theory, see equation 4.24, by a logarithmic term, and it is this term which includes the crucial effects not included in Landau theory.

Instantly it becomes clear that setting $T = 0$ in equation 5.10 gives rise to a negative term in the free energy for some value of m and that varying the quantity t via pressure **always** causes a first-order transition. Furthermore, it follows from this analysis that the first-order nature is a generic feature of all systems [67]. The first-order transition can be seen in plots of the free energy in figure 5.2. Analysis of equation 5.10 gives insight into the phase diagram at non-zero temperatures. It is clear that in this case the argument of the logarithm is never zero for any m and there exists some temperature, let us call it $T = T_{\text{tri}}$, above which the logarithmic term is never negative. This means that the quartic term of the free energy is always positive and the only type of transition that can occur is a second-order (continuous) one and this arises when the quantity t (which is now temperature dependent itself) becomes negative in some way.

Finally, application of a magnetic field h introduces further physics. We assume that we can add a term to the free energy of the form

$$\delta F = -hm, \tag{5.11}$$

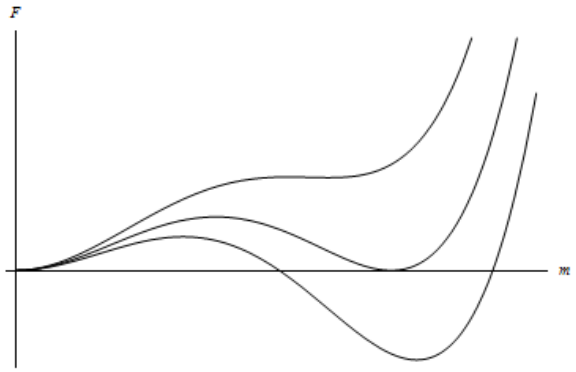

Figure 5.2: The free energy given by equation 5.9 plotted against magnetisation. Varying the parameter t, by pressure say, causes the first-order transition as the minimum at non-zero m is dragged below the $F = 0$ axis. For low (or even negative) t there exists a situation resembling the lower curve whose minimum is some $m \neq 0$, this is the ordered state. For high t the situation resembles the upper curve whose minimum is at $m = 0$, this is the unordered state. The point at which the first-order transition takes place is that where the curve's minima all touch the $F = 0$ axis, this is depicted in the middle curve.

which is consistent with derivation [76, 77].

In a similar vein to the Landau theory considered in Chapter Three, the application of a field has the effect on the zero-temperature phase diagram of suppressing the first-order transition. With increasing magnetic field, the size of the jump in magnetisation lessens until a quantum-critical end-point is reached. This is seen in figure 5.3. The details discussed here give the phase

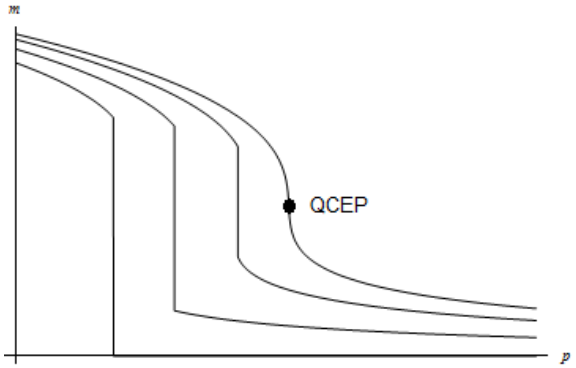

Figure 5.3: Analysis of the free energy of equation 5.9 gives rise to a quantum-critical end-point. For low applied magnetic fields there exists a jump in the order parameter as pressure is varied (the three leftmost curves). This situation comes to an end at a critical value of applied magnetic field $h = h_c$ (rightmost curve), this is the first point where the transition is suppressed to one of continuous nature as the pressure is increased.

diagram shown in figure 4.7.

5.2.4 The Clausius-Clapeyron condition

Having discussed the most basic aspects of the phase diagram associated with equation 5.10, here we further analyse some features of the phase diagram and compare to some experimental data from the material $ZrZn_2$ discussed in the previous chapter. We have demonstrated that for low temperatures and small applied magnetic fields, equation 5.10 predicts a first-order transition. It is well known that at such phase boundaries the two phases on either side are in equilibrium and therefore their Gibbs free energies are equal. From this fact one can derive the Clausius-Clapeyron condition, see for example [78, 62], which gives the slope of the curve of the phase boundary in the temperature-pressure phase diagram to be

$$\frac{dp}{dT} = \frac{\Delta S}{\Delta V}, \tag{5.12}$$

where V is volume and ΔS is the change of entropy associated with the transition. As we are considering a transition from one state at zero-temperature to another, from Nernst's theorem [78] which states that

$$\lim_{T \to 0} S \to 0, \tag{5.13}$$

we expect ΔS to be zero. So as the transition temperature tends to zero

$$\frac{dp}{dT} = 0, \tag{5.14}$$

which is to be expected from equations 5.12 and 5.13. This implies that the line of first-order transitions in the zero-field phase diagram of equation 5.10 necessarily **has** to touch the zero temperature axis at a right-angle. Here we prove that it does.

Let us make the ansatz that in equation 5.10 the coefficient of m^2 has the dependence on temperature and pressure such that

$$t\left(T, p\right) = \frac{p - p_c}{p_c} + \frac{T^2}{T_c^2} \tag{5.15}$$

where p_c denotes the point on the zero temperature axis of the phase diagram that is the continuation of the line of continuous transitions. $p_c < p_1$ where p_1 is the location of the first-order transition at $T = 0$. T_c is the temperature at which the continuous transition occurs at ambient pressure and is measured relative to T_0, which is discussed above. This choice, which is arbitrary, is not too unrealistic when compared to experimental data, see pane **b** of figure 4.5. For convenience, let us write $\beta = 1/T_c^2 > 0$. The free energy looks like

$$F(m) = \left(\frac{p - p_c}{p_c} + \beta T^2\right) m^2 + u m^4 + v m^4 \ln\left(m^2 + T^2\right). \tag{5.16}$$

The condition for a first-order transition (see figure 5.2 and its caption) is

$$F(m) = \frac{\partial F}{\partial m} = 0, \tag{5.17}$$

and this gives the two equations

$$\begin{aligned} \left(\frac{p - p_c}{p_c} + \beta T^2\right) m^2 + u m^4 + v m^4 \ln\left(m^2 + T^2\right) &= 0, & (5.18)\\ 2\left(\frac{p - p_c}{p_c} + \beta T^2\right) m + 4 v m^3 \ln\left(m^2 + T^2\right) + \frac{2 v m^5}{m^2 + T^2} + 4 u m^3 &= 0. & (5.19) \end{aligned}$$

We can deal with the logarithm by making the replacement

$$\ln\left(m^2 + T^2\right) \approx \ln m^2 + \frac{T^2}{m^2}, \tag{5.20}$$

which is valid for small T/m, and we deal with the term involving $\left(m^2 + T^2\right)^{-1}$ by making the replacement (which, too, is valid for small T/m)

$$\frac{1}{m^2 + T^2} \approx \frac{1}{m^2}\left(1 - \frac{T^2}{m^2}\right). \tag{5.21}$$

Substituting these expressions into equations 5.18 and 5.19 yields

$$t\left(T,p\right)+um^{2}+vm^{2}\ln m^{2}+vT^{2} = 0 \quad (5.22)$$

$$t\left(T,p\right)+2vm^{2}\ln m^{2}+vT^{2}+2um^{2}+vm^{2} = 0, \quad (5.23)$$

and subtracting one equation from the other gives a value for the magnetisation jump across the first order transition:

$$m^{2}=e^{-\left(\frac{u}{v}+1\right)}. \quad (5.24)$$

We can now substitute equation 5.24 into 5.22 to get

$$p=-k-p_{c}\left(\beta+v\right)T^{2}, \quad (5.25)$$

where

$$k=-p_{c}\left(1+ve^{-\left(\frac{u}{v}+1\right)}\right) \quad (5.26)$$

is a measure of the distance along the pressure axis of the first-order transition from p_c.

Differentiating equation 5.26 with respect to temperature gives

$$\frac{dp}{dT}=-2p_{c}\left(\beta+v\right)T \quad (5.27)$$

which tends to zero as $T\rightarrow 0$. This is in accordance with the condition given above by equation 5.14 and therefore the Clausius-Clapeyron equation is satisfied.

5.2.5 The tricritical point

Equation 5.16 dictates that the phase diagram at zero applied magnetic field consists of a line of first-order transitions at low temperatures which join to a line of continuous transitions at higher temperatures. The end-point of first-order transitions, the point at which behaviour becomes continuous, is to be referred to as the *tricritical point*. Here we look to pinpoint its location in the phase diagram and work out some details of the phase diagram around it.

Given its definition, the tricritical point occurs along the line represented by $t\left(T,p\right)=0$ and at the point where $f\left(m\right)=f'\left(m\right)=0$. If we denote the temperature where the tricritical point occurs as T^{*}, then it is true that the following conditions must be satisfied

$$vm^{4}\ln\left(m^{2}+T^{*2}\right)+um^{4} = 0 \tag{5.28}$$

$$4vm^{3}\ln\left(m^{2}+T^{*2}\right)+\frac{2vm^{5}}{m^{2}+T^{*2}}+4um^{3} = 0. \tag{5.29}$$

Solving for m gives

$$m=\sqrt{e^{-u/v}-T^{*2}}, \tag{5.30}$$

and hence

$$T^{*}=e^{-\frac{u}{2v}}, \tag{5.31}$$

in units of T_0. As we know that T^{*} must satisfy $t\left(T^{*},p^{*}\right)=0$, we can in principle find the pressure coordinate of the tricritical point p^{*}.

5.2.6 Discussion of the shape of the phase diagram

If one were to logically consider the mean-field free energy given by equation 5.16 and to ask under what circumstances certain transitions can occur, one would come to the conclusion that the low-temperature first-order transition can only occur given the conditions $t\left(T,p\right)>0$ and the fourth order logarithmic term sufficiently negative to "drag" any plot of the free energy below the axis, see figure 5.2. A first-order transition can **never** occur at any part of the phase diagram where $t\left(T,p\right)<0$: the transition will always be continuous were the fourth order term to be altered. Therefore we must conclude that a line of first-order transitions must pass through that part of the phase diagram where $t\left(T,p\right)>0$, *i.e.*, lying outside of the line of continuous transitions and its continuation. The situation has to resemble figure 5.4.

Keeping this reasoning in mind, let us compare with an experimental result. Figure 5.5 shows a detail taken from data from $ZrZn_2$ in figure 4.5 [64]. We can see, comparing it to figure 5.4, that for the case of $ZrZn_2$, the first-order transition appears to live below the continuous

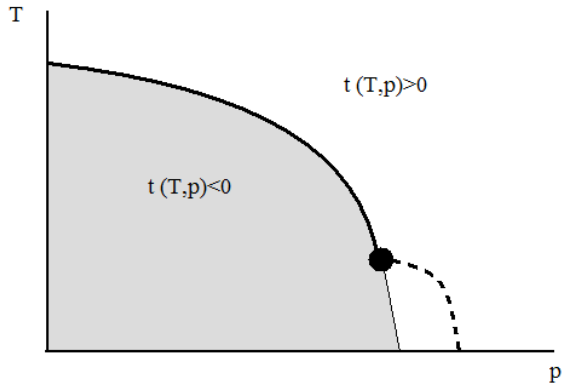

Figure 5.4: The phase diagram inferred from equation 5.16. The thick line denotes points of continuous transitions, this is where the quantity $t\left(T,p\right)$ changes sign from positive to negative (shaded region). Its continuation to zero temperature is denoted by the thinner line. The dashed line denotes points of first-order transitions and, as discussed in the text, must live in the unshaded region to be of that nature.

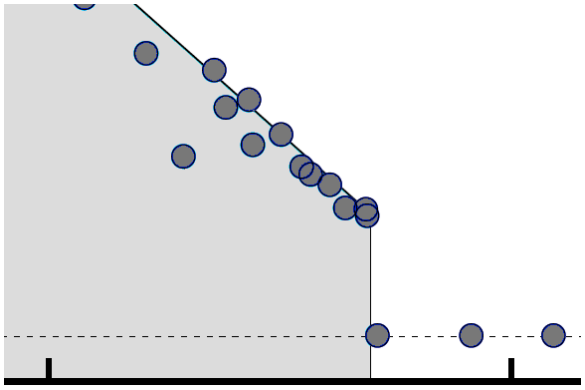

Figure 5.5: Detail from pane **b** of figure 4.5.

transition. This brings the ability of equation 5.16 to describe such a system into question.

5.2.7 Application to $ZrZn_2$

In Chapter Two we used the simplest possible Landau free energy to model $ZrZn_2$ and predict certain properties of the zero-field and zero temperature phase diagrams. We now move on to repeat this procedure, only now with the free energy given by

$$F\left(m\right)=-hm+tm^{2}+vm^{4}\ln\left(m^{2}+T^{2}\right)+um^{4}. \tag{5.32}$$

We assume that u and v are positive constants and that t is allowed to vary (via temperature or pressure) in value. The corresponding equation of state is given by

$$h = 2tm + 4vm^3 \ln\left(m^2 + T^2\right) + \frac{4vm^5}{m^2 + T^2} + 4um^3. \tag{5.33}$$

We recreate some results, and amend others, that are found in the literature [67]. To begin with, we consider the situation when the applied magnetic field is zero, $h = 0$:

$$F(m) = tm^2 + vm^4 \ln\left(m^2 + T^2\right) + um^4. \tag{5.34}$$

Using the condition for a first-order transition, equation 5.17, allows us to calculate the jump in magnetisation across the transition at $T = 0$ which is given by

$$m_1 = e^{-1/2} e^{-u/2v}. \tag{5.35}$$

This, when substituted into the equation of state, equation 5.33, gives the corresponding value of the parameter t at the transition, which we call t_1 to be

$$t_1 = ve^{-1} e^{-u/v}. \tag{5.36}$$

Imagine now that we apply a magnetic field, $h \neq 0$. As discussed previously, this has the effect of suppressing the first-order transition - reducing the jump in magnetisation until the transition becomes continuous, see figure 5.2. The point at zero-temperature at which the transition first becomes continuous is called the quantum-critical end-point. Let us say that this occurs at a value of the magnetisation $m = m_c$, at a value of the parameter $t = t_c$ and at a value of the applied field $h = h_c$. At this point equation 5.32 satisfies

$$f'(m_c) = f''(m_c) = f'''(m_c) = 0. \tag{5.37}$$

This gives the set of equations

$$\begin{aligned} 2t_c m_c + 4vm_c^3 \ln m_c^2 + 2vm_c^3 + 4um_c^3 &= h_c & (5.38)\\ 2t_c + 12vm_c^2 \ln m_c^2 + 14vm_c^2 + 12um_c^2 &= 0 & (5.39)\\ 24vm_c \ln m_c^2 + 52vm_c + 24um_c &= 0. & (5.40) \end{aligned}$$

Solving equation 5.40 gives either $m_c = 0$ or

$$m_c = e^{-13/12} e^{-u/2v}, \tag{5.41}$$

which when substituted into equation 5.39 yields

$$t_c = 6vm_c^2 = 6ve^{-13/6} e^{-u/v}. \tag{5.42}$$

Finally, use of both equation 5.41 and 5.42, along with equation 5.38 gives

$$h_c = \frac{16}{3} ve^{-13/4} e^{-3u/2v}. \tag{5.43}$$

We can now use data from experimental measurements to place values on the parameters mentioned here. At the quantum-critical end-point, the inverse susceptibility is given by

$$\frac{\partial h}{\partial m} \equiv \chi^{-1} = 2t_c + 12vm_c \ln m_c^2 + 14vm_c^2 + 12um_c^2, \tag{5.44}$$

which can be rewritten using 5.42 as

$$\chi^{-1} = 14vm_c^2. \tag{5.45}$$

This, in turn, allows us to rewrite h_c in terms of χ^{-1} and m_1, given by equation 5.35, as

$$h_c = \frac{8}{21} \chi^{-1} e^{-7/12} m_1 \tag{5.46}$$

which differs from the corresponding result in [67].

Using experimental data [64], we can estimate a value for the magnetic field required to drive the system to its quantum-critical end-point. Susceptibility measurements from figure 4.6 and magnetisation data from plate **a** of figure 4.5 give $\chi \approx 0.01\mu_{\rm B}$ and $m_1 \approx 0.05\mu_{\rm B}$. Therefore, from equation 5.46

$$h_c = 0.05 \cdot \frac{8}{21} \cdot \frac{1}{0.01} e^{-7/12} \approx 1\mathrm{T}, \tag{5.47}$$

which is in agreement with equation 4.33, but differs by an order of magnitude from that found by other workers – for example reference [67] finds $h_c = 0.1$T.

From equation 5.35, one can infer that $u \approx 5v$ and this allows us to compute, from equation 5.41, m_c to be

$$m_c = 0.03\mu_{\rm B}. \tag{5.48}$$

It quickly follows from equation 5.43 that

$$v \approx 7000\mu_{\rm B}^{-4}, \tag{5.49}$$

and that therefore

$$u \approx 5v = 35000\mu_{\rm B}^{-4}. \tag{5.50}$$

5.3 Features of the density of states

So far in this chapter we have discussed a theory that predicts the appearance of a first-order quantum phase transition, and subsequently the existence of a quantum-critical end-point of such transitions, based on the effects of soft particle-hole excitations which, it has been argued, exist generically in all itinerant ferromagnetic materials. These effects are independent of any features of the band structure.

Here we consider a simpler, yet competing, theory [36, 73, 79] which does depend on features of the band structure which enter the theory straightforwardly via the density of states. We discussed the Stoner model in §2.4.5 and commented on its apparent breakdown at higher

temperatures. Here we show a derivation and use the resulting free energy to analyse the zero temperature phase diagram's various transitions. As we will see, first-order magnetic transitions can be predicted depending on the topology of the density of states.

5.3.1 Derivation of the Stoner free energy

The starting point for Stoner theory is to apply the Hartree-Fock approximation to the single-band Hubbard model which is given by equation 2.33. In this approximation, we imagine that an electron in the band feels some "mean-field" (therefore this field is independent of the electron's wave-vector) from all other electrons. The mean-field depends on the total magnetisation of the system M and any applied magnetic field h. As such, a single electron's total energy is given by

$$E_{k\sigma} = \epsilon_k + \sigma\Delta, \tag{5.51}$$

where $\sigma = \pm 1$ is the electron's spin orientation (up or down) and half[1] of the band splitting Δ is given by

$$\Delta = IM + \mu_{\mathrm{B}} h. \tag{5.52}$$

Here I is the value of the usual Hubbard U divided by the number of atomic sites in our sample N_0.

The total number of electrons and the overall magnetisation of the system are given, respectively, by

$$N = \int d\epsilon \rho(\epsilon) \left[f(\epsilon - \Delta) + f(\epsilon + \Delta) \right] \tag{5.53}$$

and

$$M = \frac{1}{2} \int d\epsilon \rho(\epsilon) \left[f(\epsilon - \Delta) - f(\epsilon + \Delta) \right]. \tag{5.54}$$

Here $f(x)$ is the usual Fermi-Dirac distribution function, explicitly given by

$$f(x) = \left[\exp(x - \mu)/T + 1 \right]^{-1}, \tag{5.55}$$

[1] The actual band splitting is 2Δ

and it is the appearance of this function which gives rise to a temperature dependence of the Stoner model.

Writing down a mean-field (or Hartree-Fock) free energy amounts to computing the quantity

$$F\left(M,T\right)=\Omega_0+\mu N\left(M,t\right)-IM^2-hM \tag{5.56}$$

where Ω_0 is the grand canonical potential for the non-interacting system (*i.e.*, $I=0$) and is given by

$$\Omega_0\left(\mu,M,T\right)=-T\sum_\sigma\int d\epsilon\rho\left(\epsilon\right)\ln\left(1+\exp\left[-\left(\epsilon+\sigma\Delta-\mu\right)/T\right]\right)+2\Delta M. \tag{5.57}$$

Manipulation of equations 5.56 and 5.57, along with the employment of the standard Sommerfeld expansion [30], allows us to write down the free energy at, in principle, any finite temperature.

$$F\left(M,T\right)=F_0\left(0,T\right)+\left(\frac{1}{2\chi\left(T\right)}-I\right)M^2+\frac{\omega\left(T\right)}{4}M^4+\cdots-hM, \tag{5.58}$$

with

$$\chi\left(T\right)=\frac{1}{2}\rho\left(\epsilon_F\right)\left(1-\frac{\alpha\pi^2}{6}T^2+\cdots\right), \tag{5.59}$$

and

$$\omega\left(T\right)=\frac{\beta}{\rho\left(\epsilon_F\right)^3}\left(1+\frac{\gamma\pi^2}{6}T^2+\cdots\right). \tag{5.60}$$

Here

$$\beta=\left(\frac{\rho'\left(\epsilon_F\right)}{\rho\left(\epsilon_F\right)}\right)^2-\frac{\rho''\left(\epsilon_F\right)}{3\rho\left(\epsilon_F\right)} \tag{5.61}$$

is a quantity which, we will see, is of some importance and α and γ are other functions of the density of states and its derivatives evaluated at the Fermi energy.

Setting the temperature to zero in equations 5.58, 5.59 and 5.60 means the zero temperature

Stoner free energy looks like

$$F(M,0) = \left(\frac{1}{2\chi(0)} - I\right) M^2 + \omega(0) M^4 + \cdots - hM, \tag{5.62}$$

where

$$\chi(0) = \frac{1}{2}\rho(\epsilon_F), \tag{5.63}$$

and

$$\omega(0) = \frac{1}{\rho(\epsilon_F)^3}\left[\left(\frac{\rho'(\epsilon_F)}{\rho(\epsilon_F)}\right)^2 - \frac{\rho''(\epsilon_F)}{3\rho(\epsilon_F)}\right]. \tag{5.64}$$

We have established a free energy which represents Stoner theory, which we propose describes itinerant ferromagnetism. In principle, this theory can be analysed to give results for both finite and zero temperatures. It is well known that the theory fails to suitably describe some systems at finite temperatures whereas the zero temperature model is more reliable [36]. In the next section we will analyse the phase diagram at zero temperature.

5.3.2 Analysis of the zero temperature, zero field Stoner model

Let us investigate the Stoner model at zero temperature, described by the free energy of equations 5.62, 5.63 and 5.64, in zero applied magnetic field $h = 0$. We wish to investigate how different features of the density of states give rise to phase transitions of various nature in our system. We imagine that changing the applied pressure of our system will vary the exchange constant I and we also allow the Fermi energy to change, that is in order to vary the parameter $\rho(\epsilon_F)$. As is always the case for models such as this, the value of the magnetisation (the order parameter) is the one which minimises the free energy.

A second-order (or continuous) transition into an ordered ferromagnetic state occurs when the coefficient of the term of lowest order in M changes sign from positive to negative. This is the Stoner criterion for ferromagnetism:

$$I\rho(\epsilon_F) > 1. \tag{5.65}$$

Furthermore, a first-order transition into the ordered state can be achieved when the term of order M^2 is positive and the term of order M^4 is sufficiently negative to drag the free energy curve negative. The value of the order parameter at the curve's minimum must therefore jump discontinuously from $m = 0$ to some non-zero value.

Enforcing the necessary conditions for the onset of a first-order transition, namely inquiring where $F'(m) = 0$, $F(m) < 0$ and ensuring that $I\rho(\epsilon_F) < 1$ leads to the condition for a first-order transition [79] to be:

$$\rho(\epsilon_F)\,\rho''(\epsilon_F) > 3\left(\rho'(\epsilon_F)\right)^2. \tag{5.66}$$

Let us consider some generic cases where equation 5.66 would hold true. Firstly it is clear that in situations where the Fermi energy lies at a region of high density of states (and where the locality is sufficiently curved, a point we will consider shortly), the inequality would hold. For example, the Fermi energy might fall close to a van Hove singularity. This is thought to be the case in the multi-layer ruthenates, those materials whose chemical formula takes the form $Sr_{n+1}Ru_nO_{3n+1}$ [73].

A second scenario where equation 5.66 might be satisfied is if the Fermi energy lies in some local minimum (that is, some region of positive curvature) which itself resides at a high density of states. This is claimed [73] to be the case in MnSi. See figure 5.6.

In the next few sections, we will consider condition 5.66 more closely. We will investigate various features of the density of states that may or may not give rise to first-order transitions.

5.3.3 Approach to a van Hove singularity

It is claimed that systems whose Fermi energy lies close to a van Hove singularity would display a first-order transition at zero temperature. Let us make the ansatz that the density of states diverges as an inverse power law:

$$\rho(x) = \frac{1}{x^n}, \tag{5.67}$$

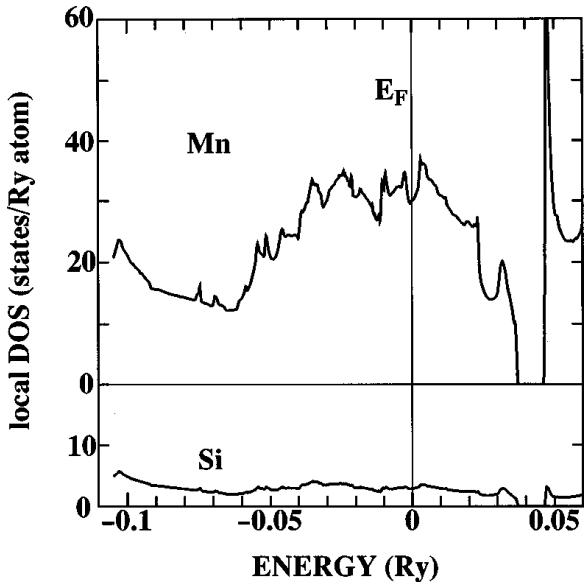

Figure 5.6: From [80]. The calculated local density of states of MnSi. The Fermi energy lies at a (high) local minimum in the density of states which, it is claimed, is the explanation in Stoner theory of a first-order transition.

where x labels the position of the Fermi energy and the van Hove singularity lies at $x = 0$. It is assumed from the outset that $n > 0$.

Now from condition 5.66, it is straightforward to show that a requirement on n, *i.e.*, the severity of the divergence, is

$$n^2 - \frac{1}{3} n\,(n+1) < 0. \tag{5.68}$$

This in turn implies that

$$n < 1/2. \tag{5.69}$$

Figure 5.7 shows plots of $\omega\,(x)$ for a number of values of n. All plots lying below the horizontal axis are for values of n that are less than $1/2$ and give rise to the possibility of a first-order transition. All those lying above the horizontal axis are for values of n that are greater than $1/2$, no first-order transition can occur in such scenarios.

Therefore, only weak power laws give rise to a first-order transition. This is clearly due to the limitations on the curvature of higher powers: in such cases it tends to zero for high values of the density of states, for example as the van Hove singularity is approached. For the situations where $n < 1/2$, the generic phase diagram is pictured in figure 5.8. The figure shows both

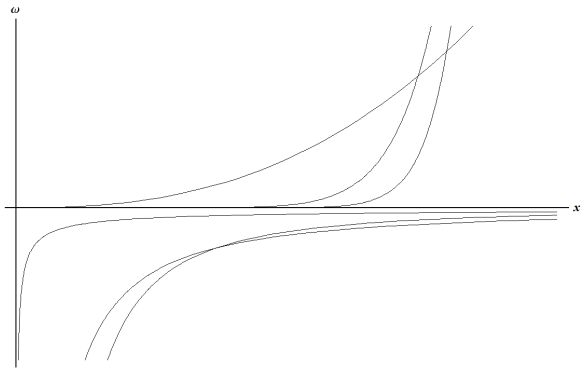

Figure 5.7: Various plots of the coefficient of the fourth order term in Stoner theory. In all cases the density of states obeys the law $\rho(x) = 1/x^n$ and a van Hove singularity occurs at $x = 0$. If $n < 1/2$ (all plots below the horizontal axis) then the fourth order term is negative and the possibility of a first-order transition arises. If $n > 1/2$ (all plots above the horizontal axis) then a first-order transition can never occur.

first-order and continuous transitions as well as the existence of a quantum-critical end-point of continuous transitions. For cases when $n > 1/2$, where no first-order transition and only continuous transitions can occur, the situation is shown in figure 5.9.

5.3.4 Logarithmic divergence

As a second case, let us consider an approach to a van Hove singularity that is logarithmic. The density of states therefore looks like

$$\rho(x) = \frac{1}{\ln(x)}, \tag{5.70}$$

and we assume we approach the van Hove singularity (which is situated at the singular point of equation 5.70, $x = 1$) from the right, *i.e.*, $x > 1$.

This situation is somewhat different from the case of the power law seen above. Figure 5.10 shows a plot of the fourth order term's coefficient as one moves away from the van Hove singularity. When this quantity is positive, *i.e.*, close to the singularity, no first-order transition can exist. Continuous transitions occur by varying the exchange constant I. However, moving away from the singularity means the graph does become negative and the possibility of a first-order transition arises. Indeed, inserting equation 5.70 into the condition 5.66 means that first-

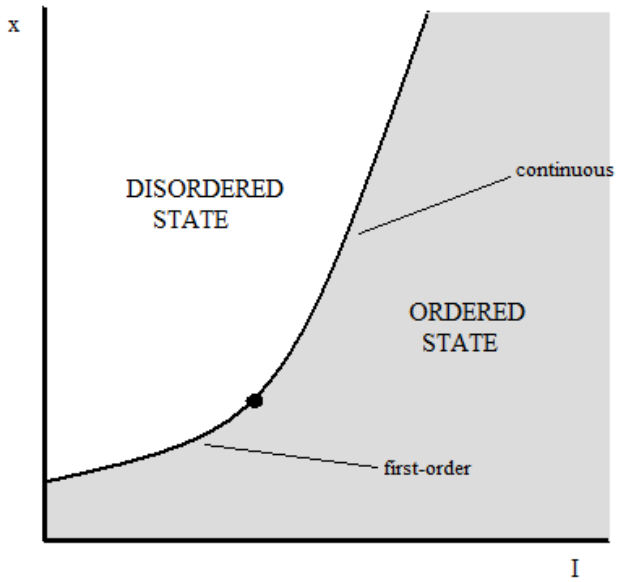

Figure 5.8: Stoner model phase diagram for an approach to a van Hove singularity that takes the form of equation 5.67 where $n < 1/2$. For such cases both a first-order and continuous transition is possible depending on the proximity to the van Hove singularity. The two different behaviours are separated by a critical end-point (denoted by a dot).

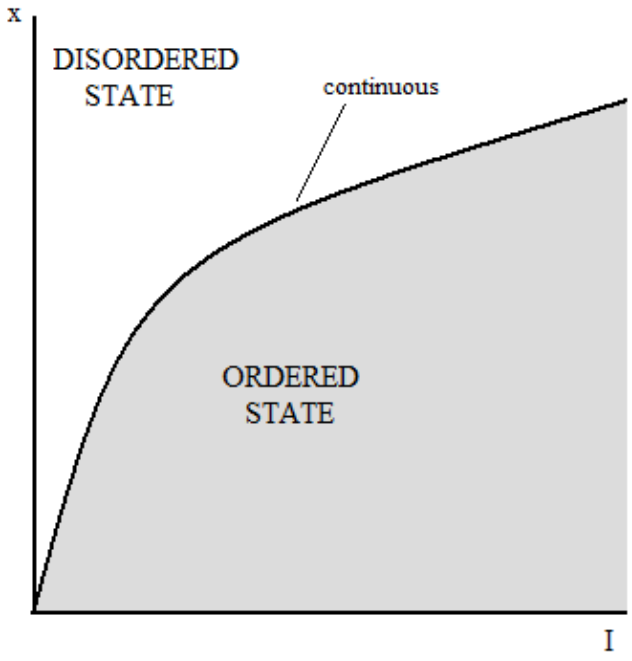

Figure 5.9: Stoner model phase diagram for an approach to a van Hove singularity that takes the form of equation 5.67 where $n > 1/2$. In these scenarios **only** continuous transitions are seen.

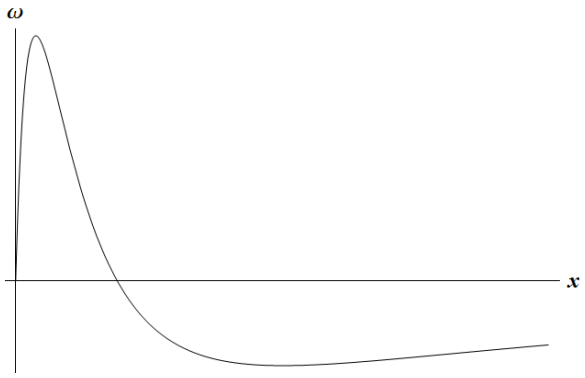

Figure 5.10: A plot of the fourth order term $\omega(x)$ of the Stoner model for a case where the density of states has a logarithmic approach to a van Hove singularity. Far from the singularity (large x) the plot is negative, giving rise to the possibility of a first-order transition. Close to the singularity, *i.e.* as $x \to 1$, the plot becomes positive and the only possibility is a continuous transition.

order transitions are seen for all $x > e \approx 2.72$. Figure 5.11 shows the phase diagram for this case.

5.3.5 Consideration of $ZrZn_2$

A detail from figure 4.8 showing the density of states of $ZrZn_2$ is shown in figure 5.12, the Fermi energy is indicated by the dotted line. It is ambiguous whether the density of states is linear or slightly curved at the Fermi energy.

Let us consider the very straightforward case where the density of states is linear in the vicinity of the Fermi energy:

$$\rho(x) = ax, \tag{5.71}$$

where a is any real number. It is clear that any linear density of states (*i.e.*, any value of a), which therefore has zero curvature, cannot satisfy condition 5.66. The square of the slope of the density of states is obviously never negative and this, in turn, implies that the fourth order term of the Stoner free energy is never negative. Therefore no first-order transitions should exist within Stoner theory for situations where the Fermi energy lies at a linear part of the density of states. In such systems, only second-order transitions can occur via the variation of the exchange coupling I.

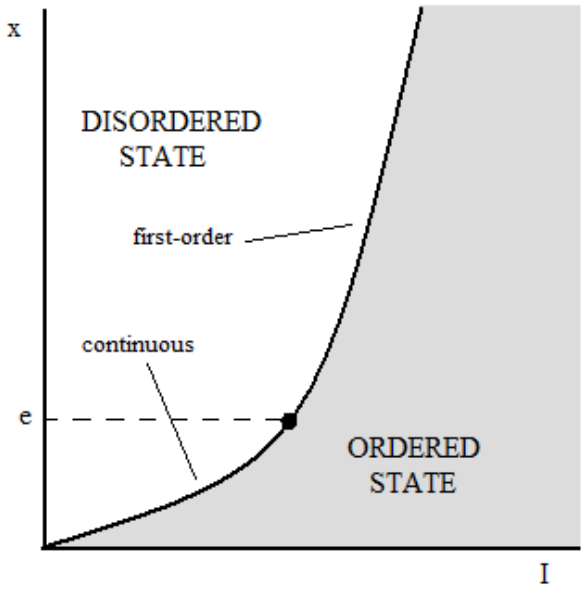

Figure 5.11: The zero temperature phase diagram described by Stoner theory for an approach to a van Hove singularity that is logarithmic. Far from the van Hove singularity the transitions are first-order, whereas close to the singularity the transition is continuous. A critical end-point separates first- and second-order behaviour. In the units used here (discussed in text) this critical end-point occurs when $x = e$.

Figure 5.12: A detail from figure 4.8. The density of states of $ZrZn_2$ **possibly** appears to be linear at the Fermi energy, denoted by the dotted line. As discussed in the text, this may indicate that Stoner theory is not a sufficient explanation of the observed first-order transition.

If the density of states is linear at the Fermi energy, this, therefore, might indicate that Stoner theory may be at odds with experimentally found first-order transitions [64]. However, our considerations above show that (among other things such as the value of the density of states at the Fermi energy) a very subtle variation in the curvature of the density of states can lead to a first-order transition. Until more refined information is found out about the shape of the density of states of $ZrZn_2$, it is impossible to conclude that the explanation of the appearance of a first-order transition lies here.

5.4 Summary

This chapter has been concerned with the appearance of first-order transitions in certain itinerant ferromagnetic systems, particularly placing emphasis on $ZrZn_2$ which was discussed at length earlier in the thesis. We introduced, discussed and applied to $ZrZn_2$ two competing theories which purport to explain the first-order behaviour.

Firstly, in §5.2, we saw how the failure to include certain modes in Hertz-Millis theory misses some important physics. Technically, this means that the Lindhard function should be corrected (see figure 5.1) by an entity which is seen to be divergent. This means that a Hertz-Millis-like expansion in terms of the order parameter (the coefficients of which are therefore now no longer numbers) does not exist. At the mean-field level (see §5.2.2) this gives rise to an extra logarithmic term as well as the usual Landau theory expansion, this is given by equation

5.10.

Using this new mean-field theory, we qualitatively discussed the temperature-pressure-magnetic field phase diagram it gives. As well as displaying the first-order transition of interest to us, application of a magnetic field suppresses the first-order nature (§5.2.3). We moved on to prove that equation 5.10 obeys the Clausius-Clapeyron condition (§5.2.4) before comparing to the experimental example of $ZrZn_2$ (§5.2.6). We found that the current experimental data hasn't sufficient resolution to support an explanation of first-order behaviour by equation 5.10.

Finally we applied the mean-field theory to $ZrZn_2$ and found values for certain parameters of the theory (§5.2.7) These agree with reference [67] with the exception of the required magnetic field to suppress the first-order behaviour sufficiently to be at a quantum-critical end-point. We calculated this to be an order of magnitude different from results of other workers.

In §5.3 we concentrated on another explantaion of the first-order transition, namely Stoner theory – an older and simpler theory which uses information about the density of states. After deriving a Stoner free energy (§5.3.1), we studied the general properties that a density of states must have to cause first- and second-order transtions in some system at zero temperature (§5.3.2). Then in sections 5.3.3 and 5.3.4 we continued to infer zero temperature phase diagrams for systems appraoching a van Hove singularity for the case of a power-law divergence, $\rho \sim x^{-n}$, and a logarithmic divergence, $\rho \sim 1/\ln x$ (where x measures the distance from the van Hove singularity, which is situated at $x = 0$ and $x = 1$ for the respective cases). The results showed that the phase diagram relies very subtly on the shape of the density of states and an attempted application to the case of $ZrZn_2$ in §5.3.5 gave no indication that Stoner theory is an explanation of the existence of first-order transitions.

Unfortunately the experimental data of $ZrZn_2$ doesn't allow the possibility to draw any conclusions on which of the two theories discussed in this chapter is correct. For further progress to be made via these routes, clearer experimental results would need to be supplied.

Chapter 6

Novel phases in itinerant systems

6.1 Introduction

In considering quantum criticality in itinerant ferromagnets we have encountered many phenomena. Arguably one could summarise these phenomena by the "fish-tail" diagram of figure 4.7 and it is worthwhile briefly reiterating the physics it shows.

Lowering the temperature, in ambient conditions, gives rise to a classical paramagnet-ferromagnet phase transition which can be seen in, say, $SrRuO_3$ [81]. However certain materials are seen to have their transition temperature lowered by the variation of some other parameter, x say, in their Hamiltonian and as it is lowered one might imagine forcing the transition to zero temperature where now the change of phase takes place via the variation of x. Yet, as the (speculative) quantum critical point is approached, along a line of critical points, we have seen examples of systems, notably $ZrZn_2$ in this thesis, that reach a critical end-point and the transition, for lower temperatures, becomes first-order.

So that we can reach a "naked" quantum critical point, there exists methods that push the critical end-point itself to zero temperature, thus reaching a quantum-critical end-point. This involves the application of some extra parameter x'. We speculated on this for $ZrZn_2$, in which the quantum-critical end-point has yet to be experimentally reached, in Chapter Four and the itinerant metamagnet $Sr_3Ru_2O_7$ has actually had its quantum-critical end-point reached via the variation of magnetic field and field direction [42].

Even in those systems that offer a route to quantum criticality, the situation is not as straightforward as we have thus far indicated. In general, and with the advent of a huge range of subtle experimental probing of the phase diagram surrounding quantum critical points, often the system under scrutiny chooses to "escape" into some strange (and sometimes unexpected) state before quantum criticality is reached – the quantum critical point is hidden by some novel state. Furthermore, some of these states seem to exhibit *dark order*: their order parameter is not obvious despite thermodynamics quantity indicating a transition. We use the term "dark order" rather than that used in the literature, *hidden order*. The ordered state is not hidden, its position can be found.

In this chapter we wish to explore one such possibility, namely the approach (from the

paramagnetic side) towards a potential Pomeranchuk instability [82] near some paramagnet-to-ferromagnet quantum phase transition.

To begin with in §6.2 we give a motivating overview of the sorts of novel superconducting and magnetic phases found near quantum criticality and draw from the large amount of experimental data found in the literature.

The investigation into the behaviour of the Fermi surface will require a microscopic treatment of Fermi-liquid theory and we will briefly discuss the mathematical results, whose origins lie in diagrammatics, necessary to make any judgement. We will do this in §6.3

6.2 Novel behaviour surrounding quantum critical points

Let us review a number of possibilities of the novel states that appear to "dress" the putative quantum critical point in many systems. In some case, the novel states are superconductors. As such they make use of various particle-particle pairing mechanisms. However, sometimes the novel state is one of strange magnetic nature, this time the relevant pairing mechanism to consider is one between particles and holes. In table 6.1 we present an analogy between the superconducting and magnetic scenarios.

To probe this analogy, methods based on disorder have been proposed to test for a Pomeranchuk instability, a non s-wave exotic magnetic state. Examining the effect of disorder on superconducting samples is now the *de facto* method for testing for exotic superconductivity; it is well known from Anderson's theorem [83] that s-wave superconductivity is robust against disorder, whereas non s-wave superconductivity is not [84]. Indeed, it has been shown that a similar argument can be applied to Pomeranchuk instabilities [85].

6.2.1 Superconductivity near quantum criticality

Early examples of superconductivity found near quantum criticality were found by the Cambridge group in a series of antiferromagnetic metals [86]. Take, for example, $CePd_2Si_2$ which begins to superconduct as the antiferromagnetic transition temperature is lowered with the ap-

Table 6.1: Various examples of the novel states that appear at quantum criticality. On the left are examples where the pairing mechanism is particle-particle and on the right particle-hole.

	Superconductivity (particle-particle pairing)	Magnetism (particle-hole pairing)
Conventional	s-wave superconductivity $\Delta = \sum_{k',\sigma} V_{k,k'} \langle c^\dagger_{k'\sigma} c^\dagger_{-k'\bar{\sigma}} \rangle$	Stoner theory M=$\sum_{k,\sigma,\sigma'} g_{\sigma,\sigma'} \langle c^\dagger_{k\sigma} c^\dagger_{k\sigma'} \rangle$
Unconventional	p- or d-wave superconductivity $\Delta(k) = \sum_{k',\sigma} V_{k,k'} \langle c^\dagger_{k'\sigma} c^\dagger_{-k'\bar{\sigma}} \rangle$	Pomeranchuk instability $\mathrm{M}(k) = \sum_{k';\sigma,\sigma'} g_{k,k';\sigma,\sigma'} \langle c^\dagger_{k'\sigma} c_{k'\sigma'} \rangle$
Inhomogeneous	*e.g.*, FFLO state $\Delta(q) = \sum_{k,k',\sigma} V_{k,k'} \langle c^\dagger_{k'+q/2,\sigma} c^\dagger_{-k'+q/2,\bar{\sigma}} \rangle$	*e.g.*, spiral spin state $\mathrm{M}(q) = \sum_{k,\sigma} g_{k,k';\sigma,\sigma'} \langle c^\dagger_{k'+q/2,\sigma} c_{k'-q/2,\sigma'} \rangle$

plication of pressure. Figure 6.1 shows the phase diagram, as the quantum critical point is approached, superconductivity is seen to set in before it is reached. Figure 6.2 shows similar behaviour in $CeIn_3$. Note both examples show a non-Fermi-liquid exponent α for resistivity $\rho \sim T^\alpha$, these are displayed in the insets.

Superconductivity has also been seen to coexist with ferromagnetism in some systems. For example, UGe_2 can be tuned, with very high hydrostatic pressures, towards a quantum critical point. The system is observed to enter a superconducting phase [87], see figure 6.3.

Thus far, we have tuned to some superconducting phase, close to a quantum critical point, with pressure. However, one might speculate that a magnetic field might be used to tune to superconductivity near quantum criticality in some materials. First thoughts might consider this approach naïve – after all, superconductors expel magnetic fields, which costs the system energy, and usually only moderate fields of a few Tesla are sufficient to remove the system from any superconducting phase. Intriguingly, though, situations have been found where a magnetic field of substantial magnitude has managed to persuade a system to superconduct.

Take, for example, URhGe [88], a close relation of UGe_2. Early investigations revealed that URhGe entered a superconducting phase at low temperatures and in ambient conditions, this superconductivity was suppressed with a field of 2 T. A spin rotation (of the moments located on uranium atoms) at high fields was found and it was speculated that this might be connected to a metamagnetic quantum-critical end-point, see figure 6.4. However, further investigations

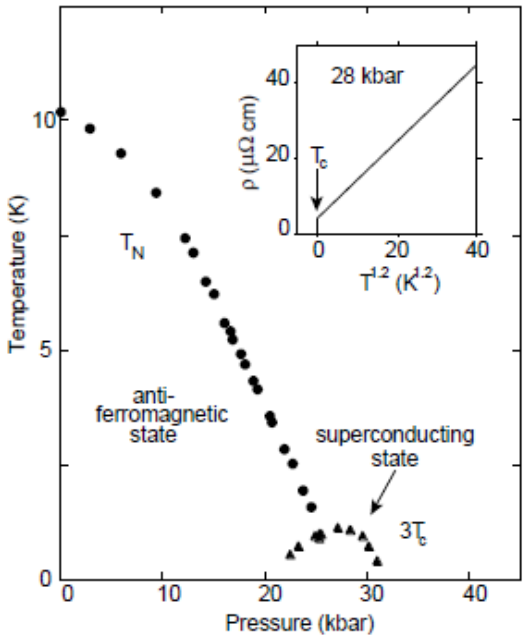

Figure 6.1: From [86]. The temperature-pressure phase diagram of $CePd_2Si_2$. As pressure is increased, the antiferromagnetic transition temperature is reduced. Close to quantum criticality the material chooses to become superconducting at a temperature $T = T_c$. The inset show non-Fermi-liquid behaviour of the resistivity and the location of T_c.

found that superconductivity returns to the system and surrounds these end-points, in quite substantial magnetic fields of the range $8 - 13$ T. See figure 6.5.

We have seen the emergence of superconductivity close to quantum criticality, but the strangely behaving phases extend further in character. In some systems new types of magnetic order emerge, next we will concentrate on a few such situations.

6.2.2 Strange magnetic regions of MnSi

MnSi, as discussed in Chapter Two, is an itinerant helimagnet that undergoes its transition from a paramagnet in ambient conditions at 29.5 K. Its order is observed to be long-ranged and three-dimensional, but is seen to be suppressed under hydrostatic pressure until disappearing discontinuously at $p_c = 14.6$ kbar [48].

Investigations under further pressure [89] have revealed a region of non-Fermi-liquid behaviour in which static magnetic order is observed, despite bulk properties indicating a loss of

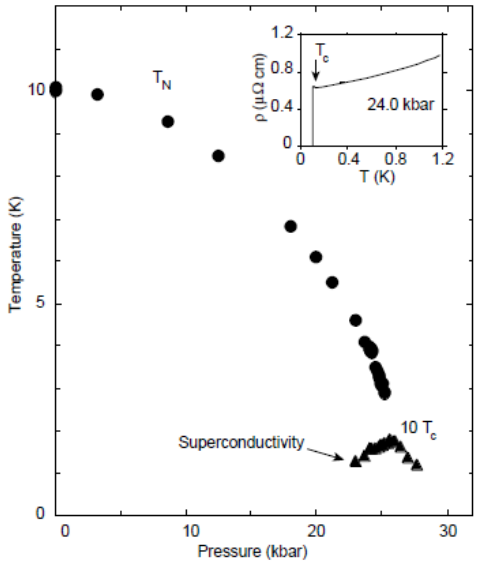

Figure 6.2: After [86]. The appearance of superconductivity near pressure tuned quantum criticality in $CeIn_3$. The inset shows the temperature dependence of the resistivity near the critical pressure.

order. Neutron scattering experiments have shown that in this phase there exists a pattern of quasi-static moments (analogous to a liquid crystal phase) which displays some semblance of long-range order.

Further neutron scattering experiments [90] have contributed information on MnSi's magnetic phase diagram, finding strange magnetism near the paramagnet-helimagnet phase boundary, see the A-phase in figure 6.7. If a magnetic field is applied (in any arbitrary direction relative to the atomic lattice) to a sample tuned to this boundary, a so-named *skyrmion lattice* [91, 92] is formed. This lattice has a magnetic structure with hexagonal symmetry, see figure 6.8, and consists of an array of topologically stable entities called *skyrmions*.

6.2.3 Nematic phase in $Sr_3Ru_2O_7$

It is proposed that there exists phases of electronic liquids that resemble nematic liquid crystals [93]. Experimentally, one can identify such phases by probing the itinerant properties and finding a lack of rotational symmetry. One such possibility of a nematic phase is given by a region near a magnetic-field tuned quantum critical point in metamagnetic $Sr_3Ru_2O_7$ [94, 95].

When sufficiently clean crystals (residual resistivity $\sim 0.4\mu\Omega$ cm) of $Sr_3Ru_2O_7$ were pro-

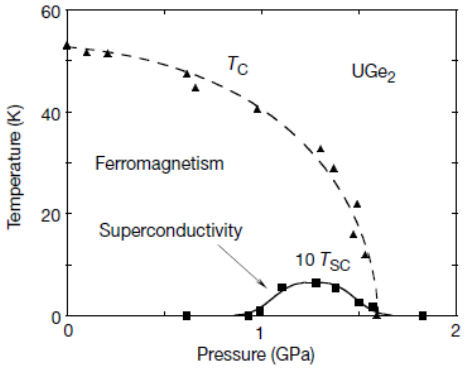

Figure 6.3: From [87]. The temperature-pressure phase diagram of UGe_2 shows the coexistence of ferromagnetism and superconductivity close to the pressure tuned quantum critical point.

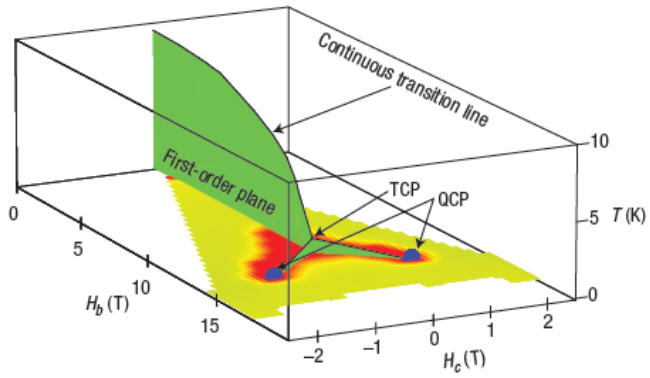

Figure 6.4: From [88]. The temperature-magnetic field phase diagram of URhGe for field in the bc plane. It displays many interesting phenomena of itinerant systems. A line of critical points reaches a tricritical point and this, in turn, can be tuned to zero temperature quantum critical points. Red regions indicate the appearance of superconductivity.

duced, a strangely behaving region was identified via measurements of resistivity and susceptibility. Figure 6.9 shows resistivity as a function of applied magnetic field, the series of sudden peaks suggest the existence of some low temperature phase. Evidence for a change of phase is supplied by thermodynamic quantities and an empirical phase diagram can be mapped out using thermodynamic quantities revealing a small region of some new phase, see figure 6.10.

Further probing of this phase [95] does indeed reveal behaviour that could be linked to some nematic phase. Figure 6.11 show resistivity measurements to be anisotropic. Plotting the difference between the resistivities in the aa and bb directions reveals a peak at low temperatures and at the applied magnetic fields necessary to be close to the quantum-critical end-point. It is

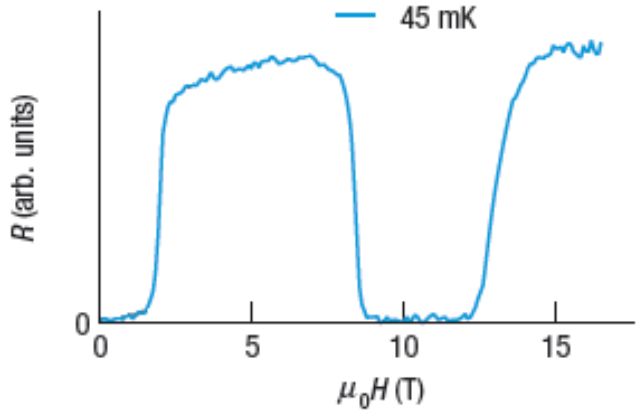

Figure 6.5: After [88]. The resistance of URhGe at a temperature of 45mK. The zero-field superconducting state is seen to be suppressed by a field of approximately 2 T. However, the possibility of superconductivity in this system arises once more at field (of suitable orientation) of approximately 8 T and this superconducting state is seen to exist for higher fields too.

argued that such behaviour could be explained by a nematic phase discussed above.

6.3 Pomeranchuk instabilities near ferromagnetic quantum critical points

We now turn to a situation of interest to us here, namely *Pomeranchuk instabilities*: a certain class of Fermi surface distortion [82]. The nematic phase that appears to mask quantum criticality may possibly be explained by a Fermi surface that has been subjected to a Pomeranchuk instability. The aim of this section is to investigate the possibility that an approach to a quantum critical point could enhance the possibility of such a situation.

6.3.1 Pomeranchuk instabilities

Pomeranchuk instabilities occurs when the Fermi surface distorts in some angular momentum channel, which we label with l. Figure 6.12 shows four such instabilities in the channels $l = 2, 3, 4, 5$. Pomeranchuk showed that an instability in the channel l arises when the following

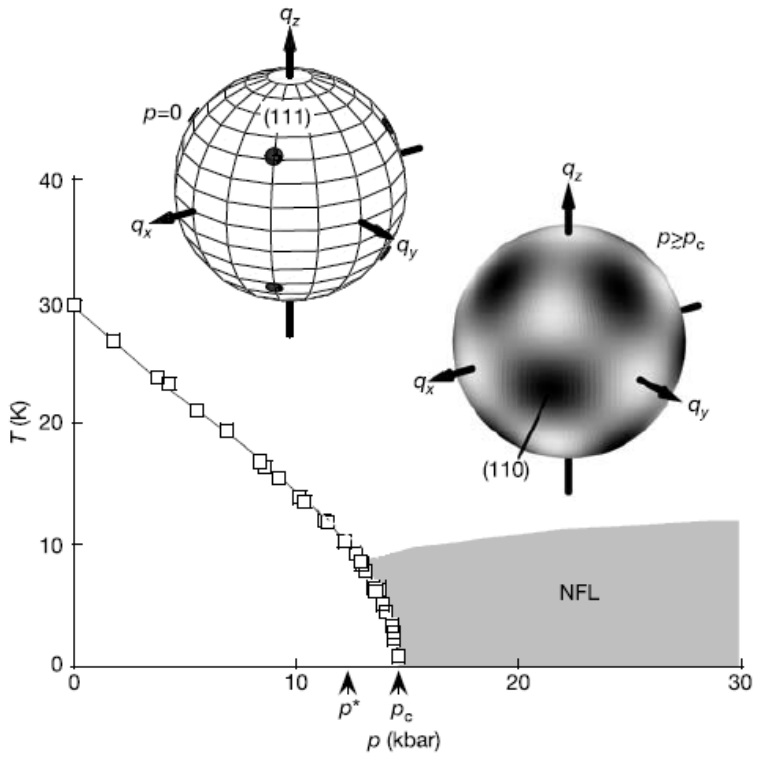

Figure 6.6: After [89]. The phase diagram of MnSi shows a region of helimagnetism reached by passing through some pressure dependent continuous transition line T_c. After a pressure p^*, the transition is first order and reaches zero temperature at $p = p_c$. The shaded region is a non-Fermi-liquid (NFL) and shows strange magnetic behaviour (discussed in text). The insets show the position of elastic neutron scattering intensity in reciprocal space at both zero pressure (left), where clear Bragg peaks (the black dots) are observed, and in the NFL region (right) where the intensity varies. The amount of shading approximately follows the changes in intensity.

condition is satisfied:

$$1 + \frac{1}{2l+1} F_l^{s,a} < 0, \tag{6.1}$$

where $F_l^{s,a}$ is a spin symmetric (labelled by s) or spin-antisymmetric (labelled by a) Landau parameter.

Pomeranchuk instabilities have sparked much interest in the condensed matter community. For example, instabilities in the $l = 2$ channel have been thought to exist in quantum Hall systems [97] and in $Sr_3Ru_2O_7$ [94] and URu_2Si_2 [98] – in each case it is proposed that a Fermi-liquid might enter some *nematic* state through such an instability. Furthermore, it is reported that the Hubbard model may, too, have a distorted Fermi surface [99].

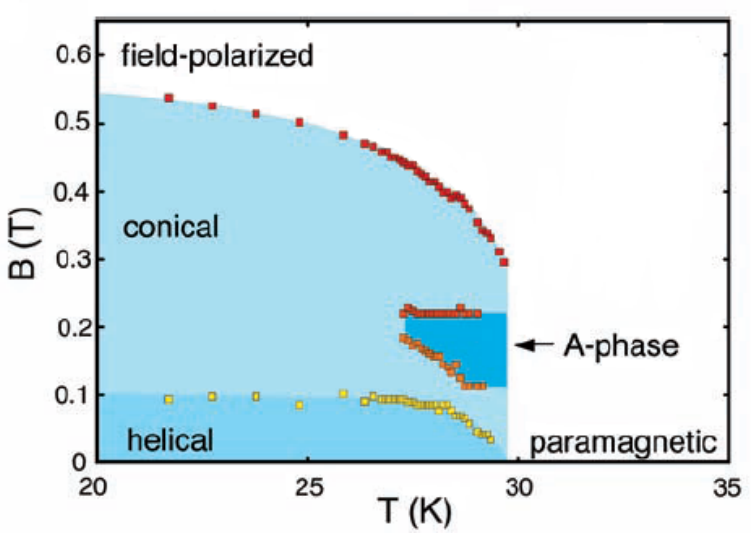

Figure 6.7: After [90]. The magnetic phase diagram of MnSi. Application of a magnetic field may give rise to a number of magnetic states: the low temperature helical order unpins and the system displays conical order. However, the interesting phase is that called the "A-phase" in the figure. This phase, a skyrmion lattice, has strange magnetic order.

6.3.2 In the vicinity of a ferromagnetic quantum critical point

The issue we wish to address here is whether the critical fluctuations occurring on the approach towards a ferromagnetic quantum critical point (see figure 6.13) might favour the formation of some Pomeranchuk instability, giving rise to a distorted Fermi surface. In the literature, there do exist mean-field treatments [100].

Imagine varying a parameter x at zero temperature such that a system is moved towards its paramagnet-ferromagnet quantum critical point. We assume that the paramagnetic region is a Fermi-liquid, this is very reasonable at zero temperature. As a quantum critical point is approached, ferromagnetic fluctuations must increase (diverging at criticality) and we wish to use this fact to see if a distorted Fermi surface state, caused by a Pomeranchuk instability, is a favourable state.

6.3.3 Fermi-liquid theory – microscopics

The content of this section has its origins in the seminal work on Fermi-liquids by Landau [8], although here we will follow reference [52].

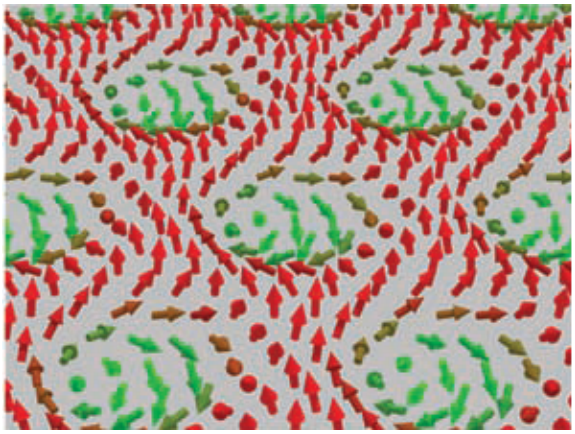

Figure 6.8: Real-space depiction of the skyrmion phase in MnSi [90].

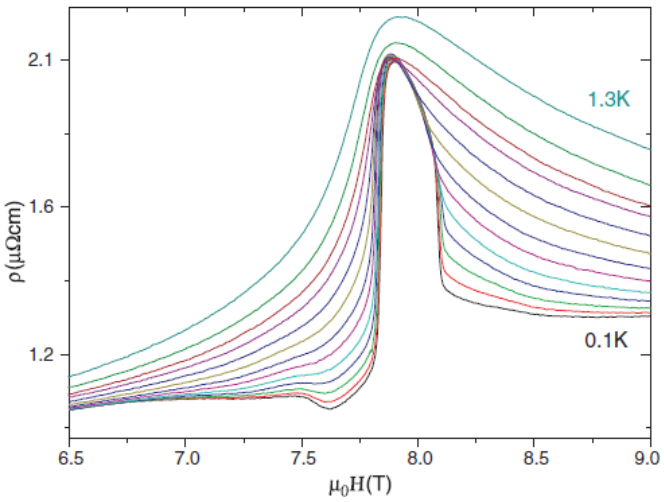

Figure 6.9: From [94]. The resistivity of $Sr_3Ru_2O_7$ shows a variety of peaks around the magnetic field required for quantum criticality. This is an indication of the existence of some strange magnetic phase.

Let us write the single-particle Green's function as

$$G(P) = \frac{z}{\omega - \mu - v_F(p - k_F) + i\eta \mathrm{sgn}(\omega - \mu)} \tag{6.2}$$

where z is the quasiparticle residue, μ chemical potential, k_F the Fermi momentum and η is a positive infinitesimal. Note that we use the four-vector notation $P \equiv (\mathbf{p}, \omega)$.

Calculating the vertex function Γ amounts to computing the integral equation represented by the diagram shown in figure 6.14:

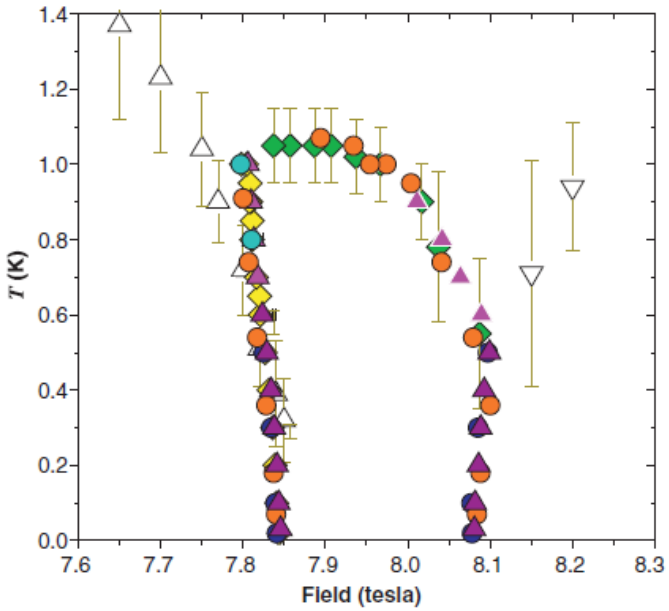

Figure 6.10: From [94]. The temperature-magnetic field phase diagram of $Sr_3Ru_2O_7$ inferred from a variety of thermodynamic quantities. The quantum critical point of this system appears to be hidden by a strange phase.

$$\Gamma\left(P_1, P_2; K\right) = \tilde{\Gamma}\left(P_1, P_2; K=0\right) - i\int \frac{d^4Q}{\left(2\pi\right)^4}\tilde{\Gamma}\left(P_1\right)G\left(Q\right)G\left(Q+K\right)\Gamma\left(Q, P_2; K\right) \quad (6.3)$$

where $\tilde{\Gamma}$ denotes the part of Γ that is not singular at $K = 0$. However, in general, the Green's functions' poles do give rise to singularities in Γ when $K = 0$ and furthermore care must be taken as the following limits

$$\Gamma^{\omega}\left(P_1, P_2\right) = \lim_{\omega\to 0}\lim_{k\to 0}\Gamma\left(P_1, P_2; K\right) \quad (6.4)$$

$$\Gamma^{k}\left(P_1, P_2\right) = \lim_{k\to 0}\lim_{\omega\to 0}\Gamma\left(P_1, P_2; K\right), \quad (6.5)$$

do not commute. That is

$$\Gamma^{\omega}\left(P_1, P_2\right) \neq \Gamma^{k}\left(P_1, P_2\right). \quad (6.6)$$

Physically, Γ^{ω} and Γ^{k} correspond to two different things. Firstly, Γ^{ω} represents virtual excitations of small transfers of energy. It can be related to the Landau interaction function $f\left(\hat{p}, \hat{q}\right)$ [52] via the relation

$$f\left(\hat{p}, \hat{q}\right) = z^2\Gamma^{\omega}\left(\hat{p}, \hat{q}\right). \quad (6.7)$$

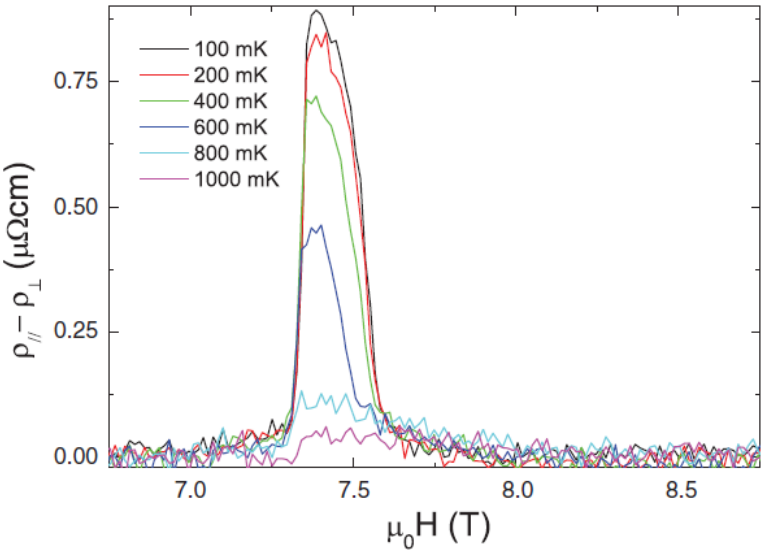

Figure 6.11: After [95]. The difference in resistivity in the aa and bb directions in $Sr_3Ru_2O_7$. The peak indicates anisotropy in the materials itinerant properties. This points to the possibility that $Sr_3Ru_2O_7$'s novel phase near its quantum critical point is a nematic phase (discussed in text).

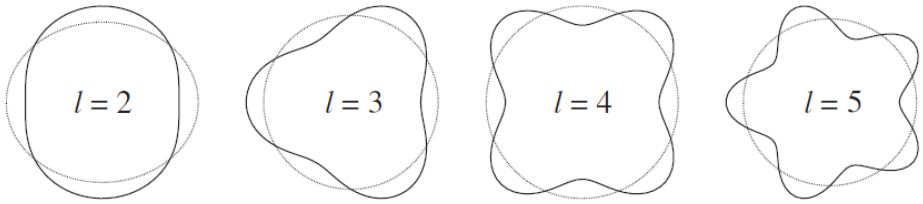

Figure 6.12: After [96]. Pomeranchuk instabilities of the circular Fermi surface (given by a dotted line in each case) in angular momentum channels $l = 2, 3, 4, 5$.

Γ^k is the forward scattering amplitude, *i.e.*, it corresponds to actual physical scattering. It can be related to Γ^ω by equations 6.4 and 6.5. Expansion of the interaction function in terms of Legendre polynomials relates Γ^k, via the Legendre coefficient B_l, to the Landau parameters:

$$\Gamma^k \sim B_l = \frac{F_l^s}{1 + \frac{F_l^s}{2l+1}}. \tag{6.8}$$

Note the denominator of the right-hand side of this equation gives rise to a Pomeranchuk instability at the point when it becomes zero. Notice, too, that the connection between scattering and the Landau functional is only in the same angular momentum channel, that labelled by l. So if ferromagnetic fluctuations ($l = 0$) diverge by being in the vicinity of a paramagnetic-

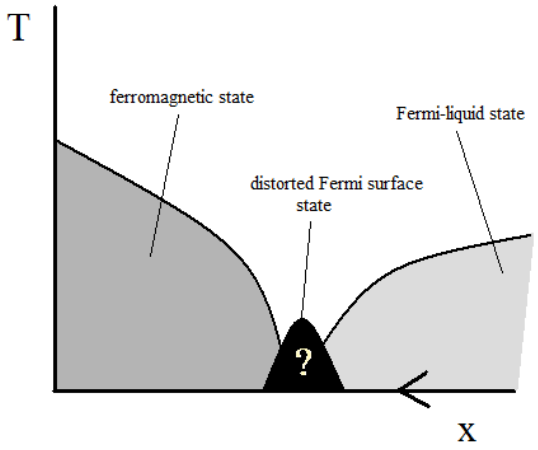

Figure 6.13: The approach to a ferromagnetic quantum critical point from the paramagnetic phase at zero temperature. We assume that Fermi-liquid theory applies here and intend to investigate whether the quantum phase transition into a ferromagnet is preempted by a Pomeranchuk instability into some novel phase (denoted here by "?") with a distorted Fermi surface in the $l \neq 0$ channel.

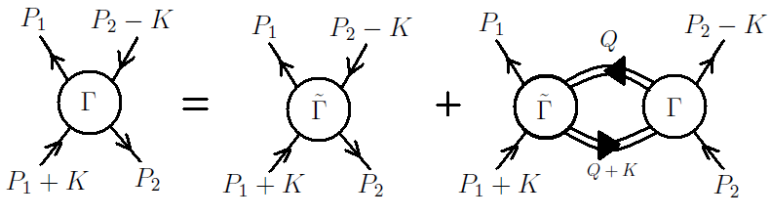

Figure 6.14: The diagram representing the vertex function Γ.

ferromagnetic quantum phase transition, it is only the Stoner instability that is enhanced.

This argument would imply that a continuous Pomeranchuk-like distortion of the Fermi surface is not favoured by ferromagnetic critical fluctuations. This is the salient result of this chapter. Note, however, that we have assumed a continuous transition and our result does not imply anything about first order transitions which are seen experimentally.

6.4 Summary

This chapter has been concerned with the fact that systems, when driven to any quantum-critical point in their phase diagram, tend to opt for some novel state rather than exhibit a bare quantum critical point. Often these states are of exotic superconducting or magnetic nature and in general

are not well understood: a choice of suitable order parameter often is not obvious and the state is described as having dark order.

In §6.1 we introduced various examples of such novel states (see figure 6.1 before concentrating on systems that display superconductivity near quantum criticality (§6.2.1). Of the superconductors, notable examples of pressure tuned systems are the antiferromagnet $CePd_2Si_2$ and the ferromagnet UGe_2, whose superconductivity coexists with ferromagnetism. We also briefly discussed the magnetic-field tuned material URhGe, whose superconductivity in ambient conditions disappears at a moderate field, only to (rather unexpectedly) return to surround quantum criticality at very high fields.

In §6.2.2, we considered MnSi, whose most notable strange phase is a skyrmion lattice. Then in §6.2.3 we reviewed the strange phase surrounding quantum criticality in $Sr_3Ru_2O_7$ which, it has been proposed, is a nematic phase.

The final part of this chapter (§6.3) was an investigation into the existence of distorted Fermi surface phases (caused by, say, a Pomeranchuk instability (see §6.3.1)) which surround ferromagnetic quantum criticality and arise because of increasing ferromagnetic fluctuations. We found it is possible to address some key questions with the microscopic formulation of Landau's Fermi-liquid theory, see §6.3.3, where scattering is straightforwardly related to Landau parameters. We concluded that an approach to a ferromagnetic quantum critical point actually fails to enhance the possibility of a nematic phase. In fact, only the Stoner instability is enhanced. Note, however, that this only applies to a continuous transitions. We have made no conclusions about the first-order transitions that are observed in experiment.

Chapter 7

Thesis discussion

This thesis has primarily concentrated on various aspects of quantum criticality in itinerant ferromagnets. In this chapter we will discuss the main results found and the conclusions made in the main body of the text.

Chapters Two and Three consisted of mainly background material. They contained the necessary foundations for the investigations appearing in rest of the thesis. §2.2 discussed one of the standard models of condensed matter physics, an attempted explanation of the low temperature properties of metals – Fermi-liquid theory. We showed how a model of independent electrons can be adiabatically mapped onto a model of quasiparticles (§2.2.3), the excitations of Fermi-liquid theory, which gives a more realistic treatment of the interactions that are really present in metals. We gave some examples of systems that do appear to be well described by Fermi-liquid theory (§2.2.7) but also some situations where the low temperature properties of metals are not Fermi-liquid in nature (§2.2.8).

In order to introduce quantum criticality some time was spent covering critical phenomena in §2.3. An overview of classical criticality was given before comparing to, and contrasting with, criticality at zero temperature (see 2.2.3) where quantum phase transitions are first properly treated. Itinerant ferromagnetism was introduced in §2.4 where a preliminary discussion of classical (§2.4.1) and localised quantum magnetism (§2.4.2) led to the consideration of itinerancy. Through the tight-binding (§2.4.3) and Hubbard models (§2.4.4), we arrived at the Stoner model (§2.4.5), a simple, yet powerful, theory of itinerant ferromagnetism.

§2.5 saw a review of experiments performed in the vicinity of quantum criticality in itinerant electron systems. In all cases considered, there existed some degree of non-Fermi-liquid behaviour in some of the systems' experimental quantities. We considered systems where doping (§2.5.1) is the tuning parameter at zero temperature as well as field induced quantum criticality and metamagnetism (§2.5.2), before pressure induced (§2.5.3) and finally natural quantum critical (§2.5.4) systems.

Chapter Three gave an overview of Hertz-Millis theory, a theory of quantum criticality in itinerant systems. In order to derive the Hertz-Millis action (§3.3), we firstly had to introduce the fermionic functional integral formalism (§3.2). The action is analysed (see §3.5) using the

renormalization group technique which is introduced in §3.4. The analysis gives rise to a set of renormalization group equations which, when solved (§3.6), describe the generic phase diagram (see figure 3.6) and give the set of critical exponents of quantum critical itinerant systems (see tables 3.1 and 3.2.

Chapter Four describes the first application of Hertz-Millis theory to a quantum-critical end-point in a three-dimensional system. We concentrate on, and compute the form of the magnetic susceptibility (which is done in §4.3.1) and compute the specific heat capacity, via the free energy, in §4.3.2. Results are given in figures 4.1, 4.2 and 4.3. Speculation on an experimental application leads us to consider the material $ZrZn_2$. In §4.4 we review this compound and its phase diagram. $ZrZn_2$ has a low temperature first-order transition (which can be made as pressure is varied) which meets the higher temperature continuous transition at a critical end-point. Assuming that this can be suppressed by a magnetic field to a quantum-critical end-point, we attempt to write down the simplest mean-field theory to capture the physics seen (§4.5) and an application to $ZrZn_2$ (§4.5.3) leads us to conclude that despite requiring only a moderate field, a substantial pressure would be required to reach the quantum-critical end-point.

Chapter Five concentrated on the appearance of a first-order transition in itinerant ferromagnetic systems. The chapter is divided into two parts, one for each of two different theories of the first-order transition's existence. The first theory (§5.2) takes into account some modes that were left out of Hertz-Millis theory. It is claimed that these modes cause the first-order transition and a derivation of an effective mean-field theory adds an extra term to the usual Landau theory.

After discussing the phase diagram this mean-field theory gives (§5.2.3) we prove in §5.2.4 that it complies with the Clausius-Clapeyron condition – the first-order transition on show touches the zero temperature axis at a right-angle. We go on to discuss the shape of the phase diagram and question whether the theory provides a good description of the data from $ZrZn_2$ (§5.2.6). We fit the theory to $ZrZn_2$ and use it to predict the location of its quantum-critical end-point. We find agreement with our earlier mean-field theory and disagreement with other workers. This is seen in §5.2.7.

The second theory of the first-order transition is given in §5.3. This theory attempts to explain a material displaying a first-order transition via the features of its density of states. In §5.3.1 we derive Stoner theory and go on to consider its zero temperature phase diagram (§5.3.2). We consider both a power law (§5.3.3) and a logarithmic (§5.3.4) approach to a van Hove singularity in the density of states and infer phase diagrams for each case. The phase diagrams are shown in figures 5.8, 5.9 and 5.11. We conclude that the appearance of a first-order transition depends quite subtly on the density of states and a consideration of $ZrZn_2$ (§5.3.5) fails to give rise to positive results due to lack of the necessary detail of its density of states in the literature.

Chapter Six was concerned with the appearance of novel states in the vicinity of quantum critical points. We introduced (see §6.2) the types of strange phases to be found, which are either superconducting or magnetic in nature, and gave an analogy between the two. In §6.2.1 we considered the experimental realisation of superconductivity near quantum critical points of various nature and went on to consider the strange magnetic phases to be found in MnSi (§6.2.2) and $Sr_3Ru_2O_7$ (§6.2.3).

In §6.3 we introduced Pomeranchuk instabilities (see §6.3.1), a certain type of Fermi surface distortion, and questioned (in §6.3.2) whether an approach towards a ferromagnetic quantum critical point, where the ferromagnetic fluctuations diverge, would give rise to a Pomeranchuk instability. The answer is to be found in the microscopic theory of Fermi-liquids (§6.3.3) and we concluded that a distorted Fermi surface due to a Pomeranchuk instability would not be favoured and that only the Stoner instability can be affected.

List of references

[1] D. Pines and P. Nozieres, *The Theory of Quantum Liquids - Volume I* (Addison Wesley, California, 1989).

[2] N. Wiser and D. J. Amit, *Quantum Fluids* (Gordon and Breach, USA, 1970).

[3] G. Baym and C. J. Pethick., *Landau Fermi-liquid Theory* (John Wiley and Sons, USA, 1991).

[4] W. Pauli, Z. Phys. **41**, 81 (1927).

[5] J. R. Hook and H. E. Hall, *Solid State Physics* (Wiley, UK, 1990).

[6] L. D. Landau, Sov. Phys.-JETP **3**, 920 (1956).

[7] L. D. Landau, Sov. Phys.-JETP **5**, 101 (1957).

[8] L. D. Landau, Sov. Phys.-JETP **8**, 70 (1958).

[9] P. Anderson, *Basic Notions of Condensed Matter Physics* (Addison Wesley, USA, 1984).

[10] A. J. Schofield, Contemporary Physics **40**, 95 (1999).

[11] E. Abrahams, Phys. Rev. **95**, 839 (1954).

[12] A. J. Leggett, Rev. Mod. Phys. **47**, 331 (1975).

[13] G. R. Stewart, Z. Fisk, J. O. Willis, and J. L. Smith, Phys. Rev. Lett. **52**, 679 (1984).

[14] L. Taillefer and G. G. Lonzarich, Phys. Rev. Lett. **60**, 1570 (1988).

[15] J. Bardeen, L. N. Cooper, and J. R. Schrieffer, Phys. Rev. **108**, 1175 (1957).

[16] J. G. Bednorz and K. A. Müller, Z. Phys. B **64**, 189 (1986).

[17] H. Takagi, B. Batlogg, H. L. Kao, J. Kwo, R. J. Cava, J. J. Krajewski, and W. F. Peck, Phys. Rev. Lett. **69**, 2975 (1992).

[18] J. M. Harris, Y. F. Yan, P. Matl, N. P. Ong, P. W. Anderson, T. Kimura, and K. Kitazawa, Phys. Rev. Lett. **75**, 1391 (1995).

[19] F. D. M. Haldane, J. Phys. C **14**, 2585 (1981).

[20] T. Andrews, Phil. Trans. R. Soc. **159**, 575 (1869).

[21] J. D. van der Waals, PhD thesis, University of Leiden (1873).

[22] P. Curie, Ann. Chim. Phys. **5**, 289 (1895).

[23] P. Weiss, J. Phys. Radium **6**, 661 (1907).

[24] P. M. Chaikin and T. C. Lubensky, *Principles of Condensed Matter Physics*, 1st ed. (Cambridge University Press, Cambridge, 1995).

[25] R. Shankar, Rev. Mod. Phys. **66**, 129 (1994).

[26] S. Sachdev, *Quantum Phase Transitions* (Cambridge University Press, Cambridge, 1999).

[27] J. Hertz, Phys. Rev. B **4**, 1165 (1976).

[28] P. Langevin, J. Phys. **4**, 687 (1905).

[29] P. Langevin, Ann. Chim. Phys. **5**, 70 (1905).

[30] N. W. Ashcroft and N. D. Mermin, *Solid State Physics* (Saunders College Publishing, USA, 1976).

[31] W. Heisenberg, Z. Phys. **49**, 619 (1928).

[32] J. C. Slater, Phys. Rev. **49**, 537 (1936).

[33] N. F. Mott, Phil. Mag. **6**, 287 (1961).

[34] E. H. Lieb and F. Y. Wu, Phys. Rev. Lett. **20**, 1445 (1968).

[35] E. C. Stoner, Proc. R. Soc. **A 165**, 372 (1938).

[36] T. Moriya, *Spin Fluctuations in Itinerant Electron Magnetism*, 1st ed. (Springer-Verlag, Berlin, 1985).

[37] G. R. Stewart, Rev. Mod. Phys. **73**, 797 (2001).

[38] C. L. Seaman, M. B. Maple, B. W. Lee, S. Ghamaty, M. S. Torikachvili, J.-S. Kang, L. Z. Liu, J. W. Allen, and D. L. Cox, Phys. Rev. Lett. **67**, 2882 (1991).

[39] M. C. de Andrade *et al.*, Phys. Rev. Lett. **81**, 5620 (1998).

[40] K. Heuser, E.-W. Scheidt, T. Schreiner, and G. R. Stewart, Phys. Rev. B **57**, R4 198 (1998).

[41] K. Heuser, E.-W. Scheidt, T. Schreiner, and G. R. Stewart, Phys. Rev. B **58**, R15 959 (1998).

[42] R. S. Perry *et al.*, Phys. Rev. Lett. **86**, 2661 (2001).

[43] A. J. Millis, A. J. Schofield, G. G. Lonzarich, and S. A. Grigera, Phys. Rev. Lett. **88**, 217204 (2002).

[44] S. A. Grigera, R. A. Borzi, A. P. Mackenzie, S. R. Julian, R. S. Perry, and Y. Maeno, Phys. Rev. B **67**, 214427 (2003).

[45] K. Umeo, T. Takabatake, H. Ohmoto, T. Pietrus, H. v. Löhneysen, K. Koyama, S. Hane, and T. Goto, Phys. Rev. B **58**, 12095 (1998).

[46] K. Umeo, H. Kadomatsu, and T. Takabatake, Phys. Rev. B **54**, 1194 (1996).

[47] K. Umeo, H. Kadomatsu, and T. Takabatake, J. Phys.: Condens. Matter **8**, 9743 (1996).

[48] C. Pfleiderer, G. J. McMullan, S. R. Julian, and G. G. Lonzarich, Phys. Rev. B **55**, 8330 (1997).

[49] O. Trovarelli, C. Geibel, S. Mederle, C. Langhammer, F. M. Grosche, P. Gegenwart, M. Lang, G. Sparn, and F. Steglich, Phys. Rev. Lett. **85**, 626 (2000).

[50] A. J. Millis, Phys. Rev. B **48**, 7183 (1993).

[51] H. v. Löhneysen, A. Rosch, M. Vojta, and P. Wölfle, Rev. Mod. Phys. **79**, 1016 (2007).

[52] J. Negele and H. Orland, *Quantum Many-Particle Systems* (Addison-Wesley, USA, 1988).

[53] F. A. Berezin, *The Method of Second Quantization* (Academic, New York, 1966).

[54] J. Hubbard, Phys. Rev. Lett. **3**, 77 (1954).

[55] R. L. Stratonovich, Doklady Akad. Nauk SSSR **115**, 1097 (1957).

[56] J. Lindhard, Dan.Vidensk. Selsk. Mat.-Fys. Medd. **28**, 750 (1954).

[57] E. C. G. Stueckelberg and A. Petermann, Helv. Phys. Acta **26**, 499 (1953).

[58] L. P. Kadanoff, Physica **2**, 263 (1965).

[59] K. G. Wilson, Rev. Mod. Phys. **47**, 773 (1975).

[60] J. Zinn-Justin, *Quantum Field Theory and Critical Phenomena* (Clarendon, Oxford, 1989).

[61] G. D. Mahan, *Many Particle Physics*, 3rd ed. (Springer, New York, 2000).

[62] R. Bowley and M. Sánchez, *Introductory Statistical Physics*, 2nd ed. (Oxford Science Publications, Oxford, 2003).

[63] E. Grüneisen, Ann. Phys. Lpz. **26**, 393 (1908).

[64] M. Uhlarz, C. Pfleiderer, and S. M. Hayden, Phys. Rev. Lett. **93**, 256404 (2004).

[65] E. A. Yelland, S. J. C. Yates, O. Taylor, A. Griffths, S. M. Hayden, and A. Carrington, Phys. Rev. B **72**, 184436 (2005).

[66] B. T. Matthias and R. M. Bozorth, Phys. Rev. **100**, 604 (1958).

[67] D. Belitz, T. R. Kirkpatrick, and J. Rollbühler, Phys. Rev. Lett. **94**, 247205 (2005).

[68] G. G. Lonzarich, *unpublished*, Trieste Lecture Notes (1994).

[69] S. A. Grigera, A. P. MacKenzie, A. J. Schofield, S. R. Julian, and G. G. Lonzarich, Int. J. Phys. B **16**, 3258 (2002).

[70] S. J. C. Yates, G. Santi, S. M. Hayden, P. J. Meeson, and S. B. Dugdale, Phys. Rev. Lett. **90**, 057003 (2003).

[71] C. Pfleiderer, M. Uhlarz, S. M. Hayden, R. Vollmer, H. v. Löhneysen, N. R. Bernhoeft, and G. G. Lonzarich, Nature **412**, 58 (2001).

[72] E. A. Yelland *et al.*, arXiv:cond-mat/0502341v2 .

[73] B. Binz and M. Sigrist, Europhys. Lett. **65**, 816 (2004).

[74] T. Vojta, D. Belitz, R. Narayanan, and T. R. Kirkpatrick, Z. Phys. B **103**, 451 (1997).

[75] D. Belitz, T. Kirkpatrick, and T. Vojta, Phys. Rev. B **55**, 9452 (1997).

[76] T. R. Kirkpatrick and D. Belitz, Phys. Rev. Lett. **67**, 024419 (2003).

[77] D. Belitz, T. R. Kirkpatrick, M. T. Mercaldo, and S. L. Sessions, Phys. Rev. B. **63**, 174427 (2001).

[78] F. Mandl, *Statistical Physics*, 2nd ed. (Wiley, Chichester, 2000).

[79] E. P. Wohlfarth and P. Rhodes, Philos. Mag. **7**, 1817 (1962).

[80] H. Yamada and K. Terao, Phys. Rev. B **59**, 9342 (1999).

[81] R. J. Bouchard and J. L. Gillson, Mater. Res. Bull. **7**, 873 (1972).

[82] I. I. Pomeranchuk, Sov. JETP **35**, 524 (1958).

[83] P. W. Anderson, J. Phys. Chem. Solids **11**, 26 (1959).

[84] A. I. Larkin, JETP Lett. **2**, 130 (1965).

[85] A. F. Ho and A. J. Schofield, Europhys. Lett. **84**, 27007 (2008).

[86] N. D. Mathur, F. M. Grosche, S. R. Julian, I. R. Walker, D. M. Freye, R. K. W. Haselwimmer, and G. G. Lonzarich, Nature **394**, 39 (1998).

[87] S. S. Saxena *et al.*, Nature **406**, 587 (2000).

[88] F. Lévy, I. Sheikin, and A. Huxley, Nature Physics **3**, 460 (2007).

[89] C. Pfleiderer, D. Reznik, L. Pintschovius, H. v. Löhneysen, M. Garst, and A. Rosch, Nature **427**, 227 (2004).

[90] S. Mühlbauer, B. Binz, F. Jonietz, C. Pfleiderer, A. Rosch, A. Neubauer, R. Georgii, and P. Böni, Science **323**, 915 (2009).

[91] A. N. Bogdanov and A. Hubert, J. Magn. Magn. Mater. **138**, 255 (1994).

[92] A. N. Bogdanov and D. A. Yablonskii, Sov. Phys. JETP **68**, 101 (1989).

[93] S. A. Kivelson, E. Fradkin, and V. J. Emery, Nature **393**, 550 (1998).

[94] S. A. Grigera *et al.*, Science **306**, 1154 (2004).

[95] R. A. Borzi, S. A. Grigera, J. Farrell, R. S. Perry, S. J. S. Lister, S. L. Lee, D. A. Tennant, Y. Maeno, and A. P. MacKenzie, Science **315**, 214 (2007).

[96] J. Quintanilla, M. Haque, and A. J. Schofield, Phys. Rev. B **78**, 035131 (2008).

[97] E. Fradkin and S. A. Kivelson, Phys. Rev. B **59**, 8065 (1999).

[98] C. M. Varma and L. Zhu, Phys. Rev. Lett. **96**, 036405 (2006).

[99] E. C. Carter and A. J. Schofield, Phys. Rev. B **70**, 045107 (2004).

[100] H. Yamase, Phys. Rev. B **76**, 115117 (2007).